

DEVELOPMENT OF A HIGH-FIDELITY TRANSIENT AEROTHERMAL MODEL  
FOR A HELICOPTER TURBOSHAFT ENGINE FOR INLET DISTORTION AND  
ENGINE DETERIORATION SIMULATIONS

A THESIS SUBMITTED TO  
THE GRADUATE SCHOOL OF NATURAL AND APPLIED SCIENCES  
OF  
MIDDLE EAST TECHNICAL UNIVERSITY

BY

YAROSLAV NOVIKOV

IN PARTIAL FULFILLMENT OF THE REQUIREMENTS  
FOR  
THE DEGREE OF MASTER OF SCIENCE  
IN  
AEROSPACE ENGINEERING

JUNE 2012

Approval of the thesis:

**DEVELOPMENT OF A HIGH-FIDELITY TRANSIENT AEROTHERMAL MODEL FOR A  
HELICOPTER TURBOSHAFT ENGINE FOR INLET DISTORTION AND ENGINE DETERIORATION  
SIMULATIONS**

submitted by **YAROSLAV NOVIKOV** in partial fulfillment of the requirements for the degree  
of **Master of Science in Aerospace Engineering Department, Middle East Technical  
University** by,

Prof. Dr. Canan ÖZGEN  
Dean, Graduate School of **Natural and Applied Sciences**

\_\_\_\_\_

Prof. Dr. Ozan TEKİNALP  
Head of Department, **Aerospace Engineering**

\_\_\_\_\_

Asst. Prof. Dr. Oğuz UZOL  
Supervisor, **Department of Aerospace Engineering, METU**

\_\_\_\_\_

Asst. Prof. Dr. Ali Türker KUTAY  
Co-Supervisor, **Department of Aerospace Engineering, METU**

\_\_\_\_\_

**Examining Committee Members:**

Assoc. Prof. Dr. D. Funda KURTULUŞ  
Department of Aerospace Engineering, METU

\_\_\_\_\_

Assist. Prof. Dr. Oğuz UZOL  
Department of Aerospace Engineering, METU

\_\_\_\_\_

Assist. Prof. Dr. Ali Türker KUTAY  
Department of Aerospace Engineering, METU

\_\_\_\_\_

Assist. Prof. Dr. İlkay YAVRUCUK  
Department of Aerospace Engineering, METU

\_\_\_\_\_

Dr. Barış GÜMÜŞEL  
Turkish Engine Industries, TEI

\_\_\_\_\_

**Date:** 07.06.2012

**I hereby declare that all information in this document has been obtained and presented in accordance with academic rules and ethical conduct. I also declare that, as required by these rules and conduct, I have fully cited and referenced all material and results that are not original to this work.**

Name, Last Name : Yaroslav Novikov

Signature :

## **ABSTRACT**

### **DEVELOPMENT OF A HIGH-FIDELITY TRANSIENT AEROTHERMAL MODEL FOR A HELICOPTER TURBOSHAFT ENGINE FOR INLET DISTORTION AND ENGINE DETERIORATION SIMULATIONS**

Novikov, Yaroslav

M.Sc., Department of Aerospace Engineering

Supervisor : Assist. Prof. Dr. Oğuz Uzol

Co-Supervisor : Assist. Prof. Dr. Ali Türker Kutay

June 2012, 120 pages

Presented in this thesis is the development of a high-fidelity aerothermal model for GE T700 turboshaft engine. The model was constructed using thermodynamic relations governing change of flow properties across engine components, and by applying real component maps for the compressor and turbines as well as empirical relations for specific heats. Included in the model were bleed flows, turbine cooling and heat sink effects. Transient dynamics were modeled using inter-component volumes method in which mass imbalance between two engine components was used to calculate the inter-component pressure. This method allowed fast, high-accuracy and iteration-free calculation of engine states. Developed simulation model was successfully validated against previously published simulation results, and was applied in the simulation of inlet distortion and engine deterioration. Former included simulation of steady state and transient hot gas ingestion as well as transient decrease in the inlet total pressure. Engine deterioration simulations were

performed for four different cases of component deterioration with parameters defining engine degradation taken from the literature. Real time capability of the model was achieved by applying time scaling of plenum volumes which allowed for larger simulation time steps at very little cost of numerical accuracy. Finally, T700 model was used to develop a generic model by replacing empirical relations for specific heats with temperature and FAR dependent curve fits, and scaling T700 turbine maps. Developed generic aerothermal model was applied to simulate steady state performance of the Lycoming T53 turboshaft engine.

Keywords: gas turbine engine, aerothermodynamic model, transient performance, hot gas ingestion, engine degradation

## ÖZ

### **BİR HELİKOPTER TURBOŞAFT MOTORUNUN YÜKSEK DOĞRULUKLU AEROTHERMAL MODELLEMESİ VE GİRİŞTEKİ AKIŞ DÜZENSİZLİKLERİNİN VE MOTOR YIPRANMASI DURUMLARININ SİMÜLASYONU**

Novikov, Yaroslav

Yüksek Lisans, Havacılık ve Uzay Mühendisliği Bölümü

Tez Yöneticisi : Yrd. Doç. Dr. Oğuz Uzol

Ortak Tez Yöneticisi : Yrd. Doç. Dr. Ali Türker Kutay

Haziran 2012, 120 sayfa

Bu tezde, GE T700 turboşaft motorunun yüksek doğruluk dereceli aerothermal modellenmesi anlatılmaktadır. Motor modeli, değişik bileşenler içerisindeki akışkan özelliklerinin değişimini belirleyen termodinamik yasalar kullanılarak tasarlanmıştır. Modelin yüksek doğruluk seviyesi, kompresör ve türbin için gerçek bileşen haritalarının ve özgül sıcaklık terimlerinin hesaplanmasındaki ampirik denklemlerin kullanılması ile elde edilmiştir. Gerçek motora daha fazla benzerlik göstermesi için modele, kompresörden hava tahliyesi, türbin soğutması ve ısı emilmesi gibi durumlar da eklenmiş bulunmaktadır. Geçiş dinamiklerinin modellenmesinde, iki bileşen arasındaki kütle debisi farkını doğrudan basınca bağlayan bileşen-arası hacim yöntemi kullanılmaktadır. Bu sayede, model herhangi bir iterasyon gerektirmeden geçiş durumlarını yüksek bir hızla ve doğruluk oranı ile hesaplayabilmektedir. Geliştirilen aerothermal model, daha önceden yayınlanmış olan sonuçlar ile başarılı bir şekilde doğrulandıktan sonra motor girişindeki akış düzensizliklerinin

ve motor yıpranmasının simülasyonunda kullanılmıştır. Bunlardan ilki, durağan ve geçiş durumundaki sıcak hava emilmesi ile girişteki basınç düzensizliklerini içermektedir. Motor yıpranması durumu ise, literatürden alınan dört farklı senaryo kullanılarak simüle edilmiştir. Modelin gerçek zamanlı çalışma durumu, motor bileşenlerinin arasındaki hacimlerin zamanla oranlanması ile daha büyük zaman adımları kullanılarak, modelin doğruluk derecesi nerede ise hiç değiştirilmeden elde edilmiştir. T700 modeli, özgül sıcaklıkların hesaplanmasında kullanılan ampirik denklemlerin, özgül sıcaklığı akışkan sıcaklığına ve yakıt-hava oranına bağlı olarak belirleyen denklemler ile değiştirilmesi ve T700 türbin haritalarının ölçeklendirilmesi ile jenerik bir aerotermal model geliştirilmesi için de kullanılmıştır. Geliştirilen jenerik model, Lycoming T53 turboşaft motorunun durağan performansının simülasyonunda kullanılmıştır.

Anahtar kelimeler: gaz türbinli motor, aerotermodinamik modelleme, geçiş durumu, sıcak gazların emilme durumu, motor yıpranması

To my parents...

## **ACKNOWLEDGEMENT**

I would like to express my deepest gratitude to my supervisor, Assist. Prof. Dr. Oğuz Uzol who patiently supervised my work. His insight was a major contribution to some of the key concepts explored in this thesis.

I would also like to thank my co-supervisor, Assist. Prof. Dr. Ali Türker Kutay, for guiding me in matters regarding simulation and control theory.

# TABLE OF CONTENTS

ABSTRACT.....	iv
ÖZ.....	vi
ACKNOWLEDGEMENT.....	ix
TABLE OF CONTENTS.....	x
LIST OF TABLES.....	xiv
LIST OF FIGURES.....	xv
LIST OF ABBREVIATIONS .....	xviii
LIST OF SYMBOLS .....	xix
CHAPTERS	
1. INTRODUCTION.....	1
1.1 Gas Turbine Simulation Models.....	2
1.2 Aerothermodynamic Engine Models.....	4
1.3 Literature Survey .....	5
1.4 Objectives .....	10
1.5 Thesis Outline .....	11
2. AEROTHERMAL ENGINE MODELING.....	13
2.1 The GE T700 Engine .....	14
2.2 Engine Component Modeling.....	15
2.2.1 Inlet.....	15
2.2.2 Compressor.....	15
2.2.2.1 Compressor Outlet Flow Variables.....	15
2.2.2.2 Bleed Flows.....	17

2.2.2.3 Compressor Power .....	17
2.2.2.4 Reading the Compressor Map.....	17
2.2.3 Combustor .....	18
2.2.3.1 Steady State Operation .....	18
2.2.3.2 Transient Operation .....	18
2.2.3.3 Fuel Pump and Injection Modeling .....	20
2.2.4 Heat Soak Model .....	20
2.2.5 Gas Generator Turbine.....	21
2.2.6 Mixer.....	22
2.2.7 Power Turbine .....	23
2.2.8 Nozzle .....	24
2.2.9 Unsteady Mass Balance.....	24
2.2.9.1 Compressor – Combustor Plenum .....	25
2.2.9.2 Gas Generator – Power Turbine Plenum.....	25
2.2.10 Shaft Dynamics .....	25
2.2.11 Evaluation of Specific Heats .....	26
2.2.12 Integration Method .....	27
3. MODEL AND SIMULATION PARAMETERS & STABILITY.....	28
3.1 Initialization .....	28
3.2 Selection of Model Parameters .....	31
3.3 Design Point Performance Parameters of the GE T700.....	32
3.4 Selection of Simulation Parameters .....	32
3.4.1 Selection of Simulation Time Step.....	33
3.4.2 Selection of Combustor Time Constant.....	34
3.5 Combustor Modeling.....	37
3.6 Effect of Pressure Derivatives on Model Stability .....	38
3.7 Implementation of the Model in Simulink® .....	39

4. MODEL VALIDATION .....	40
4.1 Steady State Validation.....	40
4.2 Transient Validation.....	44
5. SIMULATION OF HOT GAS INGESTION AND INLET TOTAL PRESSURE DISTORTION .....	49
5.1 Introduction .....	49
5.1.1 Hot Gas Ingestion .....	49
5.1.2 Inlet Total Pressure Distortion.....	51
5.2 Simulation Methodology .....	51
5.3 Simulation of Steady State Hot Gas Ingestion .....	55
5.4 Simulation of Transient Hot Gas Ingestion .....	63
5.5 Simulation of Inlet Total Pressure Distortion .....	67
6. SIMULATION OF ENGINE DETERIORATION .....	72
6.1 Simulation Cases and Methodology .....	73
6.2 Simulation Results .....	75
7. REAL TIME IMPLEMENTATION OF AEROTHERMAL MODEL .....	84
8. DEVELOPMENT OF A GENERIC AEROTHERMAL MODEL.....	93
8.1 Evaluation of Specific Heats.....	93
8.2 Scaling of Component Maps.....	95
8.3 Steady State Simulation of Lycoming T53-L11 Turboshaft Engine .....	96
9. CONCLUSIONS AND FUTURE WORK .....	104
9.1 Conclusions.....	104
9.2 Future work .....	107
9.2.1 Remodeling of the Compressor.....	107
9.2.2 Surge Modeling.....	108
9.2.3 Dynamics of Loss Coefficients .....	108
9.2.4 Drive Train Model.....	108
BIBLIOGRAPHY .....	109

## APPENDICES

A. COMPRESSOR MAP READING.....	113
B. T700 ENGINE CONSTANTS .....	116
C. IMPLEMENTATION OF THE T700 ENGINE MODEL IN SIMULINK® .....	117
D. GE T700 COMPRESSOR MAP .....	120

## LIST OF TABLES

### TABLES

Table 2.1: Component inertia values .....	26
Table 2.2: Temperature-enthalpy relations [Ref. 19] .....	26
Table 3.1: Assumed T700 engine performance parameters.....	31
Table 3.2: Design point performance parameters.....	32
Table 5.1: Gains of the PI fuel control system .....	55
Table 5.2: Steady state engine parameters for different values of TIT .....	55
Table 6.1: Engine parameters for 100% nominal fuel flow regime for difference cases of engine deterioration .....	76
Table 6.2: Engine steady state parameters for difference cases of engine deterioration (TIT = 1575 K) .....	82
Table 7.1: Percent errors introduced with time scaling of plenum volumes .....	91
Table 7.2: CPU time per one second of simulation measured for different time steps .....	92
Table 8.1: Lycoming T53-L11 design specifications [Ref. 39].....	96
Table 8.2: Estimated performance parameters for Lycoming T53-L11 .....	97
Table B.1: T700 Engine Parameters .....	116

## LIST OF FIGURES

### FIGURES

Figure 2.1: Cross-sectional view of GE T700 showing major engine components with station numbers.....	14
Figure 3.1: Flowchart for calculation of design operating point of the engine .....	30
Figure 3.2: Response of power turbine inlet pressure to fuel step increase from 400 to 775 lbm/h (50.4 to 97.65 g/s) at different simulation time steps.....	34
Figure 3.3: Engine response to step increase in fuel flow from 400 to 775 lbm/h (50.4 to 97.65 g/s) as a function of $\tau_b$ .....	35
Figure 3.4: Influence of different combustor modeling approaches on engine response to step increase in fuel flow from 400 to 775 lbm/h (50.4 to 97.65 g/s).....	37
Figure 3.5: Effect of plenum outlet temperature derivative on system stability for the case of step decrease in fuel flow from 775 to 400 lbm/h (97.65 to 50.4 g/s) .....	38
Figure 4.1: Engine output power vs. fuel flow .....	41
Figure 4.2: Gas generator speed vs. fuel flow.....	42
Figure 4.3: Compressor exit static pressure vs. gas generator speed .....	43
Figure 4.4: Engine response to step increase in fuel flow from 400 to 775 lbm/h (50.4 to 97.65 g/s) .....	45
Figure 4.5: Engine response to step increase in fuel flow from 400 to 125 lbm/h (50.4 to 15.75 g/s) .....	46
Figure 5.1: Hot gas ingestion during on-ground operation [Ref. 28].....	50
Figure 5.2: Hot gas ingestion in ground effect hover [Ref. 28].....	50
Figure 5.3: Distortion angle in circumferential plane of engine intake .....	52
Figure 5.4: Engine response to steady state hot gas ingestion for $T_3 = T_{3,des}$ .....	57
Figure 5.5: Engine response to steady state hot gas ingestion for $T_3 = 1550 K$ .....	58
Figure 5.6: Engine response to steady state hot gas ingestion for $T_3 = 1575 K$ .....	59
Figure 5.7: Operating lines for clean and distorted sections of the compressor for different angles of distortion, $T_3 = T_{3,des}$ .....	62

Figure 5.8: Resulting compressor operating lines for different distortion angles, $T_3 = T_{3,des}$ .....	63
Figure 5.9: Real flight data for temperature and pressure distortions at the inlet .....	64
Figure 5.10: Engine response to realistic transient inlet distortion.....	65
Figure 5.11: Sample inlet total pressure distortion signal for 15% distortion amplitude, 0.1 seconds of duration .....	68
Figure 5.12: Engine response to transient inlet total pressure distortion.....	69
Figure 5.13: Variation of distortion amplitude with signal duration and distortion angle to initiate a compressor surge .....	71
Figure 6.1: Variation of gas generator speed with fuel flow for different cases of engine deterioration.....	77
Figure 6.2: Variation of compressor outlet static pressure with gas generator speed for different cases of engine deterioration .....	78
Figure 6.3: Variation of output power with fuel flow for different cases of engine deterioration.....	79
Figure 6.4: Compressor operating lines for different cases of engine deterioration .....	81
Figure 7.1: Response of power turbine inlet pressure to step increase in fuel flow from 400 to 775 lbm/h (50.4 to 97.65 g/s) for the two cases of volume time scaling.....	87
Figure 7.2: Response of compressor outlet static pressure to step increase in fuel flow from 400 to 775 lbm/h (50.4 to 97.65 g/s) for the two cases of volume time scaling .....	87
Figure 7.3: Gas generator speed dynamics as a function of simulation time step for step increase in fuel flow from 50% to 100% of design value.....	88
Figure 7.4: Compressor outlet static pressure dynamics as a function of simulation time step for step increase in fuel flow from 50% to 100% of design value .....	88
Figure 7.5: Gas generator outlet pressure dynamics as a function of simulation time step for step increase in fuel flow from 50% to 100% of design value .....	89
Figure 7.6: Gas generator speed dynamics as a function of simulation time step for step decrease in fuel flow from 100% to 50% of design value.....	89
Figure 7.7: Compressor outlet static pressure dynamics as a function of simulation time step for step decrease in fuel flow from 100% to 50% of design value .....	90
Figure 7.8: Gas generator outlet pressure dynamics as a function of simulation time step for step decrease in fuel flow from 100% to 50% of design value .....	90
Figure 8.1: Variation of fuel flow as a function of gas generator speed.....	99
Figure 8.2: Variation of compressor mass flow as a function of gas generator speed.....	100

Figure 8.3: Variation of output power as a function of gas generator speed .....	101
Figure A.1: Reading of the compressor map.....	113
Figure C.1: Individual engine blocks of the SIMULINK® model.....	117
Figure C.2: Compressor model block .....	117
Figure C.3: Combustor model block.....	118
Figure C.4: Gas generator turbine model block.....	118
Figure C.5: Power turbine model block .....	119
Figure D.1: GE T700 compressor map.....	120

## LIST OF ABBREVIATIONS

<i>FAR</i>	Fuel-to-Air Ratio
<i>HGI</i>	Hot Gas Ingestion
<i>ISA</i>	International Standard Atmosphere
<i>LHV</i>	Lower Heating Value
<i>SLS</i>	Sea Level Static
<i>TIT</i>	Turbine Inlet Temperature

## LIST OF SYMBOLS

$b_1$	First bleed fraction
$b_2$	Second bleed fraction
$b_3$	Third bleed fraction
$g_2$	Mass flow rate at compressor outlet
$g_{2p}$	Compressor mass flow rate
$g_3$	Gas generator turbine inlet mass flow rate
$g_4$	Power turbine inlet mass flow rate
$g_{4p}$	Gas generator turbine outlet mass flow rate
$g_b$	Fuel mass flow rate
$g_{cool}$	Gas generator turbine cooling mass flow rate
$h_1$	Specific enthalpy of the ambient
$h_2$	Specific enthalpy at compressor outlet
$h_3$	Specific enthalpy at gas generator turbine inlet
$h_4$	Specific enthalpy at power turbine inlet
$h_{4p}$	Specific enthalpy at gas generator outlet
$h_5$	Specific enthalpy at power turbine outlet
$J_{GG}$	Gas generator turbine assembly moment of inertia
$J_{PT}$	Power turbine assembly moment of inertia
$K_V$	Plenum volume parameter
$N_1$	High pressure spool rotational speed
$N_2$	Low pressure spool rotational speed
$P_1$	Ambient total pressure
$P_2$	Total pressure at compressor outlet
$P_{2stat}$	Static pressure at compressor outlet
$P_3$	Total pressure at combustor outlet
$P_4$	Total pressure at power turbine inlet
$P_{4p}$	Total pressure at gas generator turbine outlet

$P_5$	Total pressure at power turbine outlet
$P_C$	Compressor power
$P_{GG}$	Gas generator turbine power
$p_{loss}$	Total pressure loss coefficient due to mixing
$P_{PT}$	Power turbine output power
$R$	Specific gas constant
$T_1$	Ambient total temperature
$T_2$	Total temperature at compressor outlet
$T_3$	Total temperature at combustor outlet
$T_4$	Total temperature at power turbine inlet
$T_{4p}$	Total temperature at gas generator turbine outlet
$T_5$	Total temperature at power turbine outlet
$y_{loss}$	Combustor total pressure loss coefficient
$\gamma$	Ratio of specific heats
$\delta_0$	Ratio of inlet total pressure to ISA SLS pressure
$\Delta h_{GG}$	Gas generator turbine enthalpy drop
$\Delta h_{PT}$	Power turbine enthalpy drop
$\eta_b$	Burner efficiency
$\eta_C$	Compressor efficiency
$\eta_{GG}$	Gas generator turbine efficiency
$\eta_{mech}$	Shaft mechanical efficiency
$\theta_0$	Ratio of inlet total temperature to ISA SLS temperature
$\theta_{GG}$	Gas generator turbine inlet critical velocity parameter
$\theta_{PT}$	Power turbine inlet critical velocity parameter
$\pi_C$	Compressor outlet to inlet total pressure ratio
$\pi_{C_{stat}}$	Compressor static outlet to total inlet pressure ratio
$\tau_b$	Combustor time constant
$\tau_C$	Compressor outlet to inlet total temperature ratio
$\omega$	Shaft rotational speed

# CHAPTER 1

## INTRODUCTION

Comprehensive transient gas turbine models can simulate real aero-engines to a high level of accuracy. With a well-structured design approach, they can be used to model and simulate any engine type and configuration, and simulations of steady state and transient performance of an aero-engine operating under different conditions can be performed with a high level of confidence. Additionally, dynamic models can be used to simulate different engine-related phenomena like engine surge, its control and prevention, performance loss due to degradation of engine components, engine faults and component failures. As a reliable tool for conceptual design of a new gas turbine engine, these models can be used effectively to test available design options and study their effect on the overall engine performance, or to explore completely new design concepts. Important design changes and modifications can be applied to the real engine after having been studied in scrutiny using such models. To avoid a possible damage which can be incurred to the real engine, control system development can be based on the dynamic model of the engine. Also, these models can be easily embedded into applications which require high fidelity engine models.

Accuracy of an engine model depends on the level of complexity which is determined by the amount of included components constituting the real engine, as well as their aerothermodynamic description. Physical faithfulness of the model can be increased substantially if known empirical relations specific to the engine are used in its aerothermal modeling to allow for a more accurate and realistic calculation of flow variables at different stations of the engine. By doing so, it becomes possible to obtain a high fidelity model which closely resembles the real engine and performs exceptionally well in producing accurate engine dynamics. However, when it comes to determining physical accuracy of the model in quantitative terms, all these factors play only a secondary role. Because there

exist a number of methods which can be used to simulate a gas turbine engine, and because each of these methods has own specificities, it is the model type that determines how accurate, in numerical sense, will a developed model reproduce the performance of the real engine.

## **1.1 Gas Turbine Simulation Models**

There exist a number of gas turbine models which are commonly used for simulating engine performance under a wide range of operating conditions. Each of these models has its own specifics which determine its advantages and disadvantages relative to other models. A good source of information about most common types of engine models used in the industry and academic research is presented in Reference 1. Given below is a brief description of the most popular, according to Walsh and Fletcher, simulation models.

- **Thermodynamic Matching Transient Performance Model**

This model type is based on a steady state engine model which runs between different engine speeds. Engine speed is calculated by using unbalanced power applied on the shaft. For each guessed value of unbalanced power the model calculates corresponding fuel mass flow. This mass flow is then compared to the value which was set by the user, or the control unit. Iteration on unbalanced power is continued until fuel flow matches its inputted value. When this condition is attained, the simulation advances to the next time step. In between time steps, transient behavior of the engine is modeled using volume dynamics and other effects included in the model (combustor dynamics, heat soak etc.). This model type is very accurate at producing correct engine transients and therefore is widely used for transient simulations in early design stages of an aero-engine, as well as for control system development. The main disadvantage of these models is noise production due to inherent iterative solution methodology. Moreover, because of the large number of iterations required to advance to the next time step, real time implementation of these models is seldom possible, which significantly limits their use in hardware-in-the loop simulations.

- **Real Time Transfer Function Transient Performance Model**

As implied by the name, variation of flow parameters and change of operating state of the engine is modeled using transfer functions in Laplace domain. In order to develop a reliable model, time constants must be determined from experimental data of the engine, or some other transient performance model. While offering considerable savings in computational time and power along with overall model simplicity, these models do not provide high levels of accuracy, and application of these models is mostly limited to flight simulators, although their use for control design purposes is frequently encountered.

- **Real Time Lumped Parameter Transient Performance Model**

In this transient model type, engine dynamics are modeled using partial derivatives of all variables taken with respect to all other engine variables for a large number of engine speeds. Constructed steady state and transient parameter matrices must be populated with either experimental data, or simulation results obtained from another performance model. Accuracy offered by these models is low, therefore the field of application of lumped parameter transient models is mostly limited to flight simulators.

- **Real Time Aerothermal Transient Performance Model**

Also known as aerothermodynamic model, it is the most accurate real-time model used in the simulation of transient performance of aero-engines. High simulation accuracy is achieved by using thermodynamic laws which govern change of flow properties inside engine components. Moreover, use of components maps for the compressor and turbines substantially improves accuracy of the model. In this model type, engine transients are modeled using inter-component volumes method, and evaluation of engine states does not require an iterative solution technique. This specificity enables fast and efficient calculation of engine performance at steady state and transient operating conditions. It therefore is no surprise why aerothermal models are accepted as the most popular tool with a long history of use in both academic and industrial circles for simulating aero-engines. It is due to the apparent advantages why in present study this model was selected for developing a high fidelity transient model for a turboshaft engine.

## 1.2 Aerothermodynamic Engine Models

Aerothermodynamic engine models are developed by considering mass, momentum and energy conservation laws governing change of flow properties inside engine components. Engine transients are modeled using inter-component volumes which are used to evaluate pressure changes as a function of mass accumulation between neighboring engine components. With this approach for modeling engine transients, aerothermal models do not require an iterative solution technique to calculate engine parameters, and simulation can continuously advance in time by updating flow variable values obtained at the previous time step with their current values. This technique renders an aerothermal model fast, and under certain conditions allows it to be run in real time, thus providing considerable savings in computational time and power without compromising numerical accuracy of the model. A study performed by Rahman and Whidborne [Ref. 2], in which authors compared relative accuracy between a purely iterative solution approach and inter-component volumes method, verified this fact. Results of the study for steady state and transient operating conditions showed that inter-component volumes method followed very closely to iterative technique in terms of numerical accuracy. While, due to stability issues, time step for the iterative model had to be limited to 25 milliseconds, it was possible to use a much smaller time step of 5 milliseconds for the inter-component volumes method, thus rendering latter solution technique even more accurate since fast variations in pressures could be captured. Thus, the study verified that aerothermal models employing inter-component volumes method provide high accuracy in calculating steady state and transient performance of gas turbine engines.

Due to their ability to accurately simulate steady state operation and transient dynamics of a gas turbine engine, aerothermal models are frequently employed in preliminary stages of engine design. Important design decisions can be made by studying the effect of each design option on the overall performance of the engine by employing high computational speed and efficiency offered by aerothermal models in simulating engine dynamics under various operating conditions and load regimes. Aerothermal models can accommodate any engine component which is capable of being mathematically modeled in a simulation environment, thus making engine simulations highly versatile and accurate in predicting dynamics of a real engine. Moreover, using high-speed processing power of modern computers, aerothermal models will usually offer the capability to be run in real time. This

advantage is particularly important for developing engine control systems: to avoid a possible damage which can be incurred to the real engine, design of engine control algorithms, their testing and validation is frequently done using aerothermal models offering real time capability. With development of simulation programs incorporating advanced graphical user interfaces such as SIMULINK® by MathWorks, separate libraries containing individual engine blocks can be constructed, and the time required to develop a specific engine model be reduced considerably.

### **1.3 Literature Survey**

Advantages offered by aerothermal models are effectively used for engine design and validation purposes. Development of these models is an ongoing research topic with many studies aimed to provide a more comprehensive description of thermodynamic processes taking place inside the engine. A number of authors proposed generic aerothermal models which can be used for a variety of engine configurations by supplying relevant component performance maps. One such model is presented by Camporeale et al. in Reference 3. In the generic model developed by the authors, calculation of flow properties at each engine station was based on non-linear algebraic relations derived from engine thermodynamics. Iterative calculation technique was eliminated by arranging these relations in parallel with engine mainstream direction to obtain a forward-substitution solution scheme. Physical accuracy of the model was increased substantially by inclusion of bleed flows, cooling effects, inlet guide vane angle variation via actuation dynamics, fuel pump and temperature transducer models. The model was applied to two different types of gas turbine engines, and each was successfully validated against experimental data and numerical simulation results obtained by other authors. Results of simulation tests aimed to determine whether developed model was capable of running in real time suggested that even for simulations performed on a Pentium III computer with second order integration scheme, 1 second of simulation time corresponded to 1/6 seconds in real time, thus making it possible to directly use developed model in real time applications. It should be stated that such a large difference which exists between the CPU and simulation times can be effectively used to increase physical accuracy of the model even more by introducing a more detailed thermodynamic description of the engine and processes taking place inside individual engine components.

An implementation of Camporeale's generic aerothermal model is presented in Reference 4. In this study, authors adapted Camporeale's model for simulating single-spool Siemens V64.3 industrial gas turbine under steady state and transient operating conditions. Based on a generic compressor map, the model was successfully applied for control design purposes.

Reference 5 focused on development of a generic aerothermal model for a gas turbine engine. Similarly to Reference 3, aerothermodynamic description constituted the basis for developed generic model. The author treated engine components as black boxes for which outlet flow variables were calculated using inlet values through the thermodynamics of each component. Using graphical user interface of SIMULINK®, engine components were modeled as individual blocks and combined into a separate library. This modeling technique allowed simulation of any gas turbine configuration by connecting model blocks in appropriate sequence. Supplemented with a model of engine control system, developed aerothermal model was used to successfully simulate steady state and transient operation of two different gas turbine engines.

In Reference 6, Sanghi et al. described the development of a dynamic model for a military turbofan engine. The model was used for calculating steady state performance of the engine for different flight Mach numbers and various operating altitudes. Also investigated was a case in which high-pressure compressor of an engine in development was assumed to be deficient in terms of component mass flow. Based on steady state simulation results, authors discussed the possibility of applying minor modifications to the existing engine hardware to compensate for performance losses and meet initial design goals.

Martin et al. [Ref. 7] developed a high-fidelity aerothermodynamic model for a commercial twin-spool turbofan engine with inter-component volumes method used to simulate engine dynamics during transient operation. This comprehensive model included bleed flows, fuel system and temperature sensor dynamics, variable bleed valves for compressor inter-stage surge protection and variable stator vanes for the high-pressure compressor. Also modeled was the heat transfer from working fluid to turbine blades and casing. Performances of the fan, compressor and turbine were defined in terms of manufacturer-supplied characteristic maps. Designed control system was used to keep the engine in a safe operating range by monitoring a number of engine parameters. Developed aerothermal model was used to

evaluate engine performance at steady state and transient operation at different Mach number and altitude regimes for different thrust requirements. Authors suggested that developed model could be used for simulating engine faults and failures and constitute a reliable basis for developing fault-tolerant control algorithms to keep the engine within safe operating limits.

In Reference 8, a different approach was employed for simulating major engine components: instead of performance charts, compressor and turbine were modeled using inlet guide vane angles and flow velocities inside these components. Developed aerothermal model with inter-component volumes approach was adapted for Solar Mercury 50 industrial gas turbine, and used to simulate start-up dynamics and steady state performance of the engine.

In their study, Tagade et al. [Ref. 9] investigated engine transients which occurred during acceleration to full throttle from engine start-up. Because most compressor maps are given only for idle to full throttle regimes, authors used an extrapolation technique which allowed extension of the compressor map to full operating range of the engine. Developed aerothermal model was found to accurately match experimental data in qualitative terms, thus suggesting that with accurate description of engine components, aerothermal models offer the capability to faithfully simulate engine transients in the full operating range.

Aerothermal models are also widely used for simulating various engine related phenomena. As such, simulations performed by Larjola [Ref. 10] were aimed at investigating the effects of heat transfer on engine dynamics during low frequency transients (acceleration and deceleration). With inclusion of density change, boundary layer and clearance effects for the compressor, and modeling of heat transfer for major components of the engine, developed model was utilized to investigate the differences in engine dynamics with and without heat transfer. Simulation results suggested that heat transfer has a profound influence on engine dynamics due to the significant impact it has on compressor surge margin. This implies that inclusion of heat transfer effects is important to obtain an accurate dynamic model of an engine, especially for applications in which preventive measures are employed to avoid a possible engine surge.

In their article, Rahman and Whidborne [Ref. 11] investigated the effect of bleed flow extraction on performance of a single-spool turbojet engine, and its feasibility for improving

control and aerodynamic performance of lifting surfaces for a blended wing-body aircraft configuration by injecting extracted from the compressor bleed flow into the boundary layer of leading and trailing edge lift devices with the purpose of energizing the flow and preventing flow separation over these surfaces. In their paper, authors used a successfully validated model of a small turbojet engine to simulate various cases of bleed flow extraction and its effect on engine performance. It was pointed out that although bleed extraction for aerodynamic control purposes was indeed possible, the amount of bleed flow, and consequently the aerodynamic control, was limited by the degrading performance of the engine which had to operate at elevated turbine inlet temperatures with significantly reduced air mass flow.

Application of an aerothermal model as a propulsion system for design and development of a major aircraft component was described in Reference 12. In this study, Vallabhaneni coupled main rotor dynamics with a gas turbine engine model via two-speed ideal continuously varying transmission mechanism. A flight dynamics algorithm was introduced to simulate a basic flight control system. Developed simulation model was used to study drive train dynamics in steady forward flight regime to gain a deeper understanding in the ongoing research on the development of variable ratio transmission mechanisms.

In Reference 13, Yarlagadda investigated the feasibility of engine thrust control by adjusting compressor inlet mass flow to decrease compressor inlet pressure with the purpose of increasing compressor rotational speed at which higher pressure ratios and component efficiencies could be achieved. Simulations performed for different reduced operating inlet pressure regimes showed an overall decrease of engine performance indicated by the decrease in thermal efficiency and increase in thrust-specific fuel consumption. With some increase in the value engine specific thrust, proposed method seems to be applicable only to military aircraft for which fuel consumption is usually of secondary importance.

An example of hardware-in-the-loop simulation is given in Reference 14. Montazeri-Gh et al. described the development of a real time aerothermal model for a single spool turbojet engine without bypass or bleed flow effects for hardware-in-the-loop simulations. The model was used to design and validate an engine control system regulating fuel flow. Developed controller was programmed to an electronic control unit which was used as a governor in the hardware-in-the-loop simulations with the turbojet model simulating the

engine. It was shown that real time capability of the model can be realized without altering simulation time step by uncoupling high sampling rate controller from the engine model, and transferring control functionality to a second processor, or computer, which works in parallel with the low sampling rate engine model in a multi-rate simulation. Proposed simulation methodology is promising especially for real time applications because with this approach engine model accuracy is preserved while more flexibility is given to hardware-in-the-loop simulations.

For more information about past studies aimed at aerothermodynamic simulation of gas turbine engines the reader is referred to Reference 15 in which an extensive literature review is presented starting from the very first attempts of gas turbine engine simulation and ending with present advances in modeling and simulation techniques until the year of 2000.

Present study is a continuation of work previously conducted by Kocer [Ref. 16]. Kocer developed a FORTRAN-based aerothermal model for simulating a small single-spool turbojet engine operating under different fuel mass flow regimes. Simulation results were compared to experimental data, and qualitatively accurate variation of engine parameters was obtained. A modified version of the model was also used to simulate hot gas ingestion for T800-LHT-800 turboshaft engine [Ref. 17]. The model predicted expected variation of engine parameters under different ambient temperature conditions.

In Reference 18, Uzol adapted Kocer's model to simulate GE T700-GE-700 turboshaft engine. Compressor map was modeled using multi-layer neural network. Engine steady state parameters for simulation initialization were obtained by performing a complete thermodynamic analysis of the engine by assuming the design point on the compressor map, estimating component efficiencies and the gas generator turbine inlet temperature. Calculation of specific heats was based on polynomial curve fits, and temperatures at component outlets were calculated using an iterative technique by assuming that efficiencies of the compressor and turbines remained constant in the entire operating range of the engine. Developed model accurately predicted engine transients and variation of engine parameters under various operating conditions, and a satisfactory match was obtained with previously published simulation results.

A study which is frequently quoted throughout the thesis belongs to Mark Ballin [Ref.19]. In this study, author developed a real-time high-fidelity aerothermodynamic model for GE T700 turboshaft engine. Modeling of engine components included empirical relations for calculating specific heat capacity values at different stations of the engine and enthalpy drops across the turbines. The gas generator turbine was also modeled using empirically determined value for the mass flow parameter at design point conditions. Modeling of transient dynamics was achieved by using inter-component volumes methods, with three plenum volumes used in the simulation model: one between the compressor and combustor, one for the combustor, and another one between the gas generator and power turbines. Evaluation of combustor mass flow was once again based on an empirically determined constant. The inclusion of a large number of empirical relations significantly limited application of the model in simulating other engines. Therefore in present study aerothermal modeling was based on a more generic approach for simulating engine performance: engine dynamics was modeled using only two plenum volumes, while gas generator turbine was modeled using a general expression for a choked turbine. Included in the model were pressure loss coefficients to account for skin friction and turbulence in the combustion chamber, as well as for mixing effects at the gas generator turbine. Moreover, used in present study was a dynamic combustor model in which, unlike the steady state approach employed in Ballin's model, combustor outlet temperature was calculated as a function of energy imbalance across the component with dynamics of the temperature variation dictated by the volume of the combustor. It will be shown in the following chapters of the thesis that the two models produced similar results for steady state performance of the engine. However, due to substantial differences in the modeling of engine components, the two models differ in terms of transient performance of the engine.

#### **1.4 Objectives**

Objective of the present study is to develop a comprehensive aerothermal model for the GE T700-GE-700 turboshaft engine in SIMULINK®. Engine-specific empirical relations will be used to obtain an accurate thermodynamic representation of the engine. An accurate estimation of design operating point of the engine will be obtained by using component matching technique coupled with a full thermodynamic analysis of the engine.

Developed aerothermodynamic model will be used to simulate steady state and transient performance of the engine, and for investigating engine response to different cases of inlet distortion. Moreover, developed model will be employed to simulate different scenarios of engine deterioration. Each deterioration case will be studied in terms of its impact on the overall performance of the engine. Finally, a generic version of the model will be developed and used in the simulation of Lycoming T53 turboshaft engine under steady state operating conditions.

## **1.5 Thesis Outline**

Chapter 2 deals with the aerothermodynamic modeling of the engine. Each component of the engine is modeled using conservation laws which govern change of flow properties across engine components. To render developed model more accurate, empirical relations for specific heats are used along with a model for heat sink, while compressor and turbines are modeled using component performance maps.

Chapter 3 discusses selection of unknown engine parameters: gas generator turbine efficiency and pressure loss coefficients for the combustor and turbine cooling. Also discussed is the selection of simulation time step and combustor time constant. Some emphasis is made on model stability and on ways for improving it.

Validation of the model is presented in Chapter 4. Steady state and transient simulation results obtained with developed aerothermal model are compared against previously published simulation results. Factors causing small discrepancies in steady state results and considerable deviations in transient response of the engine are discussed in detail.

Simulation results for different cases of inlet distortion are presented in Chapter 5. A two-parallel-compressor model is developed and used to simulate steady state engine performance at elevated ambient temperatures. Then, real flight data for hot gas ingestion is used to study engine dynamics under transient distorted inlet conditions. Finally, transient inlet total pressure distortion simulations are performed to investigate the impact of such distortions on engine performance.

Chapter 6 presents simulation results for four different cases of engine deterioration. Each degradation scenario is studied in terms of its impact on the overall engine performance by comparing simulation results against nominal engine data.

Discussed in chapter 7 is the real time capability of developed model. Limitations imposed on the maximum allowable simulation time step by numerical instabilities occurring at large time steps are removed by applying time scaling of control volumes to obtain a stable aerothermal model with real time capability without sacrificing its numerical accuracy.

Chapter 8 discusses the development of a generic aerothermal model. Replacing empirical relations used in the T700 engine model for evaluating specific heat capacities with a generic way of calculating these parameters, and scaling down component maps of the T700 engine with its design point parameters yields a generic model which can be applied to different engines via appropriate scaling of performance maps. Developed generic model is used to simulate steady state performance of Lycoming T53 turboshaft engine.

Chapter 9 contains a summary of present work, and suggestions for improvement of the model.

## CHAPTER 2

### AEROTHERMAL ENGINE MODELING

Thermodynamic processes taking place inside engine components and transient dynamics of a gas turbine are generally represented by a set of algebraic relations and differential equations which are used for calculating variation of engine flow parameters in time. Inter-component volumes method is a widely used approach to account for various time-dependent variations such as mass imbalance and energy accumulation between engine components which especially occur during engine transients. This method was shown to be of high practical advantage in real-time applications where fast but accurate calculation of transient dynamics is required [Ref. 3]. It should be added that inter-component volumes method makes iterative solution technique, i.e. the highly accurate method for calculating operating state of the engine, impractical due to its high demand for simulation time and computational power. Moreover, as was stated in Chapter 1, models incorporating inter-component volumes method usually offer superior execution time at very little cost of numerical accuracy.

Inter-component volumes are modeled using plenums, and related mass accumulation relation is derived from ideal gas law. This relation is used to account for pressure change at plenum outlets to satisfy continuity condition between two neighboring engine components. In developed simulation model, pressures at compressor and gas generator turbine outlets were calculated using the plenum relation which accounted for mass imbalance between the compressor and combustor, and between the gas generator and power turbines. The model included bleed flow extraction from the compressor inter-stage which was used for turbine cooling, as well as mixing effects due to coolant ejection from the turbine. Also taken into account was the heat soak effect. Modeled as a transfer function with varying time constants, heat soak effect accounted for turbine blades absorbing heat from hot

gases at gas generator turbine inlet where large temperature gradients frequently occur. Empirical relations given by Ballin in Reference 19 were used in the model to achieve a more faithful representation of aero-thermodynamic processes and transient dynamics of the real gas turbine engine.

## 2.1 The GE T700 Engine

GE T700 is a 1600-HP class turboshaft engine which powers UH-60 Black Hawk, AH-1W SuperCobra and AH-64 Apache helicopters. It has a 5-stage axial and a single-stage radial compressor. First two stages of the axial compressor have variable-geometry inlet guide vanes and stator vanes. The gas generator and power turbines have two stages. Cooling of turbine blades is applied only at the gas generator turbine. A simplified cross-sectional view of the T700 showing major components of the engine and station numbers used in present study is given in Figure 2.1.

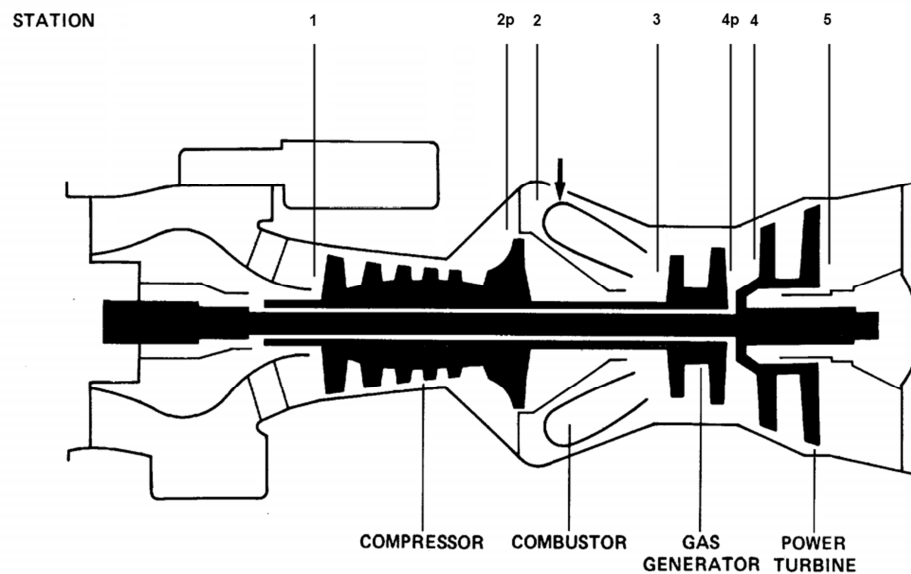


**Figure 2.1: Cross-sectional view of GE T700 showing major engine components with station numbers**

## 2.2 Engine Component Modeling

### 2.2.1 Inlet

Air ingestion through engine intake was assumed to be an isentropic and adiabatic process so that total temperature and pressure at compressor inlet were taken equal to ambient total temperature and pressure, respectively. For low Mach number regimes, total parameters of the flow can be assumed to be equal to their respective static values. This assumption was used within the entire scope of this thesis, and from this point onwards, unless stated otherwise, total flow variables will assume their total quantities without being referred to as “total” variables.

Compressor inlet flow properties were defined in terms of ambient conditions:

$$P_1 = P_{amb} \quad [2.1]$$

$$T_1 = T_{amb} \quad [2.2]$$

ISA SLS conditions were used to define the following correction parameters:

$$\delta_0 = \frac{P_{amb}}{P_{SLS}} \quad [2.3]$$

$$\theta_0 = \frac{T_{amb}}{T_{SLS}} \quad [2.4]$$

Where,

$$P_{SLS} = 101325 \text{ Pa}$$

$$T_{SLS} = 288.15 \text{ K}$$

### 2.2.2 Compressor

#### 2.2.2.1 Compressor Outlet Flow Variables

Mass flow rate going through the compressor was calculated using the performance map given by Ballin [Ref. 19]. Corrected mass flow was read from the map for a given operating state defined in terms of static-to-total pressure ratio of the component and corrected gas generator speed:

$$g_{2p_{cor}} = f(\pi_{C_{stat}}, N_{1_{cor}}) \quad [2.5]$$

The definitions for  $\pi_{C_{stat}}$  and  $N_{1_{cor}}$  are given as follows:

$$\pi_{C_{stat}} = \frac{P_{2_{stat}}}{P_1} \quad [2.6]$$

$$N_{1_{cor}} = \frac{N_1}{\sqrt{\theta_0}} \quad [2.7]$$

Static pressure at compressor outlet was taken as a fixed percentage of the total pressure [Ref. 19]:

$$P_{2_{stat}} = 0.956 \cdot P_2 \quad [2.8]$$

Mass flow rate at compressor outlet was uncorrected with respect to operating ambient conditions by using the correction parameters defined by Equations 2.3 and 2.4:

$$g_{2p} = g_{2p_{cor}} \frac{\delta_0}{\sqrt{\theta_0}} \quad [2.9]$$

Compressor outlet temperature is usually evaluated using the definition of compressor efficiency:

$$\eta_c = \frac{\pi_c^{\frac{\gamma-1}{\gamma}} - 1}{\tau_c - 1} \quad [2.10]$$

It is customary to embed compressor efficiency information in the performance map of the component. In Reference 19, efficiency contours were not given as part of the compressor characteristic map. Instead, the variation of compressor temperature ratio with static-to-total pressure ratio was given, so that temperature at compressor outlet was calculated as follows:

$$T_2 = T_1 \cdot f\left(\frac{P_{2_{stat}}}{P_1}\right) \quad [2.11]$$

### 2.2.2.2 Bleed Flows

In the T700 engine, a total of four different bleed flows are extracted: two from the 4<sup>th</sup> compressor stage and two from the diffuser. Bleed flow fractions, i.e.  $b_1$ ,  $b_2$  and  $b_3$  in Equation 2.12, were, as given in Ballin [Ref. 19], defined as functions of corrected rotational speed of the gas generator turbine and corrected compressor mass flow rate.

$$g_{bleed} = g_{2p} \cdot (b_1 + b_2 + b_3 + 0.0025) \quad [2.12]$$

Mass flow rate at the inlet of the first plenum was calculated in terms of compressor mass flow less bleed flows:

$$g_2 = g_{2p} - g_{bleed} \quad [2.13]$$

### 2.2.2.3 Compressor Power

Power required by the compressor is proportional to the core mass flow and enthalpy rise across the component. Accounted for in compressor power relation were the extracted bleed flows: bled air flows do not contribute to the power requirement of the compressor in the downstream direction from the location of bleed flow extraction. Therefore, these must be excluded from the power relation:

$$P_C = g_{2p}(h_2 - h_1) - 0.29 \cdot g_{2p}h_2(b_1 + b_2) \quad [2.14]$$

Equation 2.14 assumes that air temperature at bleed flow extraction location in component inter-stage equals 71% of component outlet temperature [Ref. 19].

### 2.2.2.4 Reading the Compressor Map

Compressor performance map given in Reference 19 was used to read corrected mass flow rate of the component as a function of corrected rotational speed of the gas generator and static-to-total pressure ratio of the compressor. The map was digitized with every RPM line being represented using 6 points which were equally spaced over each speed line. The digitized map was stored in a MATLAB-compatible file, and contained information for mass flow and pressure ratio for each speed line given in the map. A MATLAB code read this file and calculated corrected mass flow using two inputs: static-to-total pressure ratio and corrected speed of the compressor. The code then scanned for two RPM values given in the

map such that current RPM value would remain between these two values. A line for the running RPM was constructed by assuming linear speed variation between bounding RPM lines, and corrected mass flow corresponding to the running RPM was calculated as a function of static-to-total pressure ratio. Details of map reading are given in Appendix A.

### 2.2.3 Combustor

Similar to the method used by Camporeale et al. [Ref. 3], in the current simulation model the combustor was modeled as a pure energy accumulator. Therefore, no mass imbalance was considered for this component, and combustor exit pressure was taken as a fixed percentage of its inlet value. By doing so, rate of pressure change at combustor outlet during transient operating conditions becomes linearly proportional to the rate of pressure change at the downstream plenum outlet with burner pressure drop coefficient, hence rendering evaluation of combustor outlet pressure by considering mass flow imbalance unnecessary.

#### 2.2.3.1 Steady State Operation

Processes taking place inside the combustor are governed by energy and mass conservation laws. Diffuser outlet and fuel mass flows constitute the net mass inflow at combustor inlet:

$$g_3 = g_b + g_2 \quad [2.15]$$

Energy conservation was used to obtain flow parameters at component outlet:

$$g_3 h_3 = g_2 h_2 + g_b \eta_b LHV \quad [2.16]$$

All of the unburned fuel was accounted for by the burner efficiency. Fuel enthalpy was assumed to be negligible in comparison with its heating value. As will be explained in Chapter 3, Equation 2.16 was used for evaluating fuel mass flow rate by assuming a value for combustor exit temperature during evaluation of design operating point of the engine.

#### 2.2.3.2 Transient Operation

Gas generator turbine inlet temperature (TIT) was calculated using a combustor model. A number of methods were proposed in the literature to model combustor dynamics. The simplest method is to read combustor outlet temperature from charts prepared for different heating value of the fuel as a function of combustor inlet temperature and FAR.

In the second approach, combustor is modeled as a steady-state device in which component dynamics are governed by steady state energy conservation (Equation 2.16). This was the approach used by Ballin in Reference 19 for evaluating combustor outlet temperature as a function of enthalpy.

In the third approach, component outlet temperature is calculated as a function of unsteady energy accumulation inside the combustor per unit time:

$$\frac{dE}{dt} = g_2 h_2 + g_b \eta_b LHV - g_3 h_3 \quad [2.17]$$

Total energy term in Equation 2.17 is a summation of internal and kinetic energies of the flow exiting the combustor. In this study, kinetic energy of the flow was assumed to be negligible in comparison with internal energy because of low flow speed assumption. Then, above relation can be written using the definition of internal energy:

$$\frac{d(m_b c_{v3} T_3)}{dt} = g_2 h_2 + g_b \eta_b LHV - g_3 h_3 \quad [2.18]$$

Time variation of mass and specific heat capacity of the flow inside the combustor was assumed to be negligible in comparison with time rate of change of combustor exit temperature. Then, Equation 2.18 becomes:

$$\frac{m_b}{\gamma_3} \frac{dT_3}{dt} = \frac{g_2 h_2 + g_b \eta_b LHV - g_3 h_3}{c_{p3}} \quad [2.19]$$

All parameters in Equation 2.19, with the exception of gas mass contained in the combustor, are either known, or can be calculated. The following combustor time constant was defined to eliminate the unknown parameter:

$$\tau_b = \frac{m_b}{\gamma_3 g_3} \quad [2.20]$$

Then, the final relation for calculating temperature variation at combustor outlet becomes:

$$\frac{dT_3}{dt} = \frac{g_2 h_2 + g_b \eta_b LHV - g_3 h_3}{\tau_b g_3 c_{p3}} \quad [2.21]$$

Pressure at combustor outlet was taken as a fixed percentage of the inlet pressure:

$$P_3 = P_2 \cdot y_{loss} \quad [2.22]$$

The value of pressure drop coefficient for the combustor was estimated using an iterative method to match simulation results given in Reference 19.

### 2.2.3.3 Fuel Pump and Injection Modeling

Dynamics of the fuel pump were simulated using a transfer function [Ref. 20]. A similar approach was already applied in a number of previous studies [Ref. 21-24]. Lag time between metering of the fuel and its injection into the combustion chamber was modeled as a simple 15 millisecond transport delay. Fuel system model used in the simulation is given as follows:

$$g_{b_{metered}} \rightarrow \frac{1}{0.03s + 1} \rightarrow e^{-0.015s} \rightarrow g_b$$

Numerical values for lag time and fuel pump dynamics were taken from Reference 19.

### 2.2.4 Heat Soak Model

Heat soak effect becomes important in regions where large temperature gradients occur. Some fraction of heat released in the combustor is absorbed by turbine blades and other engine components. Heat sink effect can be modeled accurately if metal mass absorbing the heat and heat transfer coefficients of engine components are known. In Reference 19, heat sink effect for T700 engine was modeled using a transfer function:

$$\frac{T_3}{T_{3_{ns}}} = \frac{\tau_1 s + 1}{\tau_2 s + 1} \quad [2.23]$$

Values of transfer function time constants were not fixed and varied as a function of engine parameters through the following relations:

$$\tau_1 = \frac{M c_{p_m}}{h A_m} - \frac{M c_{p_m}}{W_g c_{p_g}} \quad [2.24]$$

$$\tau_2 = \frac{M c_{p_m}}{h A_m} \quad [2.25]$$

Where,

$$\frac{Mc_{p_m}}{hA_m} = \tau_{hs} \frac{\sqrt{T_3}}{g_3^{0.8}} \quad [2.26]$$

$$\frac{Mc_{p_m}}{W_g c_{p_g}} = \frac{f_{hs}(N_{1cor})}{g_3} \quad [2.27]$$

$$\tau_{hs} = 0.2067 \left( \frac{kg^{0.8} \cdot s^{1.8}}{K^{0.5}} \right) \quad [2.28]$$

As suggested by Equation 2.23, combustor outlet temperature calculated using Equation 2.21 was fed directly into the heat sink block.

### 2.2.5 Gas Generator Turbine

Gas generator turbines are designed to operate under choked flow condition for a wide operating range of the engine. Assuming that this is the case for T700 engine, introduced was the definition of mass flow parameter which allowed calculation of component mass flow rate using design point mass flow rate parameter value and current engine operating state defined by combustor outlet pressure and temperature:

$$\left( g_3 \frac{\sqrt{T_3}}{P_3} \right)_{des} = g_3 \frac{\sqrt{T_3}}{P_3} \quad [2.29]$$

At steady state operating conditions, power absorbed by the compressor is proportional to the power extracted by the gas generator turbine from hot gasses expanding over turbine blades with mechanical efficiency of the shaft:

$$P_C = \eta_{mech} \cdot P_{GG} \quad [2.30]$$

Moreover, power extracted by the gas generator turbine is proportional to the enthalpy drop across the component and mass flow rate:

$$P_{GG} = g_{4p} \cdot (h_3 - h_{4p}) \quad [2.31]$$

Pressure ratio of the turbine was calculated using the definition of turbine efficiency:

$$\eta_{GG} = \frac{\frac{c_{p3}}{c_{p4p}} - \frac{T_{4p}}{T_3}}{\frac{c_{p3}}{c_{p4p}} - \left(\frac{P_{4p}}{P_3}\right)^{\frac{\gamma-1}{\gamma}}} \quad [2.32]$$

In above equation, the ratio of specific heats was taken as an average of values at the inlet and outlet.

Enthalpy drop across the gas generator turbine was given in Reference 19 as a function of power turbine inlet to combustor outlet pressure ratio ( $P_4/P_3$ ). To account for cooling effects, in present study enthalpy drop parameter was read from the same map as a function of gas generator turbine outlet to combustor outlet pressure ratio:

$$\Delta h_{GG} = \theta_{GG} \cdot f\left(\frac{P_{4p}}{P_3}\right) \quad [2.33]$$

Then, flow enthalpy at turbine outlet was calculated as:

$$h_{4p} = h_3 - \Delta h_{GG} \quad [2.34]$$

The definition of critical velocity parameter used in Equation 2.33 was given in Reference 19 as follows:

$$\theta_{GG} = k_{GG1}T_3 + k_{GG2} \quad [2.35]$$

Numerical constants employed in Equation 3.5 are given in Appendix B.

### 2.2.6 Mixer

Cooling effects at the gas generator turbine were accounted for in a fictitious volume called the mixer. This component was placed at the outlet of the gas generator turbine and was used for adding cooling air to the mainstream flow, and for evaluating cooling effects in terms of enthalpy and pressure drop of the core gas flow at turbine outlet.

In GE T700 engine, only a fraction of bleed flow extracted from the diffuser is introduced back into the mainstream of the gas generator turbine for cooling purposes [Ref. 19]:

$$g_{cool} = 0.7826 \cdot (g_{2p} \cdot b_3) \quad [2.36]$$

$$g_4 = g_3 + g_{cool} \quad [2.37]$$

Injection of cool air into the mainstream causes a decrease in enthalpy and pressure of the core gas flow. For both of these parameters, the decrease was assumed to be equal to a fixed percentage of inlet values, so that mixer outlet values were calculated as follows:

$$h_4 = 0.9623 \cdot h_{4p} \quad [2.38]$$

$$P_4 = p_{loss} \cdot P_{4p} \quad [2.39]$$

Numerical value for enthalpy decrease due to mixing at the gas generator turbine was taken from Ballin [Ref. 19]. Because in his model Ballin did not take pressure drop due to mixing into account, in present study pressure drop coefficient for the gas generator turbine was estimated. This will be discussed in more detail in Chapter 3.

### 2.2.7 Power Turbine

Power turbine was modeled using the performance map given in Reference 19. The map was used to calculate corrected mass flow rate going through the turbine as a function of ambient to power turbine inlet pressure ratio:

$$g_{4cor} = f\left(\frac{P_{amb}}{P_4}\right) \quad [2.40]$$

Corrected mass flow was uncorrected with respect to operating state of the turbine defined in terms of pressure and temperature at the inlet:

$$g_4 = g_{4cor} \frac{P_4}{\sqrt{\theta_{PT}}} \cdot \left(\frac{1}{6894.75729} \cdot \frac{psi}{Pa}\right) \quad [2.41]$$

Power turbine critical velocity parameter was defined in Reference 19 as follows:

$$\theta_{PT} = k_{PT1} T_4 + k_{PT2} \quad [2.42]$$

Enthalpy drop across the turbine was evaluated as a function of component pressure ratio using turbine map given in Reference 19:

$$\Delta h_{PT} = \theta_{PT} \cdot f\left(\frac{P_5}{P_4}\right) \quad [2.43]$$

When multiplied by the turbine mass flow, enthalpy drop defined by Equation 2.43 yields the power output of the engine:

$$P_{PT} = g_4 \cdot \Delta h_{PT} \quad [2.44]$$

### 2.2.8 Nozzle

In Reference 19, nozzle discharge pressure was given as a function of engine speed:

$$P_5 = P_{amb} \cdot f(N_{1cor}) \quad [2.45]$$

### 2.2.9 Unsteady Mass Balance

During transient operating conditions components of the engine will operate with different mass flow rates. These differences are accounted for by using inter-component volumes in which mass imbalance between neighboring components of the engine is reflected on the inter-component pressure.

For real time applications, relation for inter-component volumes must be simple and efficient from computational point of view, but sufficiently accurate to faithfully model engine dynamics. This relation is obtained by differentiating ideal gas law in time:

$$\frac{dP_{out}}{dt} = \frac{RT_{out}}{V} \cdot \frac{dm}{dt} + \frac{Rm}{V} \cdot \frac{dT_{out}}{dt} \quad [2.46]$$

By applying ideal gas relation one more time and defining change of mass per unit time in terms of mass flow imbalance across the plenum, Equation 2.46 can be written as follows:

$$\frac{dP_{out}}{dt} = \frac{RT_{out}}{V} \cdot (g_{in} - g_{out}) + \frac{P_{out}}{T_{out}} \cdot \frac{dT_{out}}{dt} \quad [2.47]$$

Rewriting above relation in a more convenient form:

$$\frac{dP_{out}}{dt} = K_V T_{out} \cdot (g_{in} - g_{out}) + \frac{P_{out}}{T_{out}} \cdot \frac{dT_{out}}{dt} \quad [2.48]$$

Equation 2.48 links mass flow accumulation in the plenum and time derivative of outlet temperature to the change of pressure at plenum outlet per unit time. The value of plenum volume parameter dictates the rate of pressure change and therefore influences the entire dynamics of the engine. Plenum volume can either be determined empirically from the known engine configuration, or it can be estimated such that simulation results match some reference data in terms of transient response of the engine. In present study, the values for plenum volume parameters were taken from Ballin [Ref. 19]. Two plenum volumes were used in developed simulation model: one between the compressor and combustor, and another between the gas generator and power turbines.

### 2.2.9.1 Compressor – Combustor Plenum

Mass flow rate entering the first plenum, as given by Equation 2.13, is defined by compressor mass flow minus extracted bleed flows. Mass flow rate leaving the plenum is evaluated by subtracting fuel mass flow from the gas generator turbine mass flow rate calculated by Equation 2.29. Then, mass flows for the first plenum are given as:

$$g_{in} = g_2|_{Eq.2.13} \quad [2.49]$$

$$g_{out} = g_3|_{Eq.2.29} - g_b \quad [2.50]$$

### 2.2.9.2 Gas Generator – Power Turbine Plenum

Inlet mass flow for the second plenum is given by Equation 2.37 and is defined by the summation of gas generator core mass flow and cooling air. Plenum outlet mass flow equals power turbine mass flow calculated with Equation 2.41. Then, inlet and outlet mass flows for the second plenum are given as:

$$g_{in} = g_4|_{Eq.2.37} \quad [2.51]$$

$$g_{out} = g_4|_{Eq.2.41} \quad [2.52]$$

### 2.2.10 Shaft Dynamics

Dynamics of the shaft are governed by a first order differential equation:

$$\frac{dw}{dt} = \frac{1}{J_w} (P_t - P_{load} - P_{loss}) \quad [2.53]$$

The load term represents compressor power for the gas generator shaft, and load of the drive train for the power shaft. Loss term is used to account for mechanical and frictional losses as well as power drawn from the engine by pumps, generators etc.

Inertia value for the gas generator section was taken from Ballin [Ref. 19], while inertia term for the power shaft and drive train was taken from Reference 25. Inertia values used in the simulation are listed in Table 2.1.

**Table 2.1: Component inertia values**

Parameter	Value	Unit
$J_{GG}$	0.060334	$N \cdot m \cdot s^2$
$J_{PT}$	1.3694	$N \cdot m \cdot s^2$

### 2.2.11 Evaluation of Specific Heats

Calculation of specific heat capacities can be based on one of the following three methods. In the first method, a single value for specific heat capacity is assumed and used at all engine stations by disregarding its variation with temperature. Although the method is simple and fast, it will produce wrongful calculation of engine operating state. In the second approach, specific heat capacities are evaluated as a function of temperature and fuel-to-air ratio by using appropriate relations which are available in the form of curve fits [Ref. 26]. In developed model, in order to obtain a better approximation of the real engine, empirical enthalpy-temperature relations given in Reference 19 were used. These relations are given in Table 2.2 with numerical constants given in Appendix B.

**Table 2.2: Temperature-enthalpy relations [Ref. 19]**

Engine inlet	:	$h_1 = k_{h1} \cdot T_1$
Compressor outlet	:	$h_2 = k_{h21} \cdot T_2 + k_{h22}$
Burner outlet	:	$h_3 = k_{h31} \cdot T_3 + k_{h32}$
Gas generator turbine outlet	:	$T_4 = k_{T41} h_{4p} + k_{T41}$

### 2.2.12 Integration Method

A total of five differential equations were used in the model to obtain an accurate representation of engine dynamics: one for the temperature at combustor outlet (Equation 2.21), two for plenum dynamics (Equation 2.48), and another two for evaluation of shaft speeds (Equation 2.53). These relations were integrated in time by using the Euler method with fixed time step:

$$x_{i+1} = x_i + \frac{dx_i}{dt} \cdot \Delta t \quad [2.54]$$

## CHAPTER 3

### MODEL AND SIMULATION PARAMETERS & STABILITY

#### 3.1 Initialization

In an earlier study performed by Uzol [Ref. 18] on GE T700 engine, design point engine parameters were calculated by estimating compressor pressure ratio and combustor outlet temperature. In present study, evaluation of the design point was done using component matching. Because compressor and turbine performance maps were available, it was possible to apply these in such a way that would yield a unique operating point of the engine at which mass flows of the compressor and power turbine, and powers of the compressor and gas generator turbine matched. The relations which were considered for component matching are given as follows:

$$g_2 + g_b + g_{cool} = g_4 \quad [3.1]$$

$$g_{2p}(h_2 - h_1) - 0.29 \cdot g_{2p}h_2(b_1 + b_2) = g_4(h_3 - h_{4p}) \quad [3.2]$$

Left-hand-side of Equation 3.1 and Equation 3.2 is defined in terms of mass flow calculated by using the performance map of the compressor. Right-hand-side is evaluated by considering power turbine mass flow read from the turbine map as a function of pressure ratio of the component. In attempt to satisfy Equations 3.1 and 3.2, iterations were done for the following three parameters: compressor and gas generator turbine pressure ratios, and combustor outlet temperature. The first parameter was bounded by two values, i.e. a maximum and a minimum, corresponding to the 100% RPM line of the compressor. Similarly, gas generator turbine pressure ratio was limited by the values which defined operating range of the turbine on its performance map. As for the combustor outlet temperature, it was calculated by iterating between a maximum and a minimum value

which was estimated by considering typical values for the gas generator turbine inlet temperature. In the process of iterating for one of these variables, a control parameter was used to flag whether component matching had occurred or not. The inner iteration loop was used to evaluate gas generator turbine pressure ratio: a value for the pressure ratio was assumed, and corresponding enthalpy drop of the turbine was evaluated. The resulting enthalpy at the gas generator turbine outlet was used first to evaluate the temperature, and then the pressure ratio of the turbine using the definition of turbine efficiency given by Equation 2.32. At this point, the value of calculated pressure ratio was compared against its assumed value. If the two did not match, a new value for the pressure ratio was assumed, and iterations continued in this routine until either a match had occurred, or the range of possible values for the gas generator turbine pressure ratio was scanned without obtaining a match. In either case, the solution was progressed to the middle loop which was used to evaluate combustor outlet temperature. The control parameter set for the intermediate loop was the ratio of left-hand-side of Equation 3.1 to the right-hand-side of the same equation. A match was assumed to have occurred when the ratio approached the value of unity with a maximum error of  $10^{-12}$ . Again, irrespective of whether a match had occurred or not, calculations were advanced to the outer loop. In this loop, pressure ratio of the compressor was evaluated by considering power balance between the compressor and gas generator turbine. Pressure ratio was iterated for values which defined the 100% speed line on the compressor map by taking as control parameter the ratio of powers and a tolerance band of  $10^{-12}$ . For each estimated value of compressor pressure ratio, the calculations were performed until the point at which combustor outlet temperature was required. After one was assumed, calculations were continued until required was a value for the gas generator turbine pressure ratio. Once assumed, remaining engine parameters were evaluated, and iterations marched from the inner loop towards the outer loop to obtain a new estimate for compressor pressure ratio. This process was repeated until calculated was a unique combination of the three unknown parameters which yielded mass flow and power match between engine components. Flowchart for the procedure which was used in present study to evaluate design point of the engine using available maps for the compressor and turbines is shown in Figure 3.1.

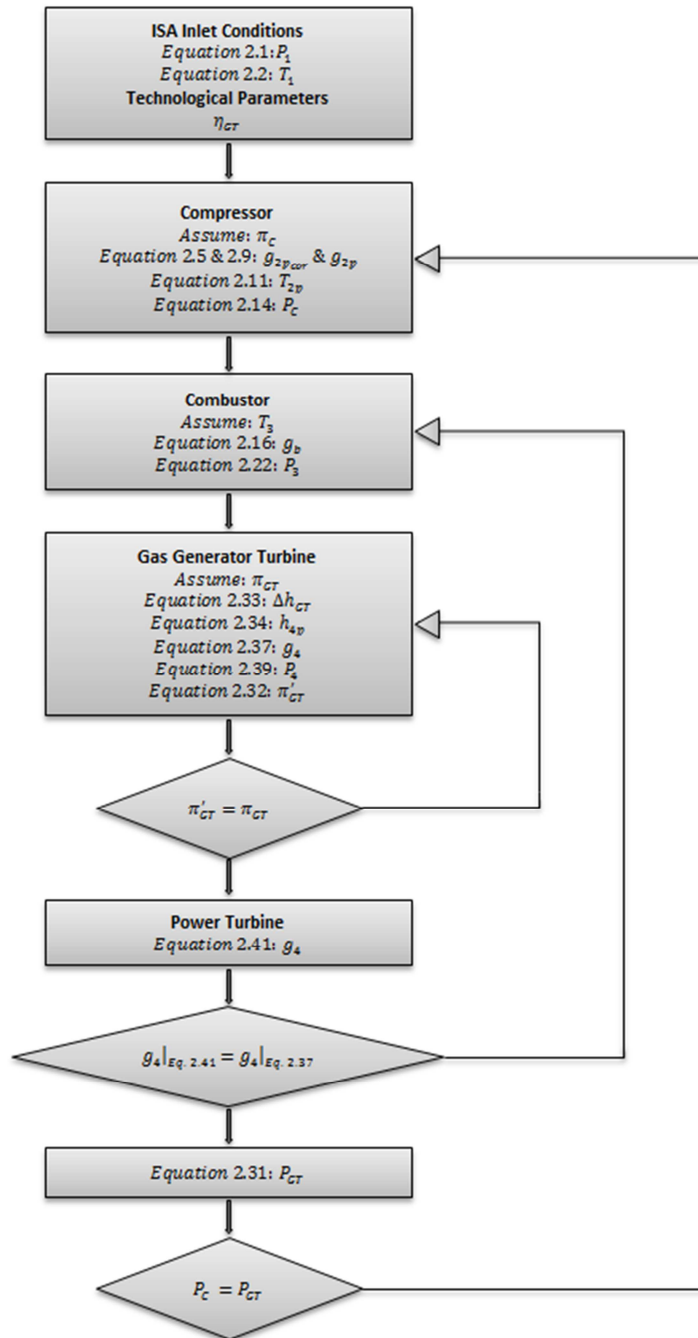


Figure 3.1: Flowchart for calculation of design operating point of the engine

### 3.2 Selection of Model Parameters

Developed aerothermal model included cooling effects at the gas generator turbine and accounted for pressure drop across the combustor. The two effects were modeled by assuming that pressure of the flow decreased by a certain percentage which remained constant in the entire operating range of the engine. These percentages were estimated since their numerical values were unknown. Moreover, also assumed was the value for efficiency of the gas generator turbine which was required for calculating pressure drop across the component during evaluation of the design operating point. The three unknown parameters were estimated by comparing design point engine parameters against simulation results given by Ballin for his model in Reference 19. In doing so, each parameter was varied within a certain range defined by typical maximum and minimum values which were found in Reference 1. Thus, algorithm for model initialization was run for all possible combinations of the three parameters until steady state design point parameters were in close match with Ballin's data [Ref. 19]. The combination of unknown parameters which yielded the best match with Ballin's simulation results is given in Table 3.1. For consistency with Ballin's model, mechanical efficiency of the shaft was taken as unity.

**Table 3.1: Assumed T700 engine performance parameters**

$\eta_{mech}$	:	1.0
$\gamma_{loss}$	:	0.97
$p_{loss}$	:	0.97
$\eta_{GT}$	:	0.804

Because in the simulation model evaluation of gas generator turbine outlet pressure was done by using a plenum volume, the use of turbine efficiency given in Table 3.1 was limited only to the calculation of component pressure ratio during the model initialization stage.

### 3.3 Design Point Performance Parameters of the GE T700

Model parameters given in Table 3.1 were used to obtain the final steady state design point parameters of the GE T700 engine. These parameters are listed in Table 3.2.

**Table 3.2: Design point performance parameters**

Parameter	Notation	Value	Unit
Compressor pressure ratio	$\pi_c$	17.53	—
Compressor core mass flow	$g_{2p}$	4.5736	$kg/s$
Compressor outlet temperature	$T_2$	733.5579	$K$
Gas generator inlet temperature	$T_3$	1525.4583	$K$
Gas generator outlet temperature	$T_4$	1093.2524	$K$
Gas generator pressure ratio	$\pi_{GG}$	0.21345	—
Power turbine outlet temperature	$T_5$	844.7305	$K$
Power turbine pressure ratio	$\pi_{PT}$	0.30250	—
Fuel mass flow rate	$g_b$	100.4259	$g/s$
Engine power output	$P_{PT}$	1768.4161	$hp$

### 3.4 Selection of Simulation Parameters

Accuracy of an aerothermal model in predicting transient dynamics of an aero-engine directly depends on how comprehensive is the thermodynamic description of engine components introduced into the model. A highly accurate engine model can be obtained if used in the model are performance maps of major engine components and empirical relations which govern change of flow properties across components of the engine. Other factors which determine model accuracy include volumes of plenums used in the simulation model to account for mass imbalance between engine components, combustor time constant which governs dynamics of combustor outlet temperature, and simulation time

step. Because each simulation parameter governs a certain dynamics, it will directly influence the transient performance of the model. For this reason, selection of numerical values for these parameters must be done carefully as incorrect values will result in wrongful engine dynamics. If known, configuration of the engine can be considered to choose proper values for plenum volumes. Combustor time constant must be determined empirically by considering the mass of gas which resides in the combustion chamber and mass flow rate across the component. Alternatively, if some reference simulation or experimental data is available, combustor time constant can be estimated by trial-and-error until good match in terms of engine transients is obtained. As for selection of simulation time step, the following two conditions must be considered: 1) the model must produce accurate engine dynamics for a given time step and 2) selected simulation time step must guarantee numerical stability of the simulation model at all times. The first condition is required to accurately capture fast changes which frequently occur in transient dynamics of combustor outlet temperature and inter-component pressures. Second condition is self-evident, and should be considered due to the simple fact that use of the simplest integration technique, i.e. Euler method, will result in large local truncation errors. Usually, in order to satisfy both conditions, a small simulation time step will be required.

#### **3.4.1 Selection of Simulation Time Step**

In present simulation model, time steps larger than  $10^{-4}$  seconds were not permissible due to cyclic oscillations which occurred in the pressure evaluated at the second plenum. Figure 3.2 illustrates these oscillations for the case of step increase in fuel flow and time step of  $5 \cdot 10^{-4}$  seconds. In the second plot of the figure shown are the first 0.1 seconds of engine response to step input in fuel flow during which oscillations were pronounced the most. These oscillations occurred because of the use of a larger time step which was insufficient to capture fast variations in pressure and due to truncation errors which were introduced by the use of Euler's method of integration. While latter effect is inherent to the integration method, former can be explained by considering volume dynamics: when dynamics of a large and a small volume are compared in terms of transient response to the same disturbance, it would be observed for a smaller volume to respond much quicker than would the larger volume. Hence, to resolve fast volume dynamics of the smaller volume, a smaller simulation time step is required. So, in some sense, plenum volumes dictate the maximum allowable simulation time step which can be used in a given simulation without

causing cyclic oscillations in the evaluation of some flow parameters. Given the limitation imposed on simulation time step by numerical instabilities, time step of  $10^{-4}$  seconds was used in all of the simulations that will follow.

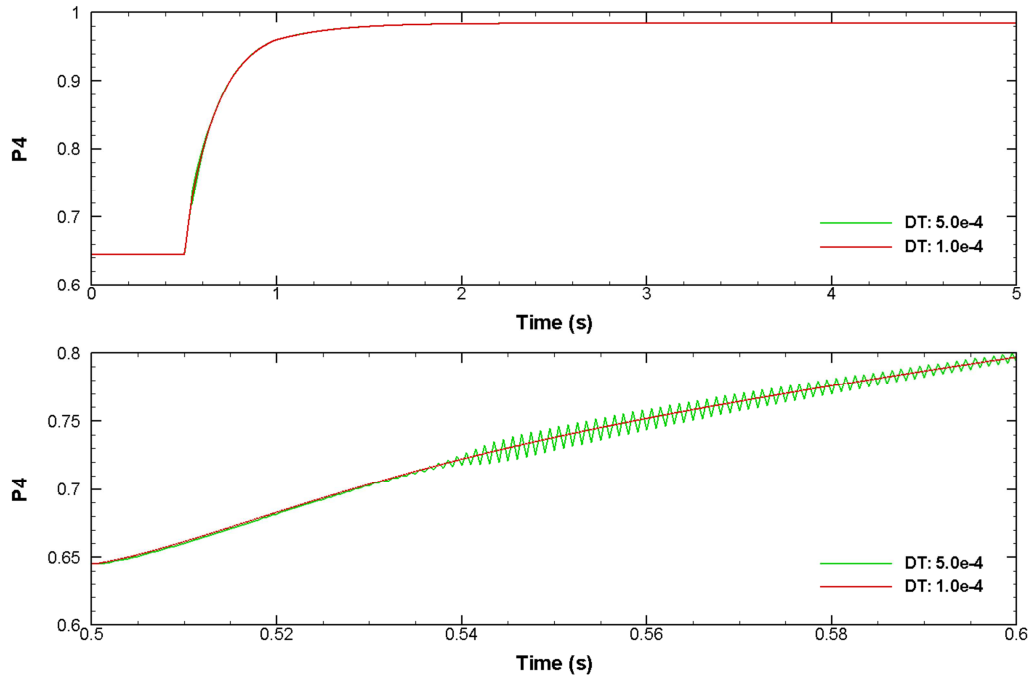


**Figure 3.2: Response of power turbine inlet pressure to fuel step increase from 400 to 775 lbm/h (50.4 to 97.65 g/s) at different simulation time steps**

### 3.4.2 Selection of Combustor Time Constant

Combustor time constant, per Equation 2.20, is defined as the ratio of gas mass contained within the combustor volume to the mass flow rate across the component. Therefore, combustor time constant can be regarded as a parameter which implicitly defines combustor volume and hence governs the dynamics of combustor outlet temperature. The influence of combustor time constant on engine dynamics was investigated by running a simulation for step increase in fuel mass flow from 400 to 775 lbm/h for four different values of combustor time constant:  $5 \cdot 10^{-2}$ ,  $10^{-2}$ ,  $5 \cdot 10^{-3}$  and  $10^{-3}$  seconds. Simulation results are given in Figure 3.3 in terms of time variation of combustor outlet temperature, gas generator speed, and compressor outlet static pressure.

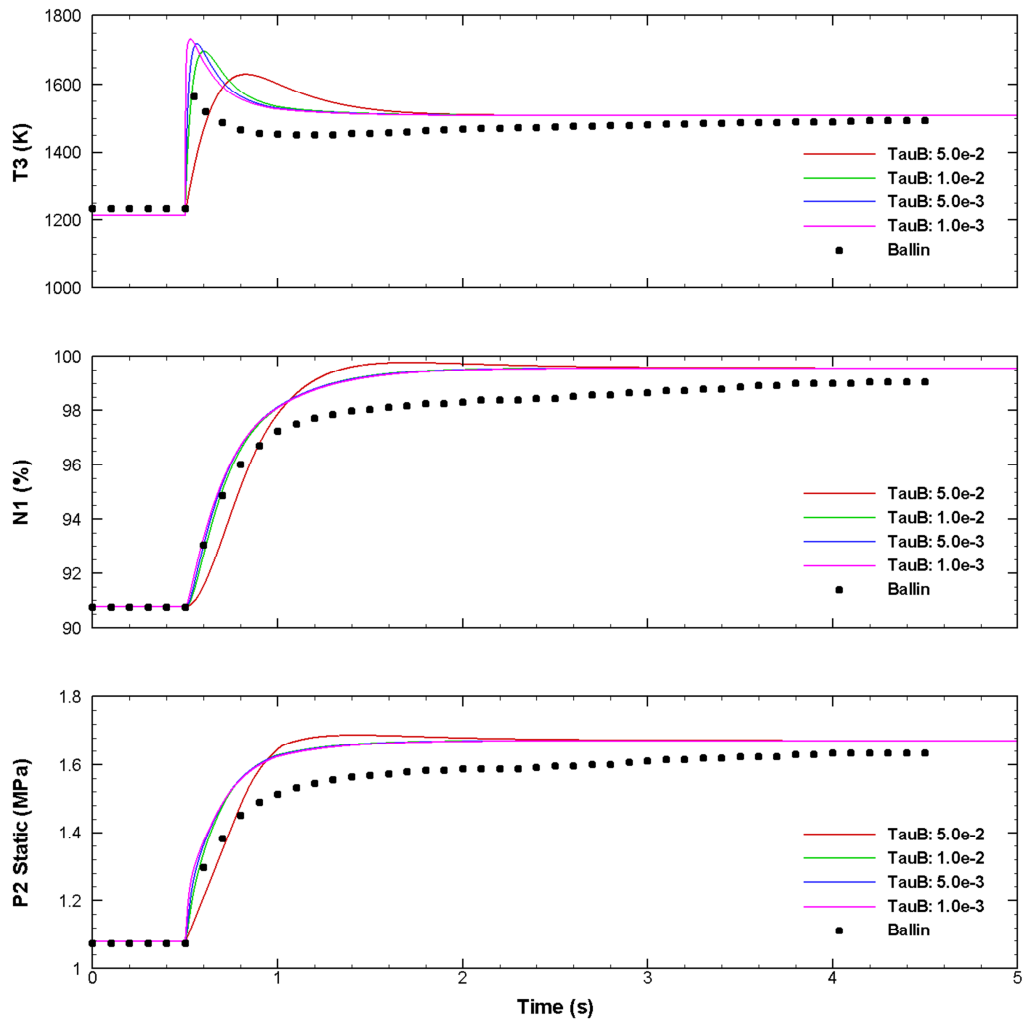


**Figure 3.3: Engine response to step increase in fuel flow from 400 to 775 lbm/h (50.4 to 97.65 g/s) as a function of  $\tau_b$**

From the first plot it is seen that a larger combustor time constant produces slower combustor dynamics: per Equation 2.21, increase in combustor time constant results in a smaller temperature gradient, and hence in a slower combustor response. On the contrary, the smallest burner time constant is seen to yield the fastest response: per Equation 2.20, a smaller combustor time constant implies, for the same mass flow rate, a lower mass of gas which is contained within the combustor, and hence a smaller combustor volume. Because, as was mentioned previously, dynamics of a smaller volume are faster than those of a larger volume, variation of temperature dynamics with combustor time constant, as it is shown in the first plot of Figure 3.3, is in agreement with the expectation.

As shown in the temperature plot of Figure 3.3, a smaller combustor time constant results in a larger temperature peak which, per Equation 2.21, is produced by the large temperature derivative. Additionally, because engine response is much slower in comparison with combustor dynamics, compressor lags in its response to increase the mass flow, and in the time duration of this lag combustor operates at a high FAR value. This, in combination with a small combustor time constant, results in a large temperature gradient and consequently a higher temperature peak.

The effect of combustor time constant on engine dynamics is given in terms of transient response of the gas generator turbine speed and compressor outlet static pressure. These are shown in the second and third plots of Figure 3.3, respectively. Time variation of the two parameters is seen to follow a trend similar to that of the combustor outlet temperature: dynamics of the engine are slower for a large combustor time constant and, conversely, engine dynamics are faster if a small combustor time constant is used.

Variations of the three engine parameters were compared against simulation results obtained by Ballin (to be referred to as “reference”) with his aerothermal model. Dynamics of combustor outlet temperature is seen to deviate from the reference in both the peak value and the time before steady state is reached. This discrepancy is partly related to the difference in the modeling of the combustor: while in present study gas generator inlet temperature was calculated using combustor dynamics defined by Equation 2.21, Ballin adopted a steady state approach in which evaluation of combustor outlet temperature was based on Equation 2.16 without giving any consideration to component dynamics. By considering combustor as a steady state device, it becomes possible to rid component model of volume dynamics which, in the present study, was defined in terms of a combustor time constant. Moreover, it is believed that due to limited computational power which was available at the time of publishing of Ballin’s results, simulation time step used in that work varied significantly from one used in present study: modern computing technology allows for the use of much smaller simulation time steps. Due to the differences in combustor modeling and simulation time step, engine dynamics obtained with present model are seen to mismatch with Ballin’s results. However, if examined more closely, it can be observed that in terms of temperature gradient combustor time constant of  $10^{-2}$  seconds produces the closest match to reference results. This value, therefore, was used in all the simulations that will follow next.

### 3.5 Combustor Modeling

As was stated previously, in the present study combustor dynamics was modeled using unsteady energy balance across the component as given by Equation 2.21. In this relation, combustor outlet mass flow can be defined in two ways: as a summation of diffuser outlet and fuel flows (Method 1) or as mass flow calculated using Equation 2.29 for a choked turbine (Method 2). The differences between two approaches are illustrated in Figure 3.4 in terms of time variation of combustor outlet temperature and power turbine inlet pressure as a response to step increase in fuel flow. As clearly seen from the figure, the peak produced for combustor outlet temperature with Method 2 is higher than for the case of Method 1. Moreover, Method 2 is seen to produce slightly faster dynamics. It may be reasonable to define combustor dynamics in terms gas generator mass flow parameter since gas generator turbine is assumed to operate under choked flow condition. This definition, however, disregards mass flows at combustor inlet, and combustor dynamics become independent from upstream conditions. It, therefore, seemed physically more correct to model combustor dynamics using inlet mass flows, i.e. Method 1.

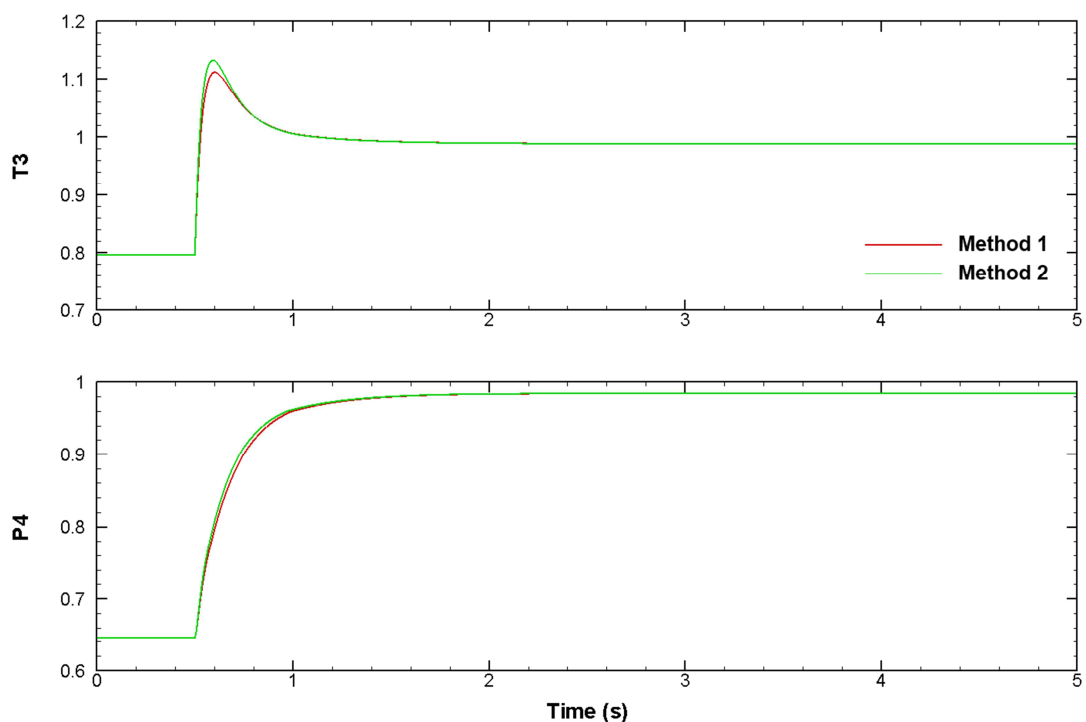


**Figure 3.4: Influence of different combustor modeling approaches on engine response to step increase in fuel flow from 400 to 775 lbm/h (50.4 to 97.65 g/s)**

### 3.6 Effect of Pressure Derivatives on Model Stability

Evaluation of pressure derivatives at the outlets of compressor and gas generator turbine was done using the plenum relation given by Equation 2.48 which accounted for mass imbalance across the plenum and temperature derivative at the outlet. Inclusion of the latter term was found to decrease numerical stability of the simulation model in the calculation of pressure at the second plenum. This decrease manifested itself in form of cyclic oscillations which are shown in Figure 3.5. One way to eliminate these oscillations was to reduce the simulation time step. However, because simulation time step was already set to a small value of  $10^{-4}$  seconds, any further reduction in time step would have resulted in considerable increase of the overall simulation time. Therefore, considering the fact that contribution of temperature derivative to pressure dynamics is small (second plot of Figure 3.5), temperature derivative part of Equation 2.48 was removed from the evaluation of pressure at the second plenum.

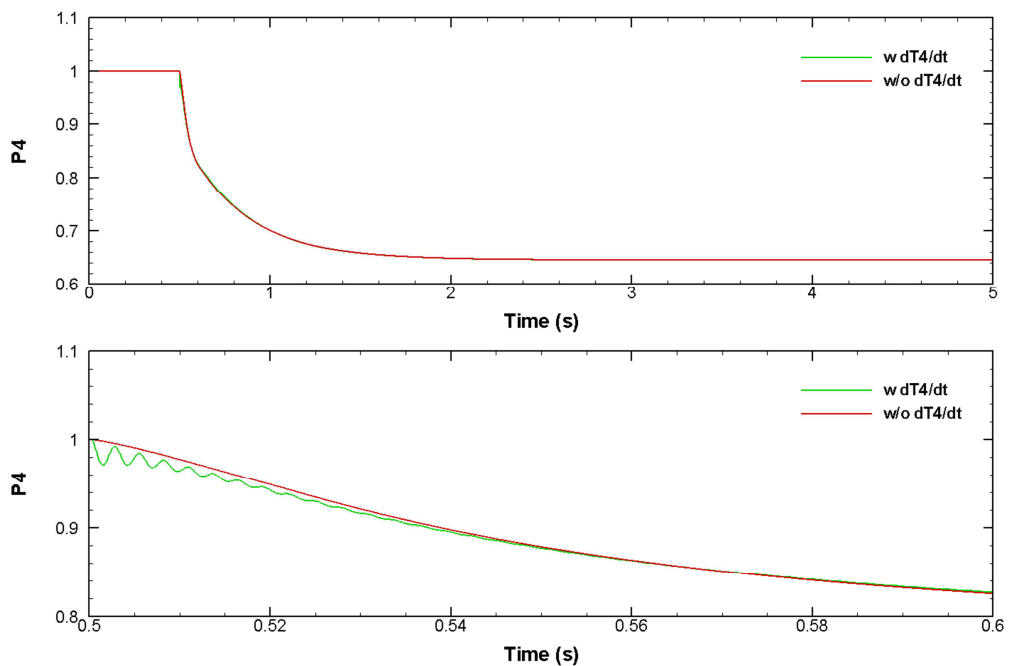


**Figure 3.5: Effect of plenum outlet temperature derivative on system stability for the case of step decrease in fuel flow from 775 to 400 lbm/h (97.65 to 50.4 g/s)**

### **3.7 Implementation of the Model in SIMULINK®**

Simulation model for GE T700 engine was built in SIMULINK® environment which provides an advanced graphical user interface. Each engine component was modeled as an individual block which was connected to other blocks in a stream-wise manner. Engine model blocks are shown in Appendix C.

## CHAPTER 4

### MODEL VALIDATION

Validation of the model was done by comparing steady state performance and transient dynamics of developed model with simulation results given in Reference 19. Steady state performance of the model was obtained by varying fuel mass flow from 100% to 15% of the design value using 5% step decreases with time step between two fuel flow regimes kept sufficiently large to allow the model to reach a steady state condition. Steady state model results obtained for standard day sea level conditions for the gas generator speed, static pressure at compressor outlet and output shaft power were compared to three different simulation results reported in Reference 19. The first set of reference results was given for the T700 aerothermal model developed by Ballin. Second and third sets were obtained using engine models developed by the General Electric: Status-81 model used for accurate modeling of transient dynamics via full thermodynamic analysis of the engine, and Unbalanced Torque model used to simulate engine dynamics for control design purposes.

Dynamic performance of the model was simulated for two fuel flow regimes: step increase from 400 to 775 lbm/h and step decrease from 400 to 125 lbm/h. Simulation results are given in terms of time evolution of compressor outlet static pressure, gas generator speed, combustor outlet temperature, power turbine inlet temperature and output torque. These were compared against Ballin and GE Status-81 model results.

#### 4.1 Steady State Validation

Figure 4.1 is the plot of engine output power as a function of fuel mass flow. Model results are in perfect match with Ballin in the entire operating range as shown in the figure. Results are also observed to match quite well with GE Status-81 model predictions.

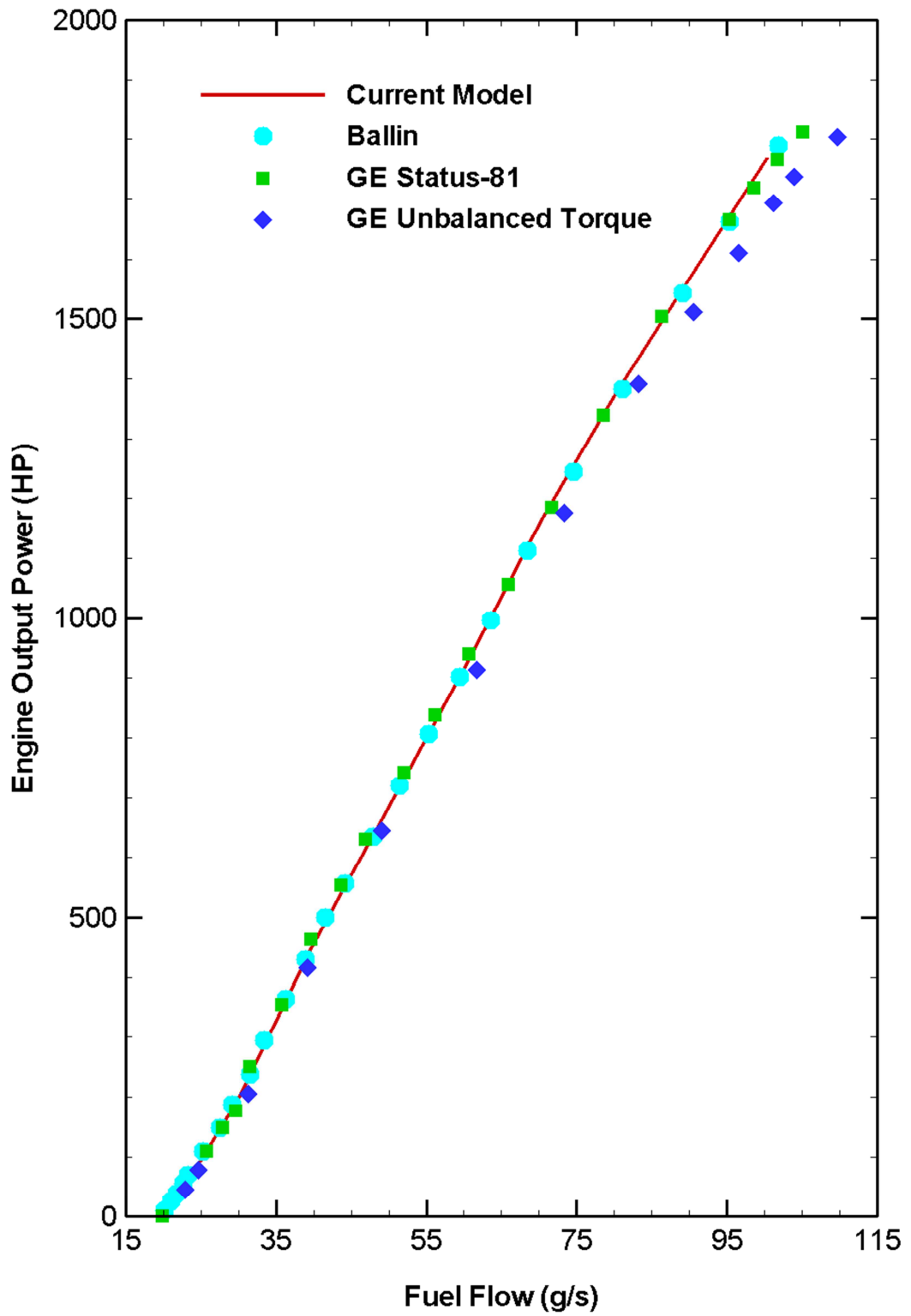


Figure 4.1: Engine output power vs. fuel flow

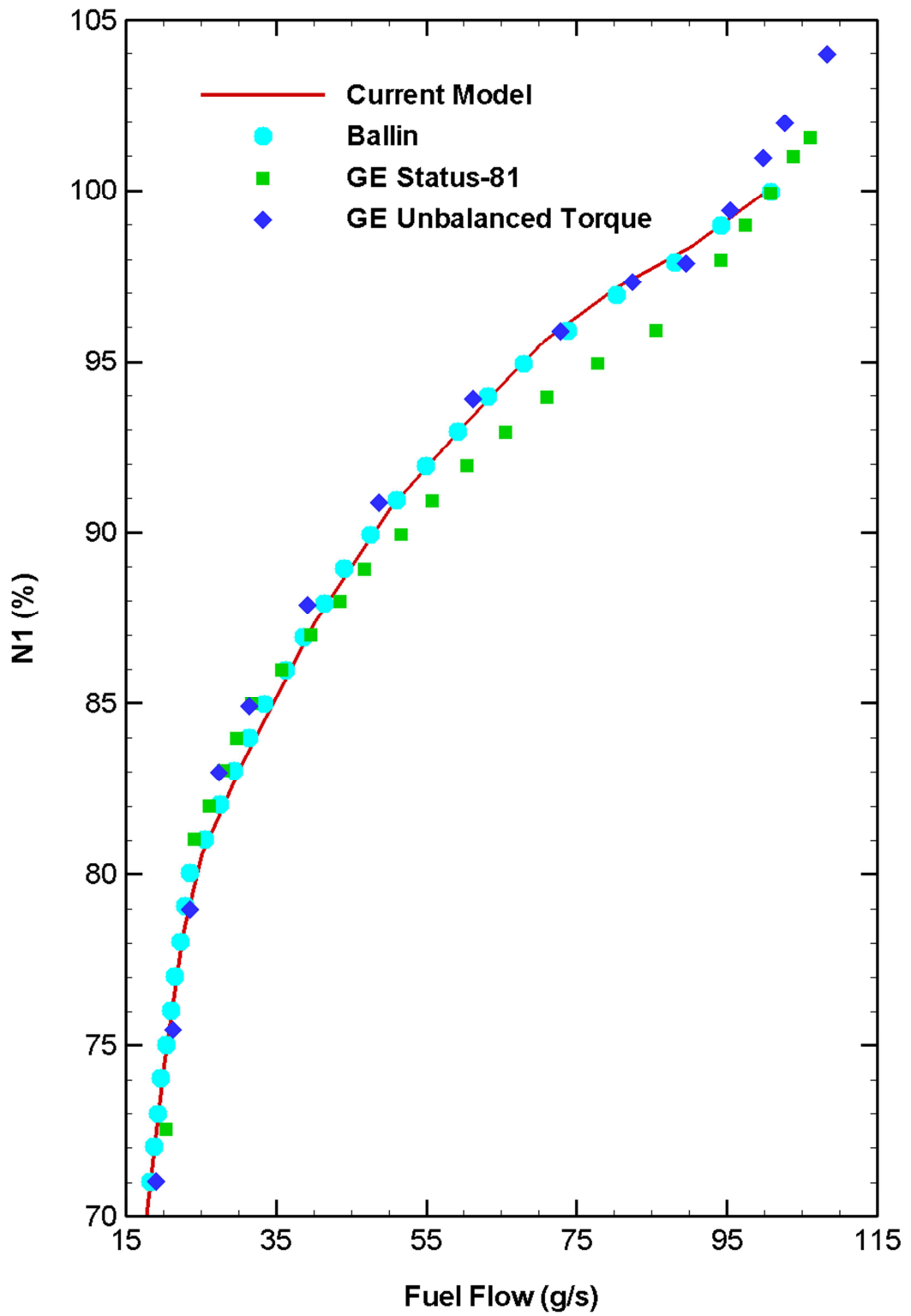


Figure 4.2: Gas generator speed vs. fuel flow

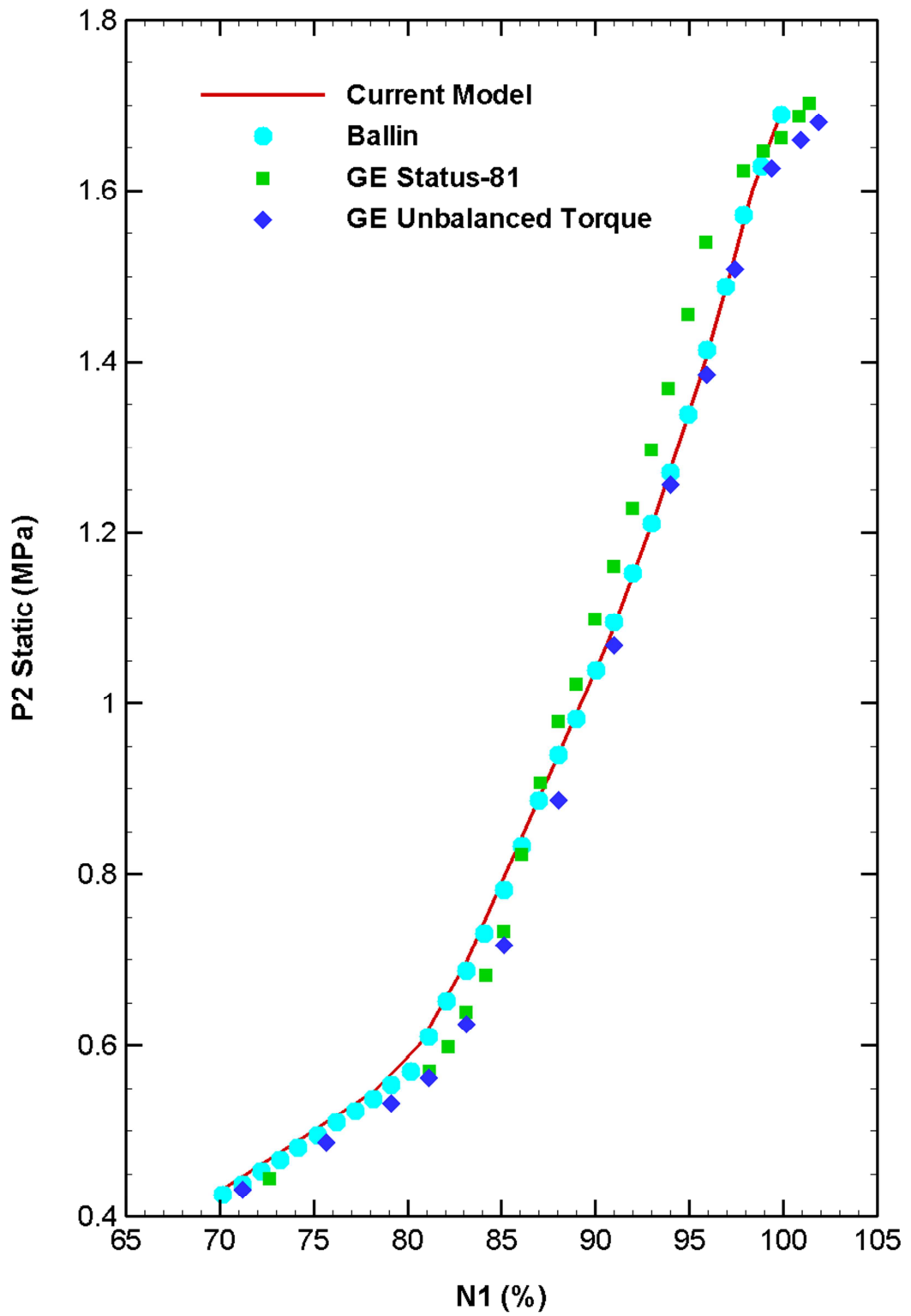


Figure 4.3: Compressor exit static pressure vs. gas generator speed

Figure 4.2 shows the variation of gas generator speed as a function of fuel flow. Simulation results match quite well with those obtained by Ballin. Some discrepancies from Status-81 model are observed in the range from 100 to 40 g/s in which for a given engine speed present model underpredicts the amount of fuel mass flow.

Figure 4.3 gives the variation of compressor outlet static pressure as a function of gas generator speed. Again, model results are in very good match with Ballin. Discrepancies from GE models are observed in the most part of the operating range.

The small discrepancies which exist between steady state simulation results obtained with present model and those obtained with Ballin's aerothermal model are due to differences in the modeling of engine components. Unlike in Ballin's model, in the current study pressure loss coefficients were employed to account for pressure drop across the combustor and due to the mixing of cooling air streams with hot core gas in the gas generator turbine. These coefficients directly influence the amount of enthalpy drop across the gas generator and power turbines since it is defined as a function of pressure drop across these components. Moreover, pressure drop coefficients were estimated by calculating design point of the engine with guessed values for these coefficients and comparing steady state engine parameters against previously published simulation results [Ref. 19] until a good match with these was obtained. Another important difference between the two models is the method of evaluation of gas generator turbine mass flow rate: while in present model evaluation was performed by considering a generic expression for a choked turbine (Equation 2.29), Ballin used a different approach by considering the critical velocity parameter for the gas generator turbine (Equation 2.35), and employing empirically determined constant for the mass flow parameter at design point. Although the two approaches are methodologically similar, they differ in the definition and evaluation of the mass flow parameter for a choked turbine and hence yield slightly different results for the value of gas generator turbine mass flow rate.

## **4.2 Transient Validation**

Model response to step increase in fuel flow from 400 to 775 lbm/h is given in Figure 4.4 in terms of compressor outlet static pressure, compressor speed, gas generator and power turbine inlet temperatures as well as the output torque.

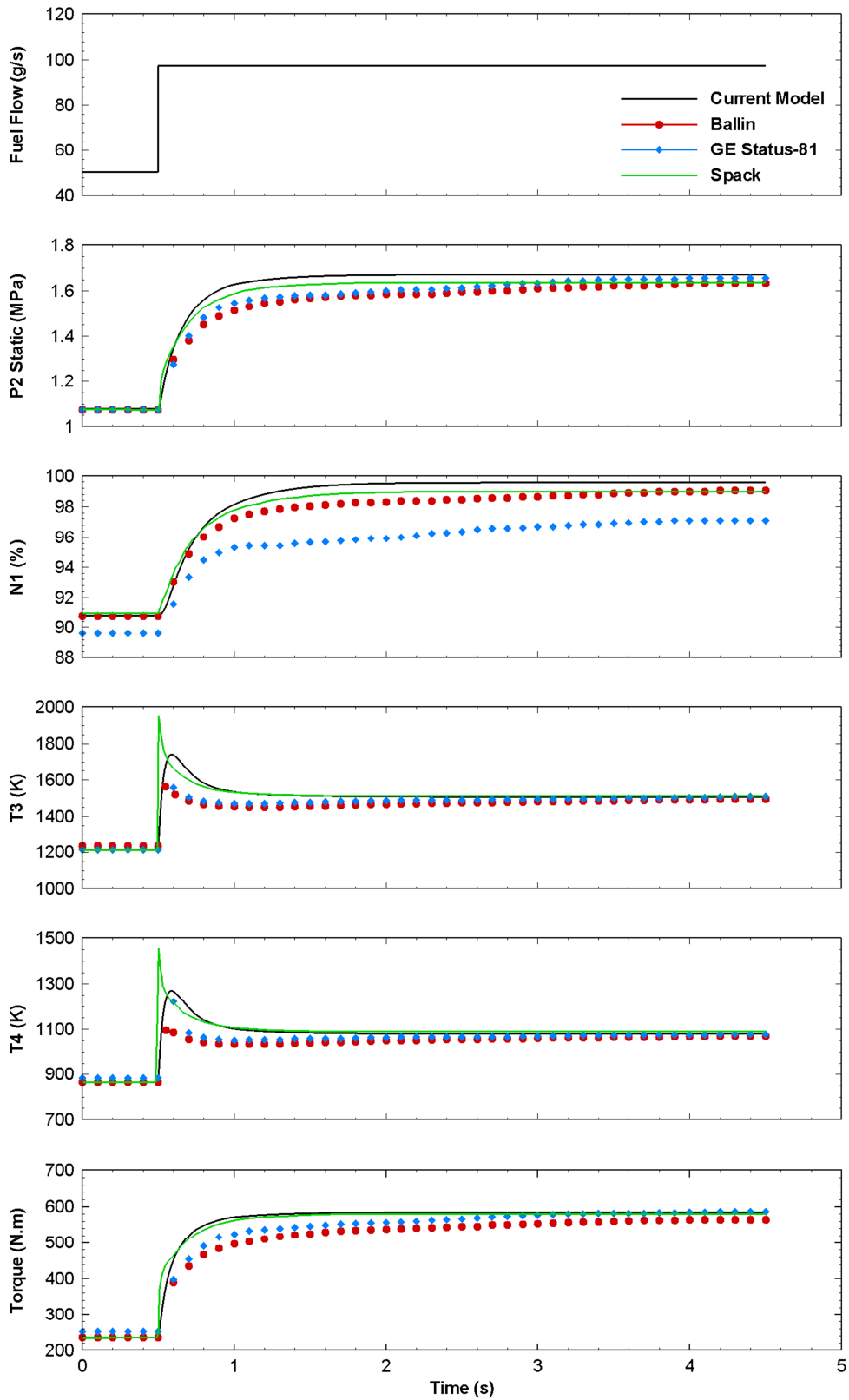


Figure 4.4: Engine response to step increase in fuel flow from 400 to 775 lbm/h (50.4 to 97.65 g/s)

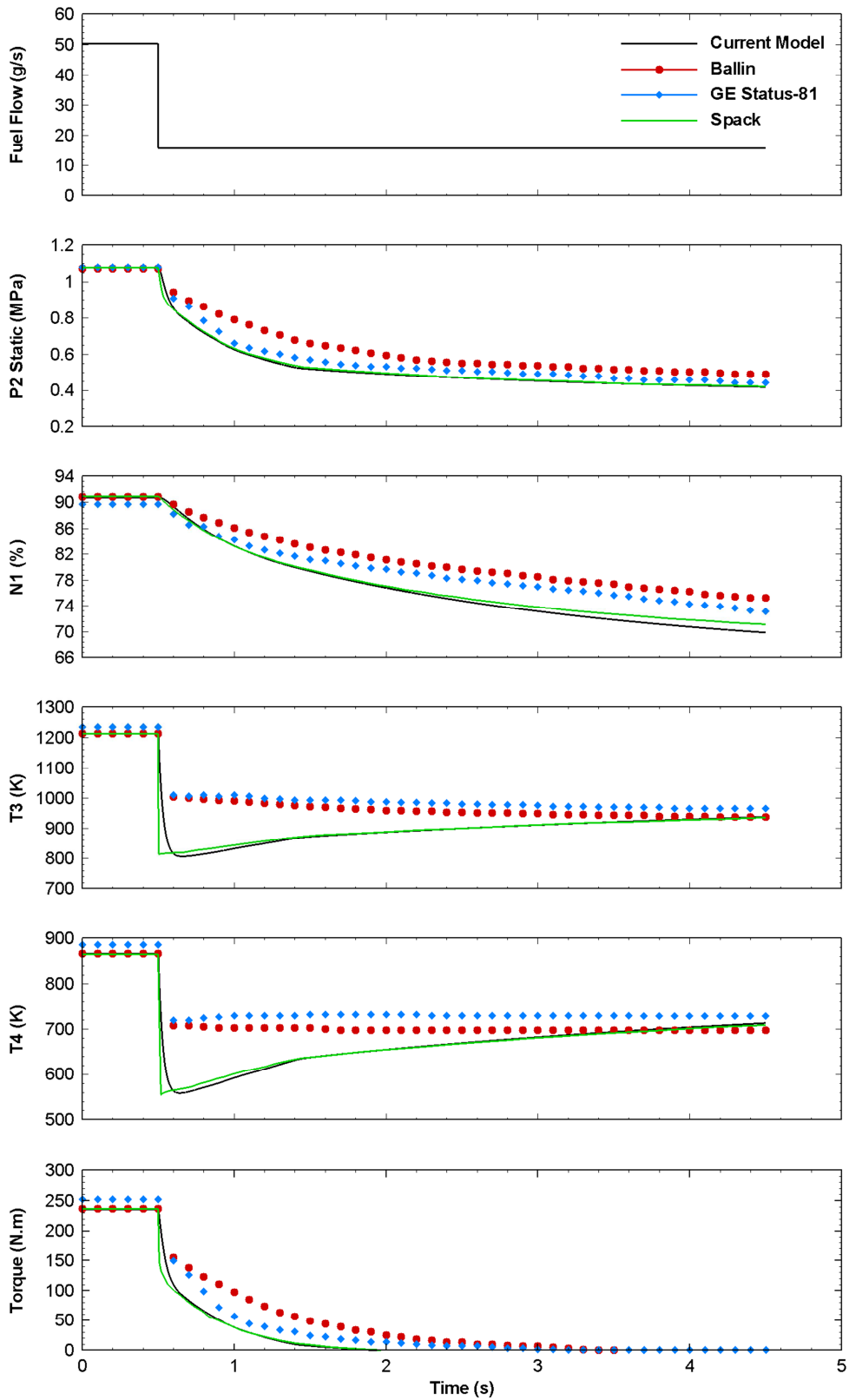


Figure 4.5: Engine response to step increase in fuel flow from 400 to 125 lbm/h (50.4 to 15.75 g/s)

Transient dynamics of the current model match simulation results obtained by Ballin and with GE Status-81 model quite well, with the only exception being the somewhat faster convergence to steady state which is seen to be the case for the present model. Temperature gradients produced as a response to step increase in fuel flow are in good agreement with Ballin. However, gas generator and power turbine inlet temperature peaks are observed to be over-predicted.

Figure 4.5 shows transient dynamics of the same engine parameters, this time for step decrease in fuel flow from 400 to 125 lbm/h. In this simulation case, discrepancies between current and reference model predictions are substantial: rate of convergence to steady state predicted by the current model for the gas generator and power turbine inlet temperatures is much slower than it is predicted by the reference models. As clearly illustrated in the temperature plots of Figure 4.5, an initial undershoot is followed by a slow rise which requires more than 5 seconds to reach a steady state condition. These deviations from reference results were initially attributed to the differences in the modeling of the combustor. In present simulation model, combustor dynamics was modeled using unsteady energy conservation which, per Equation 2.21, was used to evaluate combustor outlet temperature. In contrast, combustor model used by Ballin employed a simple relation for steady state energy balance across the component (Equation 2.16). Thus, the principal difference between the two approaches was rooted in the modeling of transient dynamics of the combustor: time- and volume-dependent temperature variation employed in current model versus quasi-steady state approach independent of these two parameters in Ballin's model. Since, as it was shown in the previous chapter, combustor time constant dictates transient dynamics of the model, it was considered to be the cause of the differences observed primarily in the temperature plots of Figure 4.5. However, a similar engine transient response was reported in a recent work conducted by Spack [Ref. 27] in which author used a direct implementation of Ballin's aerothermal model for the T700 engine. Transient validation results reported by Spack for his model were added to Figures 4.4 and 4.5 for the purpose of completeness. As clearly seen in the two figures, transient response of Spack's model to step increase and decrease in fuel flow exhibits trends similar to those predicted by the current model, therefore suggesting that the differences in modeling of the combustor were not the cause for the large deviations observed in Figure 4.5, particularly in the temperature plots. Then, because no information was provided in

Reference 19 about simulation parameters used by Ballin, no definite reasoning could be made about what exactly caused such variations in temperature profiles as they were predicted by the current model, especially considering the fact that the same dynamics were obtained with direct implementation of Ballin's model. There, however, remains one possible explanation which has to do with the choice of simulation time step. Employing high computational power capability of modern computers, it has become possible to use very small time steps for developing more accurate transient simulation models in which fast pressure variations are easily captured in the absence of a significant increase in the overall simulation time. Therefore, it becomes reasonable to assume that Ballin's real-time aerothermal model was run at simulation time steps much larger than the ones used in the current study due to the insufficient computational power which was available at the time of publishing of Ballin's results.

## CHAPTER 5

# SIMULATION OF HOT GAS INGESTION AND INLET TOTAL PRESSURE DISTORTION

### 5.1 Introduction

Helicopters are used in all kinds of environments with their engines exposed to a variety of inlet conditions. These are seldom uniform, and distortions in the inlet temperature and pressure are frequently encountered. Investigated in this chapter is the effect of such distortions on the overall performance of the engine.

#### 5.1.1 Hot Gas Ingestion

Under specific circumstances, some region of ingested air may become hotter than its surroundings. This phenomenon is termed as hot gas ingestion, or shortly HGI, and is usually caused by ingestion of engine's own exhaust gasses which circulate back into the region of engine inlet, or hot gasses expelled from the nozzle of a launched rocket. For the case of exhaust gas ingestion, this phenomenon was observed to occur most frequently during on-ground operation and hovering at close proximity to the ground under the condition of a tailwind [Ref. 28] which diverts expelled exhaust gasses into the region just above the main rotor where they are sucked and upon leaving the rotor disk are ingested by the engine. During on-ground operation when engine runs in idle mode and main rotor speed is low, exhaust gasses leaving the engine nozzle flow into the downstream without mixing with the surrounding air until, by the action of a tailwind, these gasses are diverted upstream to be sucked by the main rotor and ingested by the engine. This mechanism is schematically shown in Figure 5.1. As for the case of hovering in close proximity to the ground (i.e. in ground effect), engines operate at full throttle, main rotor speed is high, and air which is being pushed down by the rotor disk is entrapped from below by the ground.

This condition acts to enhance the mixing process of hot exhaust gasses which, by the action of a tailwind, were diverted into the upstream and sucked by the main rotor of the helicopter. Because air has no place to escape, hot exhaust gasses through the mixing process just below the rotor disk increase the average temperature of ambient air which is being ingested by the engine. The mechanism for hot gas ingestion for the case of hovering in ground effect is schematically shown in Figure 5.2.

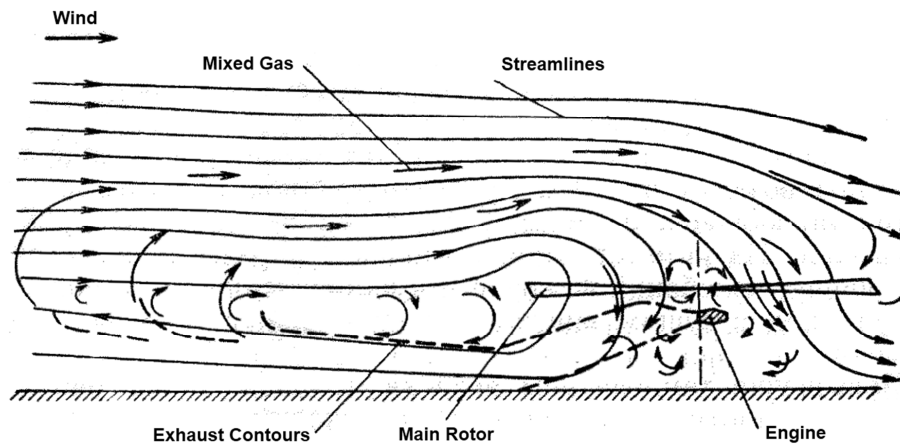


Figure 5.1: Hot gas ingestion during on-ground operation [Ref. 28]

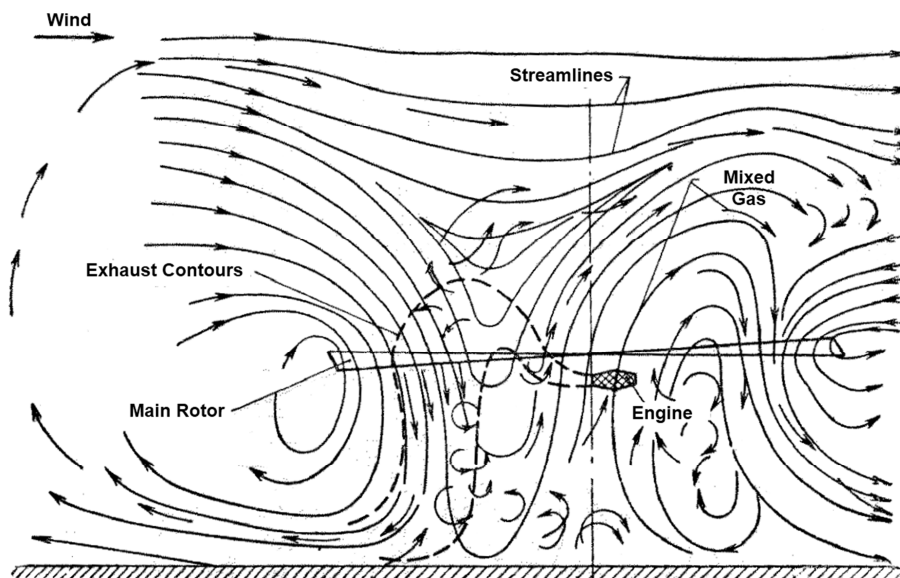


Figure 5.2: Hot gas ingestion in ground effect hover [Ref. 28]

Reference 29 reports increase in the value of inlet temperature due to mixing of exhaust gasses with surrounding air by about 10 to 15°C, and by a maximum of 25 to 30°C in localized regions of the flow.

Because under normal operating conditions ingestion of hot gasses results in decrease of engine performance and reduction in the surge margin of the compressor, hot gas ingestion becomes particularly detrimental and hence particularly important during engine operation at elevated temperature regimes (i.e. summer time, desert climate etc.) at which engine performance is already reduced.

### **5.1.2 Inlet Total Pressure Distortion**

Either being a result of flow separation at engine inlet caused by a cross wind or sudden aircraft maneuver, or ingestion of highly turbulent air or wakes of other aircraft, inlet total pressure distortion negatively affects the amount of available power of the engine and reduces stability margin of the compressor. Inlet total pressure distortion is a phenomenon which has been studied and analyzed in great detail, and numerous experiments and simulations have been performed to understand its impact on engine performance and propose methods on how to reduce the negative effects of inlet total pressure distortion.

## **5.2 Simulation Methodology**

Simulation of hot gas ingestion and inlet total pressure distortion was carried out using the so-called parallel compressor theory. Since in a real compressor mixing between hot and cold air streams ingested by the compressor is very weak [Ref. 28], each of these streams can be treated separately, and compressor performance approximated by considering that each air stream passes through a parallel compressor which is exposed to a uniform inlet flow condition and operates in parallel with other compressors each of which is exposed to a different, but uniform inlet condition. It is assumed that distortions are concentrated in a certain region at the inlet, and contribution of each parallel compressor to the performance of the original compressor is evaluated either through the angle or fraction of inlet area which is exposed to distorted ambient condition applied uniformly to the inlet of a parallel compressor. With this approach, performance of the engine can be analyzed under different inlet conditions and for various magnitudes of distortion.

In the present study, mixing of hot and cold air streams was assumed to take place in the combustor during the combustion process. No averaging of flow variables was attempted at compressor outlet, and streams were directly passed into the combustor. With this approach, evaluation of compressor outlet pressure using the plenum, which was originally placed between the compressor and combustor, impractical. Since all parallel compressors were assumed to discharge to the same static pressure at compressor outlet, and because in the present study combustor outlet pressure was taken as a fixed percentage of the inlet pressure, total pressure at compressor outlet could be directly evaluated by considering mass imbalance for the combustor. So, pressure at combustor outlet was evaluated through Equation 2.48, and compressor outlet total pressure was calculated using Equation 2.22. In the process of evaluating the pressure at combustor outlet, component outlet mass flow was calculated using Equation 2.29, while combustor inlet mass flow was evaluated by the combination of mass flows coming from individual parallel compressors, plus the fuel flow. This combination was done in proportion to the angle of distortion to which each parallel compressor was subjected in the original compressor.

In the present study, two parallel compressors were employed to simulate distorted inlet flow conditions. By denoting with  $\theta_{dst}$  the distortion angle of the distorted compressor as shown schematically in Figure 5.3, angle for compressor operating at clean inlet is given as:

$$\theta_{cln} = 360 - \theta_{dst} \quad [5.1]$$

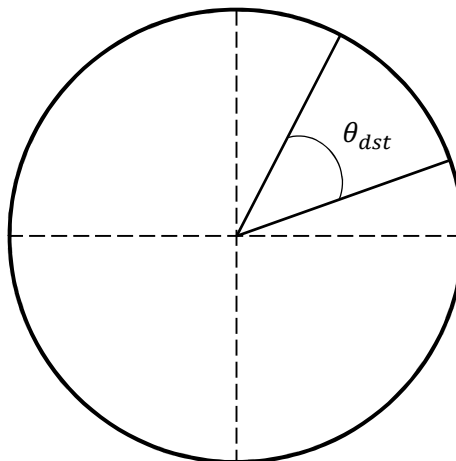


**Figure 5.3: Distortion angle in circumferential plane of engine intake**

For each parallel compressor evaluated is the core mass flow, bleed fractions and power required by the component. Combined compressor core mass flow is calculated by summing mass flows coming from the two parallel compressors in proportion to the corresponding angle of distortion:

$$g_{2p} = \left( g_{2p} \cdot \frac{\theta}{360} \right)_{dst} + \left( g_{2p} \cdot \frac{\theta}{360} \right)_{cln} \quad [5.2]$$

As was mentioned in Chapter 2, bleed flow fractions were evaluated as a function of corrected engine speed and corrected mass flow, latter term being a function of the former corrected with respect to ambient conditions at the inlet. Since inlet conditions of the two compressors are dissimilar, so are the corrected engine speeds and calculated mass flows, and hence the bleed flows extracted from each parallel compressor. Then, combined mass flow at compressor outlet after extraction of bleed flows is calculated as:

$$g_2 = \left( g_2 \cdot \frac{\theta}{360} \right)_{dst} + \left( g_2 \cdot \frac{\theta}{360} \right)_{cln} \quad [5.3]$$

Combined bleed flow for turbine cooling is evaluated as follows:

$$g_{cool} = \left( g_{2p} b_3 \cdot \frac{\theta}{360} \right)_{dst} + \left( g_{2p} b_3 \cdot \frac{\theta}{360} \right)_{cln} \quad [5.4]$$

Per Equation 2.14, compressor power is a linear function of ingested air mass flow. Then, using the definition of compressor core mass flow given by Equation 5.2, compressor power can be written as:

$$P_C = \left( P_C \cdot \frac{\theta}{360} \right)_{dst} + \left( P_C \cdot \frac{\theta}{360} \right)_{cln} \quad [5.5]$$

Combined energy which enters the combustor per unit time is evaluated by considering the energy balance at combustor inlet:

$$g_2 h_2 = \left( g_2 h_2 \cdot \frac{\theta}{360} \right)_{dst} + \left( g_2 h_2 \cdot \frac{\theta}{360} \right)_{cln} \quad [5.6]$$

Static pressure at compressor outlet was taken as a fixed percentage of the total pressure (Equation 2.8). Therefore, for present study this implied that all parallel compressors which discharged to the same static pressure also discharged to the same total pressure, which was evaluated using Equation 5.7.

$$P_2 = \frac{P_3}{\gamma_{loss}} \quad [5.7]$$

To calculate compressor outlet pressure, plenum at the interstage between the compressor and combustor was removed, and evaluation of pressure at compressor outlet was done by considering mass imbalance for the combustor. Mass flow entering the combustor is comprised of compressor outlet mass flow given by Equation 5.3 and fuel flow. Mass flow leaving the combustor is given by the gas generator mass flow calculated using Equation 2.29. Then, combustor inlet and outlet mass flows are given as follows:

$$g_{in} = g_2|_{Eq.5.3} + g_b \quad [5.8]$$

$$g_{out} = g_3|_{Eq.2.29} \quad [5.9]$$

Pressure ratio of the nozzle, per Equation 2.45, was given as a function of corrected gas generator speed. As a result of step increase in inlet temperature, step decrease in corrected gas generator speed would result in a sudden change in the value of engine discharge pressure. Because this pressure was used in Equation 2.43 to evaluate enthalpy drop across the power turbine, a sudden change in discharge pressure would result in a step variation of power output, power turbine speed and output torque. This problem was eliminated by assuming that nozzle discharged to undisturbed atmospheric pressure:

$$P_5 = P_1 \quad [5.10]$$

One of the critical parameters which define operating state of the engine is the surge margin of the compressor. This parameter, as suggested in Reference 1, is defined as follows:

$$SM = \frac{\pi_{C_{surge}} - \pi_C}{\pi_C} \cdot 100\% \quad [5.11]$$

### 5.3 Simulation of Steady State Hot Gas Ingestion

To understand how ingestion of hot air affects engine performance under steady state operating conditions, simulations with the two-parallel-compressor model were performed for different ambient temperatures varied in the range from 15°C (standard day sea level temperature) to 50°C using 5°C increments. Two PI-type controllers were used in the simulation: one to vary fuel flow to keep power shaft RPM at design speed, and another to vary the load applied on the power shaft to maintain gas generator turbine inlet temperature at a specified level. Such control configuration allowed simultaneous control of the output shaft speed and the maximum power delivery of the engine, a quantity directly related to the amount of enthalpy at combustor outlet, i.e. the gas generator turbine inlet temperature (TIT) which in the simulations for steady state hot gas ingestion was varied from design value of 1525.46 Kelvin to 1550 Kelvin, and finally to 1575 Kelvin. Gains used for the fuel control are given in Table 5.1.

**Table 5.1: Gains of the PI fuel control system**

Proportional gain	0.0023796
Integral gain	0.0028399

Simulation results are shown in Figures 5.4 to 5.6 in terms of mass flows for the fuel and compressor, compressor outlet static pressure, maximum power output and compressor surge margin. These parameters, except the latter, were normalized with respect to steady state values calculated at ISA SLS conditions for the given gas generator turbine inlet temperature. Engine parameters at steady state operating conditions are given in Table 5.2.

**Table 5.2: Steady state engine parameters for different values of TIT**

<i>TIT (K)</i>	<i>P<sub>2,stat</sub> (MPa)</i>	<i>g<sub>2p</sub> (kg/s)</i>	<i>g<sub>b</sub> (g/s)</i>	<i>Power (hp)</i>
Design	1.698	4.574	100.423	1768.42
1550	1.734	4.629	104.202	1840.65
1575	1.769	4.682	108.026	1913.36

Figure 5.4 shows simulation results which were obtained by maintaining gas generator turbine inlet temperature at design value of 1525.46 Kelvin. Variation of engine parameters is shown for four different values of distortion angle. From the first plot it is observed for fuel consumption to decrease with increasing ambient temperature: because this increase results in decrease of corrected engine speed and hence the mass flow, engine operates at increased fuel-to-air ratio which, for the purpose of keeping the gas generator turbine inlet temperature at the same level, must be decreased.

According to Equation 2.44, the decrease in core mass flow and fuel input results in reduction of power delivery of the engine. This is clearly shown in the power output plots in which power delivery is seen to decrease with increasing ambient temperature. Moreover, reduction of corrected speed and mass flow of the compressor results in decrease of pressure ratio. Because enthalpy drop across the turbine is a function of turbine pressure ratio, decrease in compressor discharge pressure adds to the reduction of engine speed and power output.

Simulation results obtained for steady state hot gas ingestion for gas generator turbine inlet temperatures of 1550 and 1575 Kelvin are similar to those shown in Figure 5.4 for design TIT. By examining the three figures it can be observed that increasing TIT results in decrease in the extent of reduction of engine performance. If, for example, engine power output plots shown in Figures 5.4 and 5.6 are compared, then it would be seen that for inlet distortion angle of 270 degrees and 40 degree ambient temperature, power loss for the case of design TIT is about 15%, while for the same inlet conditions for the case of 1575 Kelvin TIT power decreases by only 14%. The extent of this reduction is more pronounced for higher ambient temperatures and larger distortion angles, e.g. 29.5% power loss at 50°C, 360 degree distortion angle at design TIT value versus 26.3% power loss at TIT of 1575 Kelvin at the same inlet conditions.

The last plot shown in Figures 5.4 to 5.6 gives the variation of compressor surge margin. The general trend of the surge margin is to decrease with increasing ambient temperature and decreasing distortion angle with latter parameter being more influential on this reduction than the former: while only some variation is observed to take place for 360 degree distortion angle, surge margin for a 90 degree distortion angle varies drastically from 12-14% to approximately -10% for all TIT values used in the study.

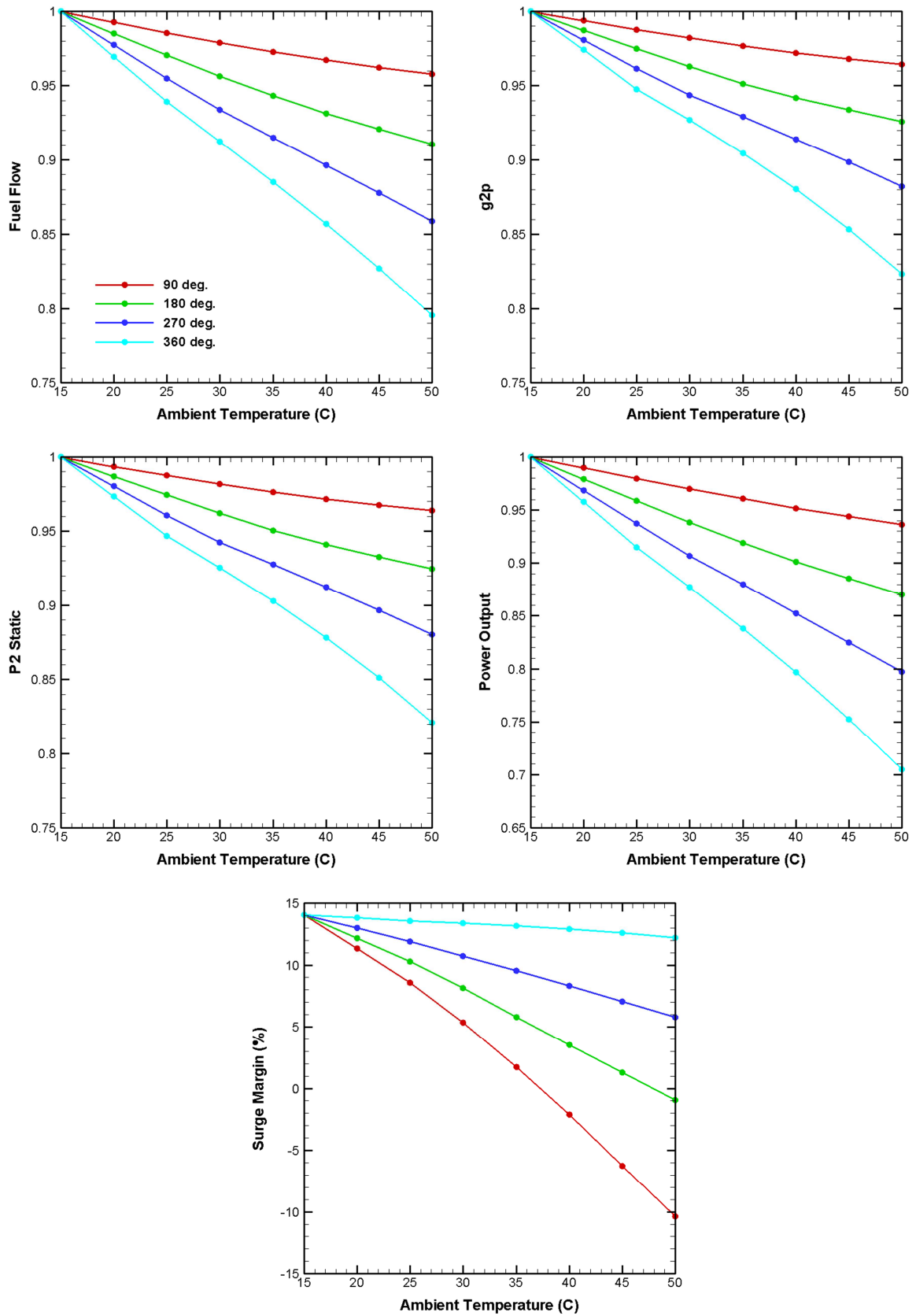


Figure 5.4: Engine response to steady state hot gas ingestion for  $T_3 = T_{3,des}$

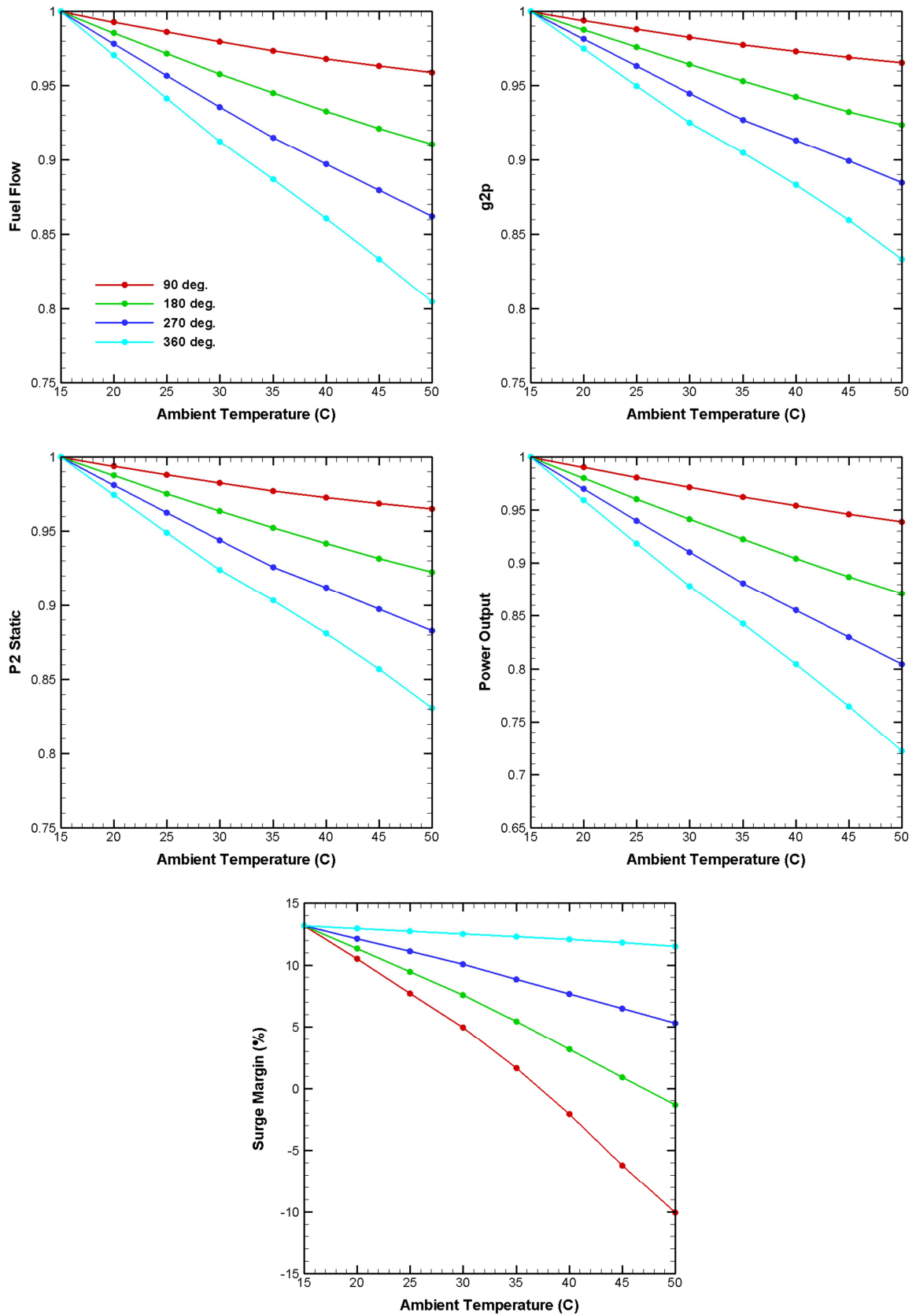


Figure 5.5: Engine response to steady state hot gas ingestion for  $T_3 = 1550 K$

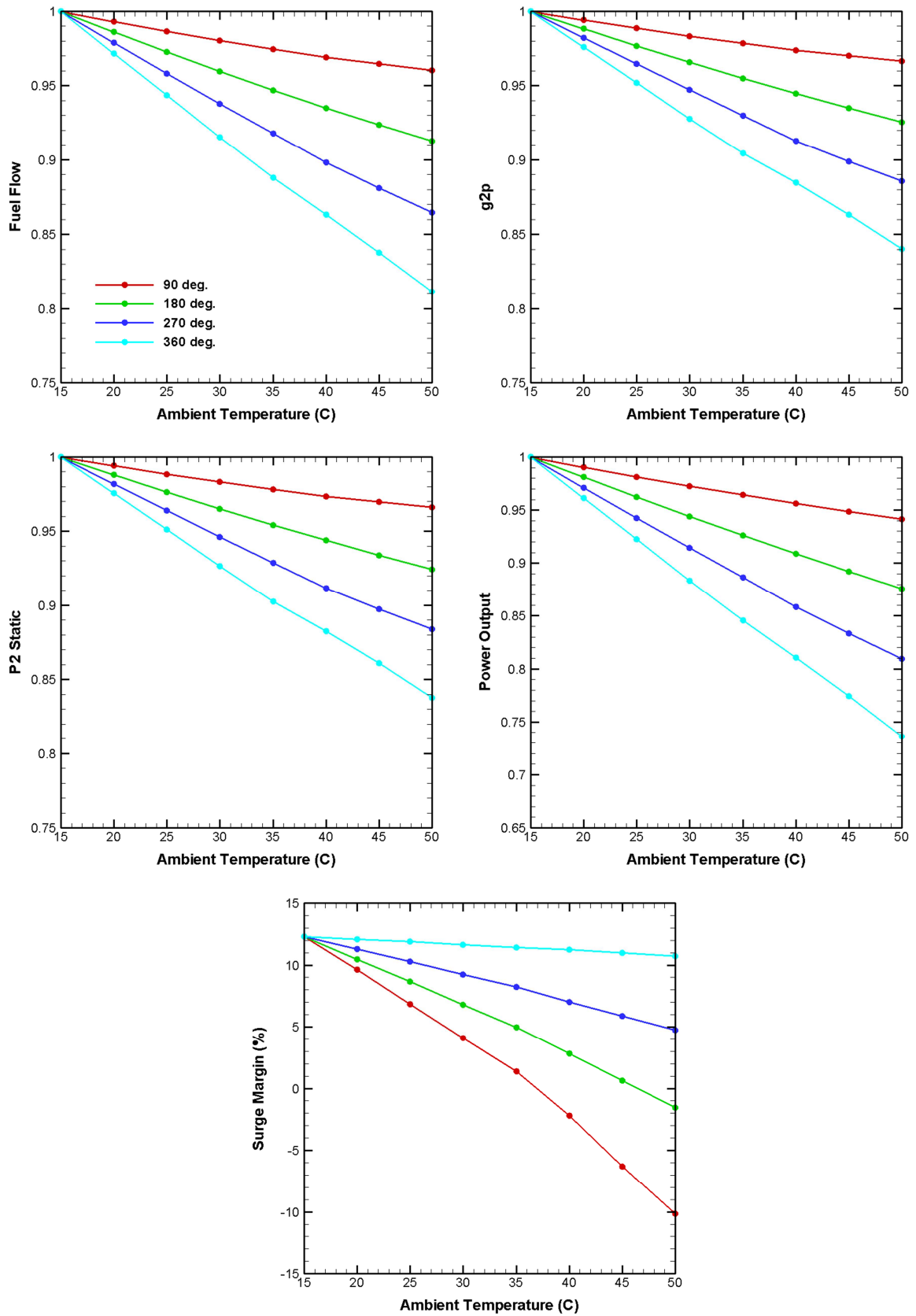


Figure 5.6: Engine response to steady state hot gas ingestion for  $T_3 = 1575 K$

As seen in all the plots for surge margin variation, out of all distortion angles it is the smallest one to yield the largest decrease in compressor surge margin: for all the three simulation cases, at approximately 37 degrees ambient temperature surge margin becomes negative to indicate compressor surge. The reason for engine stall at lower values of distortion angle is explained as follows. Part of the compressor which is exposed to distorted inlet conditions operates at reduced values of corrected speed and mass flow. Because only a small part of the compressor is exposed to the distortion, the overall effect of distorted compressor on engine performance per Equation 5.2 and 5.3 is also small. Therefore, only a small mass imbalance is generated at combustor plenum, which causes an equally small change in the value of combustor outlet pressure and hence, per Equation 5.7, in the value of compressor discharge pressure. Then, part of the compressor which is exposed to distorted inlet conditions operates at reduces corrected speed and mass flow and a discharge pressure which is not significantly different from its initial value calculated at clean inlet condition before the application of the distortion. These operating conditions result in an almost vertical shift of the operating point of the distorted compressor yielding a drastic reduction in the surge margin. With increase in distortion angle, the weight of distorted section of the compressor on the overall engine performance is increased, and change in pressure at combustor outlet becomes more pronounced. Since extent of pressure change increases with increasing angle of distortion, operating point of the distorted section of the compressor experiences a less severe displacement in the vertical (i.e. corrected mass flow), and a more pronounced shift in the horizontal direction towards lower pressure ratios is observed. In other words, operating point of the compressor moves away from the surge line to maintain a positive stability margin for the compressor.

Variation of compressor parameters as a function of ambient temperature for distorted and clean sections of the compressor are shown in Figure 5.7 for the case of design value for the gas generator turbine inlet temperature. The map is horizontally divided to separate operating lines of the distorted compressor which lie below the dashed line and those of the clean section of the compressor which lie above it. Each dot represent a certain ambient temperature, and starting from the design point at which the temperature is given by its ISA SLS value of 15°C the temperature gradually increases to 50°C.

Performance variation for the distorted section of the compressor with increasing ambient temperature is clearly illustrated with compressor lines running from design point to lower

engine speeds. Clearly seen in this figure is the sharp drop in stability limit of the compressor exposed to a 90-degree inlet distortion: engine is surged at a corrected engine speed of 96.2% at 37 degrees ambient temperature. With increase in distortion angle at the inlet, operating lines for the distorted compressor are observed to rotate away from the surge line, and no crossing of the stability limit is observed to occur for inlet distortion angle of 270 degrees and larger.

Also shown in Figure 5.7 is response of the clean section of the compressor. Since hot gas ingestion causes a decrease in the overall mass flow of the engine, clean section of the compressor must operate at a higher corrected speed to compensate for the decrease in mass flow of the distorted section. Since for a given ambient temperature small distortion angles produce a larger decrease in corrected mass flow of the distorted section, a larger mass flow must be attained by the clean section to compensate for this decrease.

Shown in Figure 5.8 are the resulting compressor running lines showing variation of engine performance as a function of ambient temperature given separately for the four distortion angles. As clearly seen in the figure, increase in the value of ambient temperature results in shifting of operating point of the compressor to a lower corrected engine speed, reduced corrected mass flow and a lower pressure ratio. The shift is observed to be shorter for smaller angles of distortion. If the four figures are superimposed on top of each other, it would be observed for compressor running lines to coincide, i.e. to lie on the same operating line given for the 360 degree distortion angle.

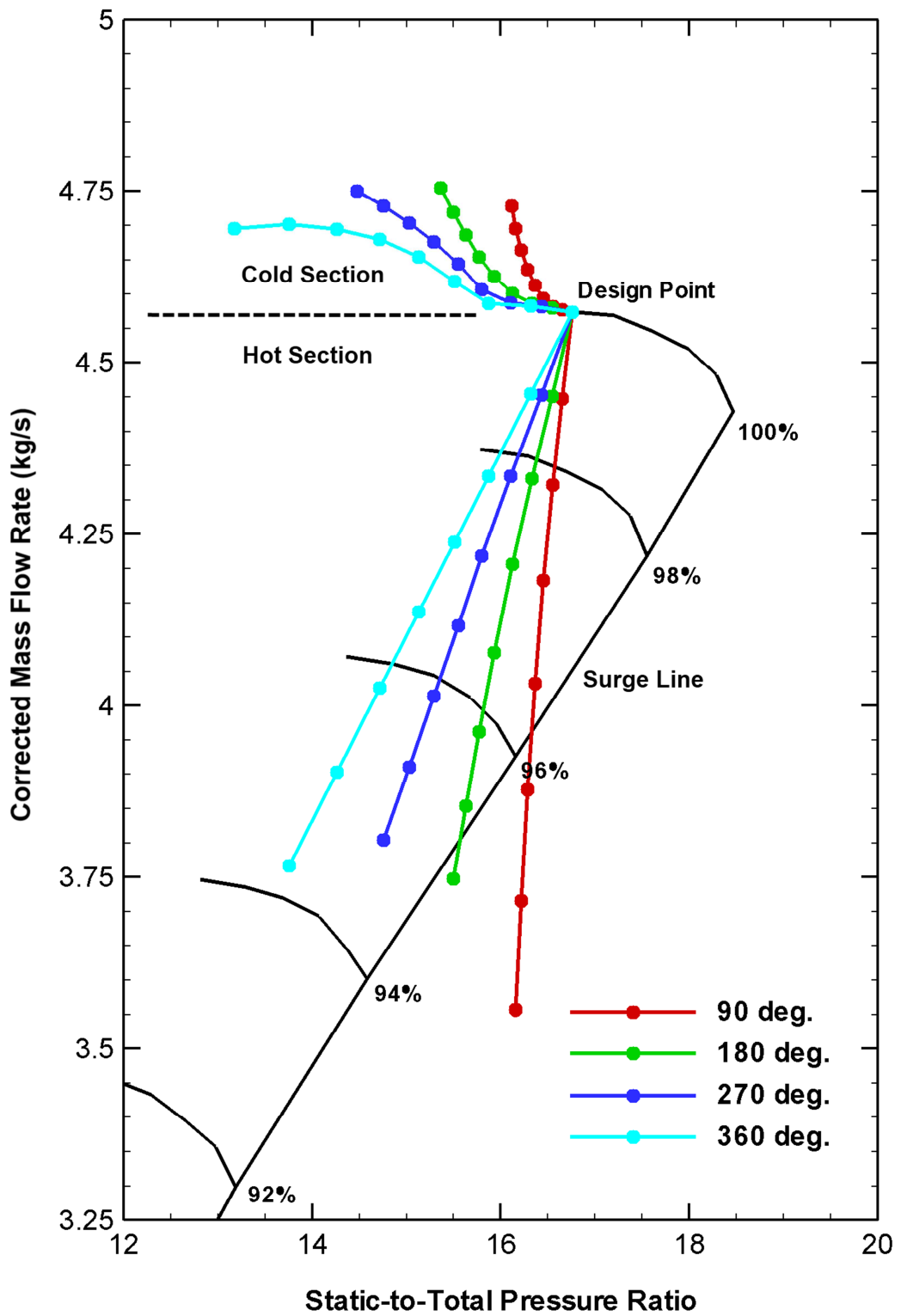


Figure 5.7: Operating lines for clean and distorted sections of the compressor for different angles of distortion,  $T_3 = T_{3,des}$

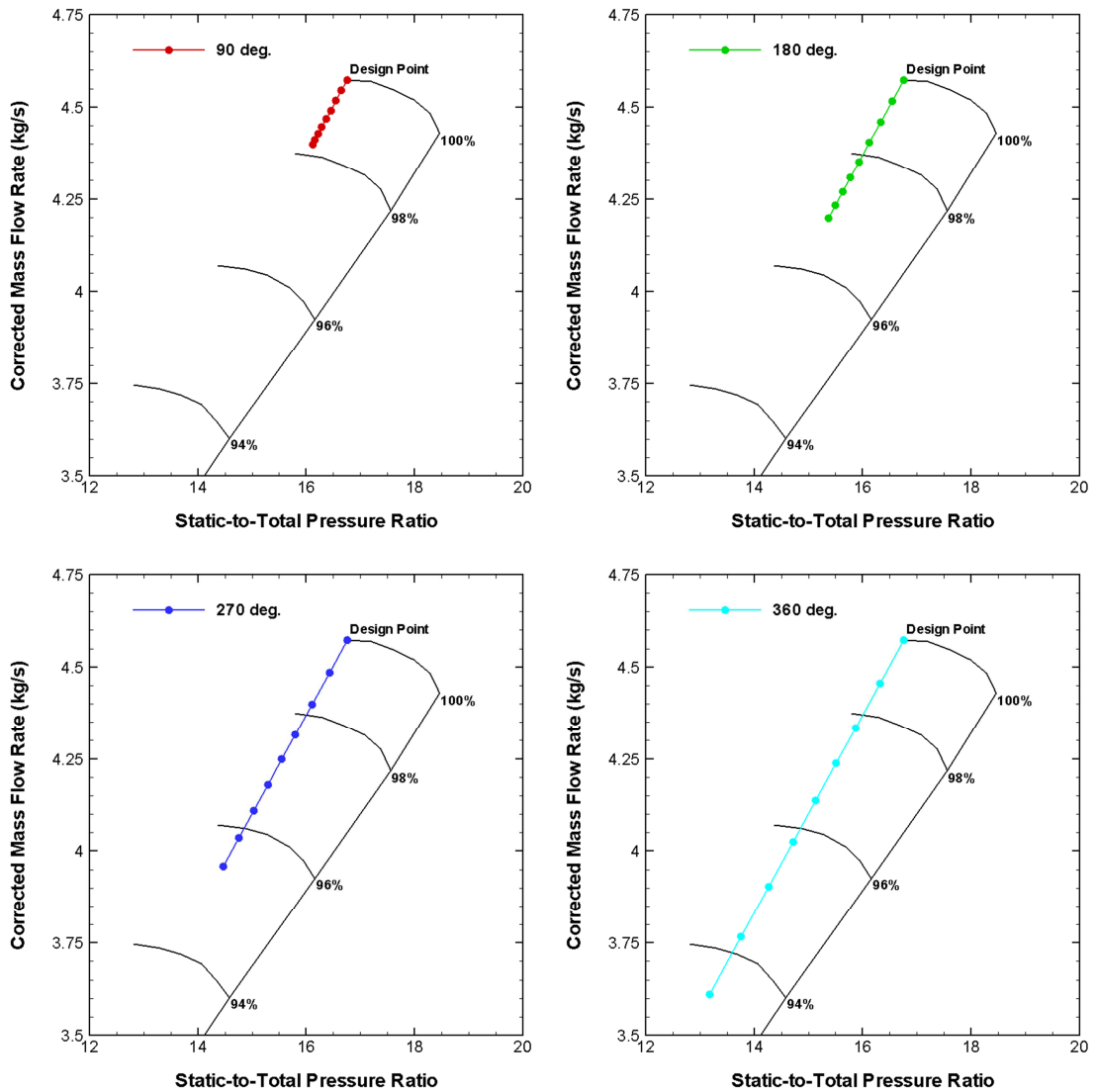
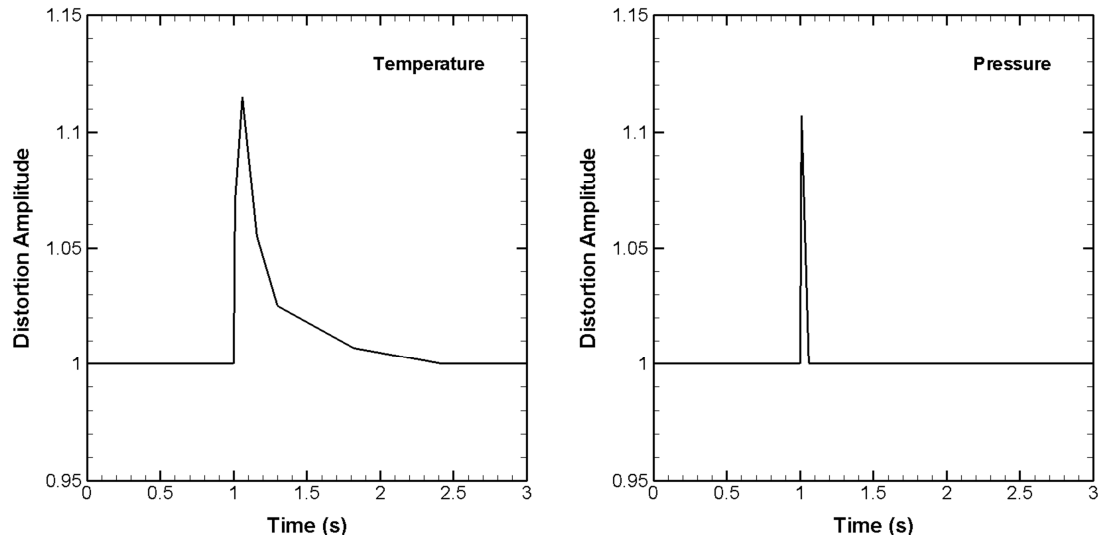


Figure 5.8: Resulting compressor operating lines for different distortion angles,  $T_3 = T_{3,des}$

## 5.4 Simulation of Transient Hot Gas Ingestion

In Reference 25 Tokarski et al. presented results of their study in which authors used an unbalanced torque model for the Lycoming T53-L-703 engine coupled to a 3DOF AH-1 Cobra helicopter model and Chandler Evans turbine assembly hydro-mechanical fuel control to investigate, and suggest methods to counteract, the negative effects of transient hot gas ingestion on torque dynamics of the power shaft and helicopter rotors. Used in this study was real flight data for pressure and temperature distortions at the inlet which was recorded after launching a pair of Mark 66 rockets. This data, a reproduction of which is

shown in Figure 5.9 for the temperature and pressure, was used to simulate transient hot gas ingestion for the T700 engine. Investigated in this study was the variation of engine dynamics as a function of extent of inlet distortion.



**Figure 5.9: Real flight data for temperature and pressure distortions at the inlet**

Simulation results are presented in Figure 5.10 in terms of fuel and compressor mass flows, compressor static discharge pressure, gas generator turbine inlet temperature and power shaft torque. Fuel flow was metered by a PI control system which maintained rotational speed of the free turbine at its design value. Simulation results for transient hot gas ingestion with application of inlet distortion as shown in Figure 5.9 indicate an initial increase in the amount of fuel flow which is inputted by the PI control into the system. Because increase in ambient temperature of ingested air results in decrease of corrected engine speed, the value of compressor mass flow must decrease, which is exactly the case as seen in the plot for mass flow in Figure 5.10. Because per Equation 2.44 power output of the turbine is linearly proportional to the mass flow, decrease in the amount of air ingested by the engine results in decrease of power delivery. To compensate for this decrease and maintain rotational speed of the power turbine at a constant value, fuel flow is increased to increase power output of the free turbine (load applied on the turbine by the drive train was assumed to remain equal to the amount of power generated by the turbine at design conditions).

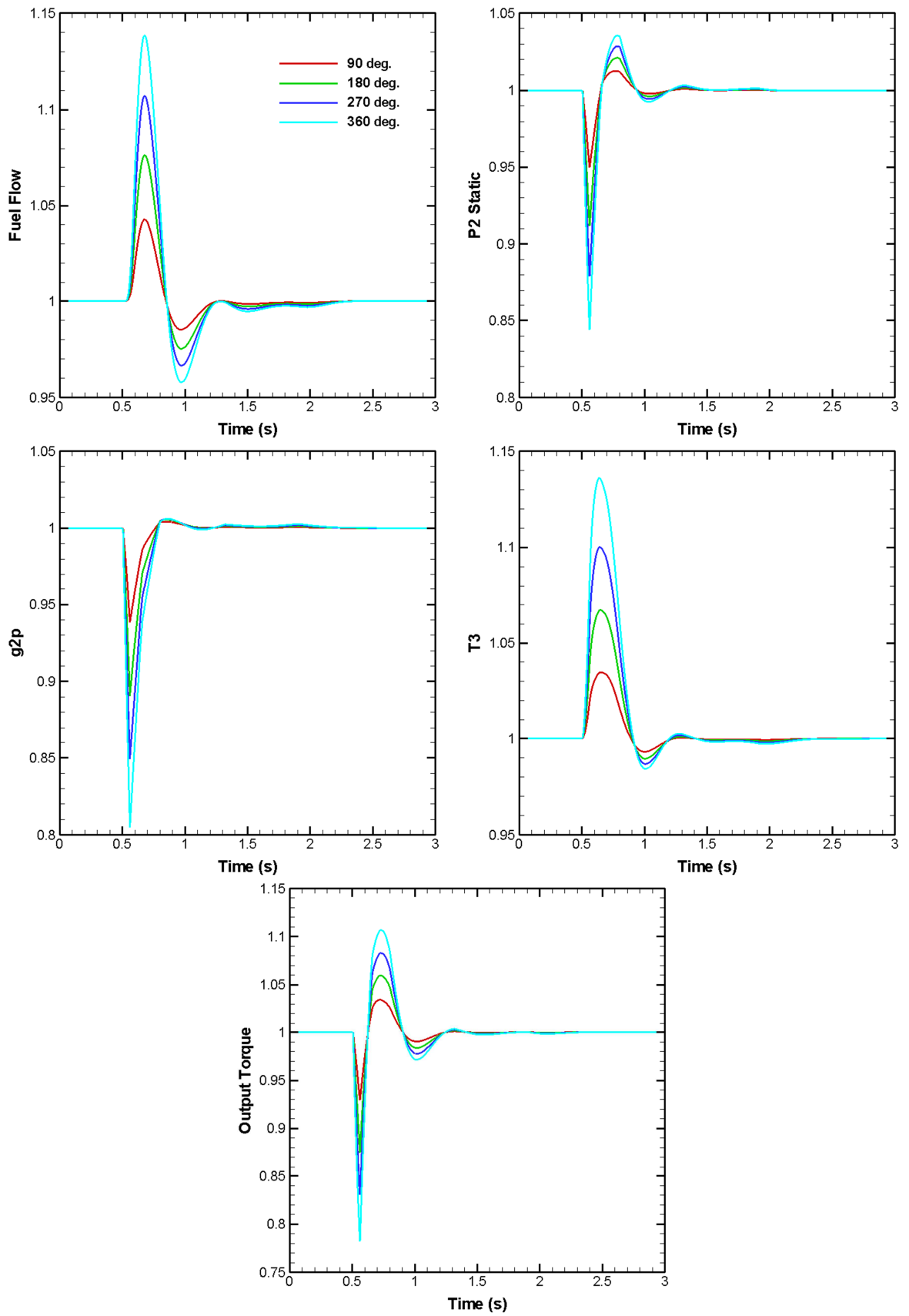


Figure 5.10: Engine response to realistic transient inlet distortion

Due to the lag time which exists between injection of the fuel and production of an engine response to the input, decrease in compressor mass flow and increase in fuel flow results in increase of FAR which leads to a substantial increase in the temperature at gas generator turbine inlet (to a temperature higher than 1700 Kelvin). Under such operating conditions, more power is produced by the free turbine than what is required to power the drive train of the helicopter, and a positive torque now applied on the power shaft acts to increase the rotational speed of the turbine. Since power shaft speed is maintained at its design value, fuel flow is reduced by engine control to remove the positive torque applied on the shaft.

From the plots in Figure 5.10 it is clear that under the same distortion conditions at the inlet, engine response is more pronounced for larger angles of distortion. For comparison, fuel input into the system is seen to increase from 4% to approximately 14% for 90 and 360 degree distortion angles, respectively. For the same distortion angles, compressor mass flow decreases by 6% and 19.5%, respectively.

Dynamics of the gas generator turbine inlet temperature are seen to closely resemble the variation of fuel flow. For the case of 90 degree inlet distortion, combustor outlet temperature is seen to increase by 3.3% from its design value. As for the case of full inlet distortion, as a result of fuel flow increase by 14% turbine inlet temperature increases by 13.7% to a value of approximately 1735 Kelvin. Considering that such temperatures are attained during launch of a single rocket, maintaining elevated temperatures during a salvo fire will inevitably cause a significant increase in the level of thermal stress experienced by turbine blades. This stress may result in the failure of thermal barrier coatings and, as a consequence, in melting or, in the worst case scenario, mechanical failure of the blades.

As clearly seen in the last plot of Figure 5.10, sharp decrease in compressor mass flow produces an equally sharp decrease in the output torque. The magnitude of resultant torque spikes generated at distortion angles of 90 and 360 degrees are read from the figure as 7% and 22% of the nominal value. Moreover, this decrease occurs in short time duration of approximately 60 milliseconds and results in a large torque gradient. Considering the high frequency at which such torque gradients are produced in gunships and attack helicopters, it is expected for fatigue life of the shaft to be relatively short with cracks forming on the surface of the shaft indicating its progressing deterioration [Ref. 30].

Dynamics of output torque shown in Figure 5.10 are consistent with simulation results reported in Reference 25: as a result of transient distortion at the inlet, engine torque initially experiences a sharp decrease, then recovers back to its nominal value, overshoots, and reaches steady state in approximately three cycles. Although simulation results reported in Reference 25 were obtained by using an active damping control system to regulate fuel flow in direct opposition to drive train resonances, trends are consistent with those predicted by the current study.

## 5.5 Simulation of Inlet Total Pressure Distortion

To investigate the negative effects of inlet total pressure distortion on engine performance, a distortion signal was applied at the inlet to decrease the total pressure of ingested air. This decrease was produced with a signal which was generated as a function signal amplitude and duration. Mathematical formulation of the signal, which in essence is a half-sine curve with both ends becoming parallel with the horizontal, is given by Equation 5.12. A sample 15% amplitude signal of 0.1 seconds of duration is shown in Figure 5.11.

$$f(A, \Delta t, t) = \left(1 - \frac{A}{2}\right) + \frac{A}{2} \cdot \sin\left(2\pi \frac{t}{\Delta t} + \frac{\pi}{2}\right) \quad [5.12]$$

Where,

- $A$  : Signal amplitude
- $\Delta t$  : Signal duration (seconds)
- $t$  : Time from zero to  $\Delta t$  (seconds)

Simulations with inlet total pressure distortion were performed using the two-parallel-compressor model in which one of the compressors was exposed to distorted inlet conditions. Simulations were run for two different distortion angles, 120 and 180 degrees, and two different 10-millisecond distortion signals: 10% and 15% reduction in the total pressure at the inlet. Results are shown in Figure 5.12 in terms of pressure ratio of the clean and distorted compressors, transient dynamics of output torque and surge margin.

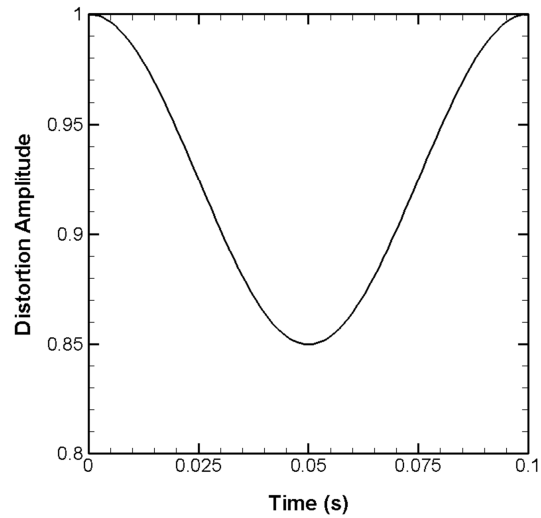


**Figure 5.11: Sample inlet total pressure distortion signal for 15% distortion amplitude, 0.1 seconds of duration**

As shown in the first plot, pressure ratio of the distorted compressor subjected to 10% distortion amplitude is increased by 8.33%. Since a 10% distortion is applied, a pressure recovery of 1.67% is achieved in the time duration of applied distortion. For 180 degree case, pressure recovery is increased, and 10% distortion produces only 7.15% increase in the value of pressure ratio of the distorted compressor. For the case of 15% distortion amplitude, 120 degree distortion angle results in 13%, 180 degree distortion angle results in 11% rise in the value of pressure ratio of the distorted compressor. So, increase in extent of distortion causes more of the pressure to be recovered by the distorted compressor.

Also shown in the two plots is the variation of pressure ratio of the clean compressor: dynamics of the clean compressor are opposite to that of the disturbed compressor. While increase in pressure ratio of the distorted compressor is due to decrease in ambient pressure, decrease in the pressure ratio of the clean compressor is due to decrease in core mass flow (per Equation 2.9, decrease in inlet pressure results in decrease of compressor mass flow) and reduction of combustor discharge pressure per Equation 2.48.

Shown in the second plot of Figure 5.12 are the dynamics of output torque. A 10% inlet distortion results in a torque spike of 4.63% for 120 degree, and 6.75% for the 180 degree distortion angle. A 15% inlet distortion produces a more drastic increase in the magnitude of the torque spike: 7.9% and 11% for 120 and 180 degree distortions, respectively.

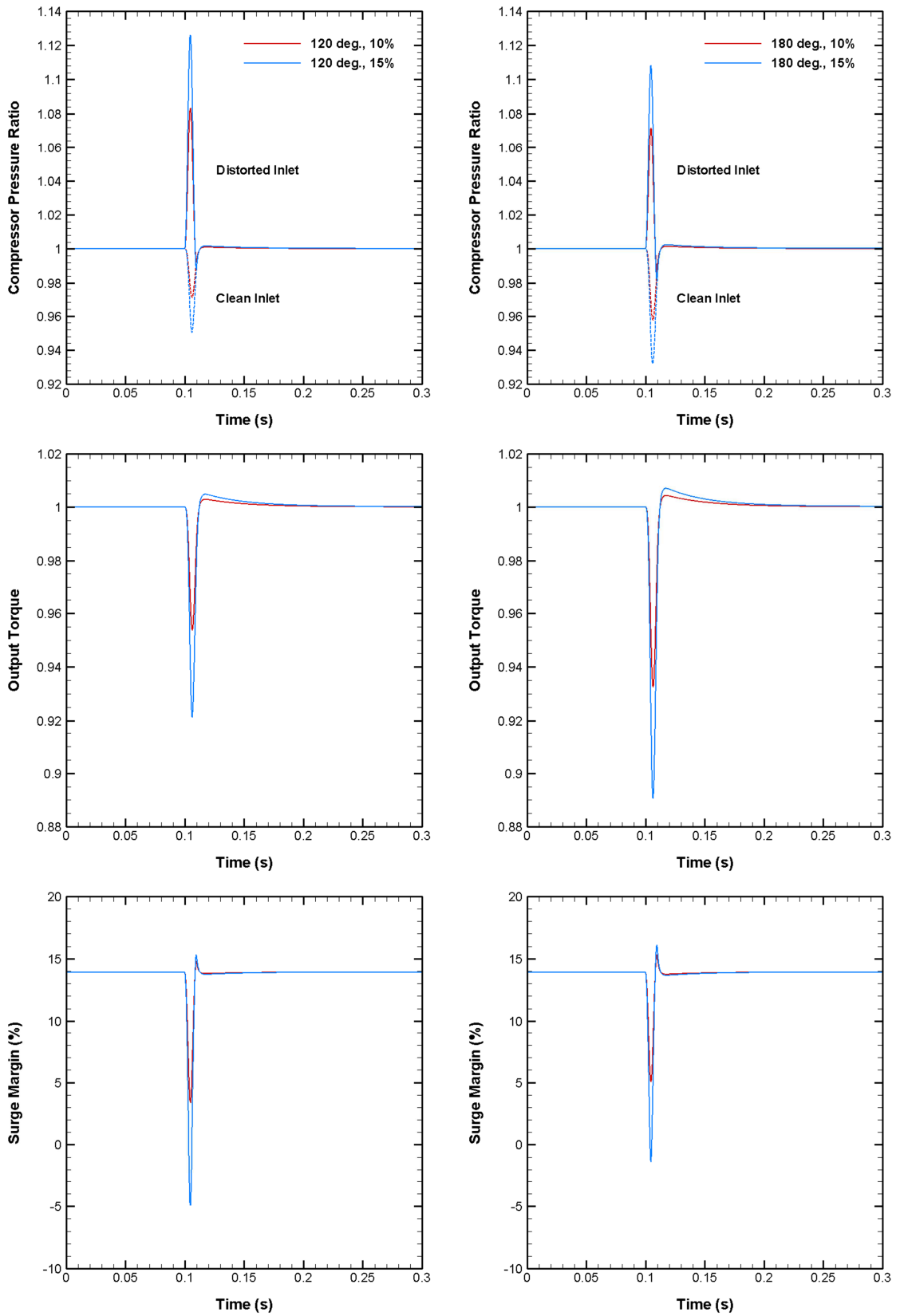
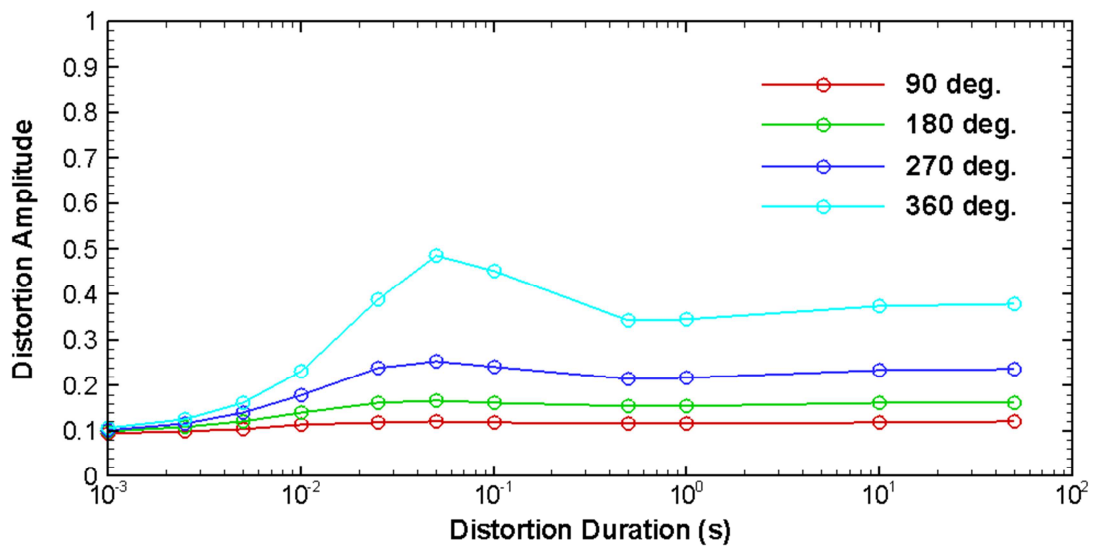


Figure 5.12: Engine response to transient inlet total pressure distortion

In the last plot of Figure 5.12 shown is the variation of compressor surge margin. It is seen for distortion amplitude of 10% to result in a significant reduction of the surge margin: down to 3.4% and 5.1% for 120 and 180 degrees, respectively. In both cases, a distortion of 15% produces a negative surge margin, implying a compressor surge. It can be observed that for the same inlet distortion signal, the decrease in stability limit of the compressor is less for the case of a larger distortion angle.

To understand how surge margin varies with signal amplitude and its duration, the model was run for different combinations of the two parameters for 90, 180, 270 and 360 degree distortion angles. Results are shown in Figure 5.13 in which plotted versus logarithmic time scale is the amplitude of the signal sufficient to initiate an engine surge, i.e. to reduce stability limit of the compressor all the way down to zero. It is clearly seen in the figure that for a given pulse duration the amplitude of distortion increases with increasing angle of inlet distortion. This behavior is explained by the increased contribution of the distorted compressor to the dynamics of the engine: because more of the flow which comes from the distorted compressor is accounted for via a larger distortion angle, engine responds more readily to any disturbance applied at the inlet of the original compressor, hence shift of operating point of the distorted compressor on its performance map is less severe in vertical direction, and stability limit of the component is maintained at a larger positive value. It can be observed that for a very small signal time duration the effect of amplitude diminishes, and stability limit of the compressor is depleted at the same rate regardless of the distortion angle. As signal duration increases, distortion amplitude required to initiate an engine surge is seen to increase. At about one seconds of pulse duration, the distortion amplitude changes only slightly, and further increase in pulse duration, depending on the distortion angle, has either no or very small effect on signal amplitude. This is caused by the fact that, with increasing time duration of the signal, engine exhibits characteristics of a steady state operation: because pulse duration is long, engine has sufficient time to approach a steady state condition at any given instant in time. These results correlate qualitatively well with simulation results obtained by Wenzel and Blaha [Ref. 31]. In their numerical simulations aimed at investigating the effect of inlet total pressure distortion on compressor performance, authors also came to the conclusion that to initiate a compressor surge the amplitude of distortion signal can be increased with increasing signal duration and distortion angle. Similarly with present study, they also found that variation curve for

the distortion amplitude levels out for very long pulse durations. Unfortunately, in present study it was not possible to obtain the variation in which for very small signal durations distortion amplitude began to increase, as was predicted in the simulations by Wenzel and Blaha. Since present model relied on a compressor map rather than internal flow dynamics, any disturbance at the inlet was immediately reflected on the corrected speed and mass flow of the compressor. Hence, only a limited understanding of engine response could be obtained. To gain more insight into the dynamics of the engine during inlet distortion, modeling of the compressor must include internal flow characteristics.



**Figure 5.13: Variation of distortion amplitude with signal duration and distortion angle to initiate a compressor surge**

## CHAPTER 6

### SIMULATION OF ENGINE DETERIORATION

With time, engine performance degrades due to deterioration of engine components. Factors decreasing engine performance can be internal, such as creep, fatigue or failure of compressor and turbine blades, and external factors which include, but are not limited with, ingestion of sand, gravel, salt water and volcanic ash. These factors are especially dangerous for helicopter engines which frequently have to work in hazardous operating conditions. For this reason, deterioration of helicopter engines is a very common problem with degradation of engine performance mostly being attributable to the deterioration of the compressor which is directly exposed to the environment. The most common causes of compressor deterioration are erosion, corrosion and fouling. Corrosion and erosion are associated with material removal which results in the shortening of compressor blades via blunting of the leading and thinning of the trailing edge, and cropping of the blade span. Moreover, erosion causes an increase in the surface roughness of the blade on its pressure side. Fouling is a term used to define material build-up on the surface of a blade: dirt, salt, volcanic ash and other particles stick to the blade and build up during operating time of the engine. It is known for compressor fouling to account for up to 85% of the overall engine performance degradation [Ref. 32]. All of the aforementioned factors of compressor deterioration result in decrease of compressor efficiency, reduction of mass flow rate and pressure delivery, and cause a reduction in the stability margin of the compressor.

Similarly to compressors, turbines are also susceptible to corrosive and erosive effects of the environment. While the former is attributed to material removal via chemical erosion of the blade by the action of such elements as chlorine and sulfur oxide which are found in the combustion products, latter is a result of ingestion of solid particles which were able to make their way into the engine downstream through the fine holes of the combustor, or a

consequence of mechanical damage caused by the impact of failed engine parts. Moreover, gas generator turbines are prone to creep and fatigue failures, former being due to the high inlet temperatures and hence high thermal stresses, and the latter due to damages sustained to the blades as a result of impact of foreign objects [Ref. 33].

All the factors mentioned for compressor and turbine deterioration result in decrease of maximum power output of the engine, and increase in fuel consumption. Considering the wide operating range and environmental conditions, helicopter engines are prone to engine performance degradation more than any other aircraft. Because they are so common, it is desirable to predict performance losses of engines operating in hazardous environmental conditions for health monitoring purposes. An accurate estimate of performance losses can be made only with the use of a comprehensive simulation model which includes aerothermodynamics of engine components as well as component maps to faithfully predict operating states of the engine. Since aerothermal models incorporate all of these requirements, they can be effectively used to simulate degradation of engine performance as a result of deterioration of individual engine components. In present study, developed aerothermodynamic simulation model for the GE T700 engine was used to simulate different cases of engine deterioration by including in the calculation of flow variables and engine parameters a number of coefficients which were used to simulate degradation of engine components.

## 6.1 Simulation Cases and Methodology

**Case 1.** Compressor was assumed to have sustained a mechanical damage which led to a 5% decrease in component efficiency. To simulate this effect, the definition of compressor efficiency given by Equation 2.10 was used to calculate the new outlet temperature:

$$\tau_{C,new} = 1 + \frac{(\tau_C - 1)_{nom}}{\alpha} \quad [6.1]$$

Per Equation 6.1, where  $\alpha$  was taken as 0.95 to simulate decrease in component efficiency by 5% from its nominal value, decrease in compressor efficiency results in increase of outlet temperature. Because enthalpy now rises to a higher value than it did for the case of nominal efficiency, power required to drive the compressor increases. However, despite

the increase in combustor outlet temperature caused by the increase of compressor outlet temperature, enthalpy drop across the gas generator turbine is insufficient to compensate for the increase in power requirement of the compressor. This results in decrease of engine speed, and reduction of mass flow and pressure delivery at compressor outlet.

**Case 2.** Gas generator turbine was assumed to have sustained a mechanical damage which led to a 5% decrease in component efficiency. This condition was simulated by decreasing the enthalpy drop across the turbine which is defined by Equation 2.33. Then, for a given flow state at the inlet, reduction in the energy extracted by the turbine produces a net negative torque applied on the high-pressure shaft. Because the turbine can no longer sustain the compressor which requires more power, engine speed decreases to attain a new steady state condition. An increase in gas generator turbine inlet temperature is expected due to increase of fuel-to-air ratio.

**Case 3.** In third scenario, gas generator turbine blades were assumed to have been eroded which led to an increase in turbine throat area by 2%. With a larger throat area, more flow can be sustained by the turbine. To simulate the effect of turbine erosion, an assumption was made that for a choked turbine mass flow increases by the same amount by which erosion causes an increase in the throat area. In other words, by applying the relation for a choked turbine to calculate its mass flow it was assumed that mass flow parameter of the turbine calculated at design conditions was still applicable for calculating mass flow of the eroded turbine. By writing Equation 2.29 in its full form to account for the throat area:

$$\left( g_3 \frac{\sqrt{T_3}}{A \cdot P_3} \right)_{des} = g_3 \frac{\sqrt{T_3}}{A \cdot P_3} \quad [6.2]$$

Then, 2% increase in throat area results in increase of mass flow by the same amount:

$$1.02 \cdot \left( g_3 \frac{\sqrt{T_3}}{P_3} \right)_{des} = g_3 \frac{\sqrt{T_3}}{P_3} \quad [6.3]$$

**Case 4.** Engine was assumed to have deteriorated with major components subjected to some extent of degradation: compressor efficiency dropped by 3%, fouling of compressor blades resulted in 5% decrease in mass flow; gas generator turbine throat area increased by 2%, and efficiency dropped by 1%. While efficiencies were modeled in a similar way as in Case 1 and Case 2, and increase in throat area as in Case 3, simulation of reduction of

compressor mass flow was achieved by scaling compressor mass flow calculated via the performance map as a function of engine speed and pressure ratio. Just for the case with decreased compressor mass flow it was found for simulation model to predict acceleration of the engine to a higher speed for the purpose of attaining the nominal value for mass flow. This was achieved by the sole increase in engine speed without causing any change in any other flow or engine parameter. Hence, the effect of mass flow reduction is increase in engine speed.

Numerical values for component deterioration assumed in the four simulation cases were taken from the literature. In Reference 34, Zhu and Saravanamuttoo used an engine model for an industrial gas turbine to simulate the effects engine deterioration. Among simulated cases was a scenario in which mechanical damage to the low pressure compressor led to a 5% drop in efficiency, mechanical damage to high pressure turbine led to a 5% efficiency decrease, and high pressure turbine erosion led to increase in throat area by 2%. In Reference 35 Kurz and Brun described performance deterioration of an engine which was exposed to jet engine exhaust and salt air. Authors simulated this condition by decreasing compressor efficiency by 2.1%, mass flow and pressure ratio by 5% and gas generator turbine efficiency by 0.5%.

## **6.2 Simulation Results**

To analyze the effect of each fault scenario, the model with included degradation effects was run for different regimes of fuel mass flow which was varied between 100% and 20% of the nominal value. Steady state simulation results are shown in Figures 6.1 to 6.3 where they are compared against nominal engine data. Steady state parameters of the engine for the four cases of engine degradation are given in Tables 6.1 and 6.2: former presents engine parameters for 100% nominal fuel mass flow regime, and the latter for gas generator turbine inlet temperature of 1575 Kelvin, a value which was assumed to represent the highest allowable limit for the TIT at which no mechanical damage was caused to turbine blades as long as the duration of such operating condition was short. Analysis at the maximum TIT was deemed important to assess in more clarity the effect of each deterioration case on the maximum power output of the engine operating under ISA SLS conditions.

Shown in Figure 6.1 is the variation of engine speed as a function of fuel flow. As can be seen in the figure, for a given fuel mass flow regime engine speed decreases from its nominal value for all cases of engine deterioration. The largest decrease in engine speed is seen to occur for Case 2 in which gas generator turbine was operated with reduces efficiency. This result is expected since decrease in gas generator turbine efficiency has a direct impact on engine speed: decrease in component efficiency reduces the enthalpy drop across the turbine and hence engine speed decreases because the turbine can no longer sustain the power levels required by the compressor. Other cases are found to produce an almost equal decrease in engine speed down to approximately 80 grams per second of fuel flow at which point with decreasing fuel flow Case 1 begins to deviate from nominal data by a larger extent. In most of the operating range decrease of engine speed for Cases 3 and 4 are almost identical.

As shown in Table 6.1, engine speed due to compressor mechanical damage decreases by 2.2% at nominal fuel flow regime. Gas generator mechanical damage is seen to produce a substantial 3.1% decrease in the speed of the engine. Speed reduction for Case 3 is small, and constitutes 1.9% of the nominal value. The cumulative effect of degradation of multiple components results in the lowest speed decrease of 1.6%. This small reduction in engine speed is attributed to the increase of compressor speed to attain a higher mass flow rate.

**Table 6.1: Engine parameters for 100% nominal fuel flow regime for difference cases of engine deterioration**

	$N_1$ (%)	Power (hp)	TIT (K)	SFC ( $\frac{kg}{hp \cdot h}$ )
Nominal	100.0	1768.41	1525.457	0.2044
Case 1	97.83 (-2.2%)	1722.19 (-2.6%)	1576.37 (+3.3%)	0.2099 (+2.7%)
Case 2	96.91 (-3.1%)	1695.75 (-4.1%)	1578.15 (+3.5%)	0.2132 (+4.3%)
Case 3	98.07 (-1.9%)	1736.31 (-1.8%)	1545.23 (+1.3%)	0.2082 (+1.9%)
Case 4	98.35 (-1.6%)	1683.61 (-4.8%)	1583.58 (+3.8%)	0.2147 (+5.0%)

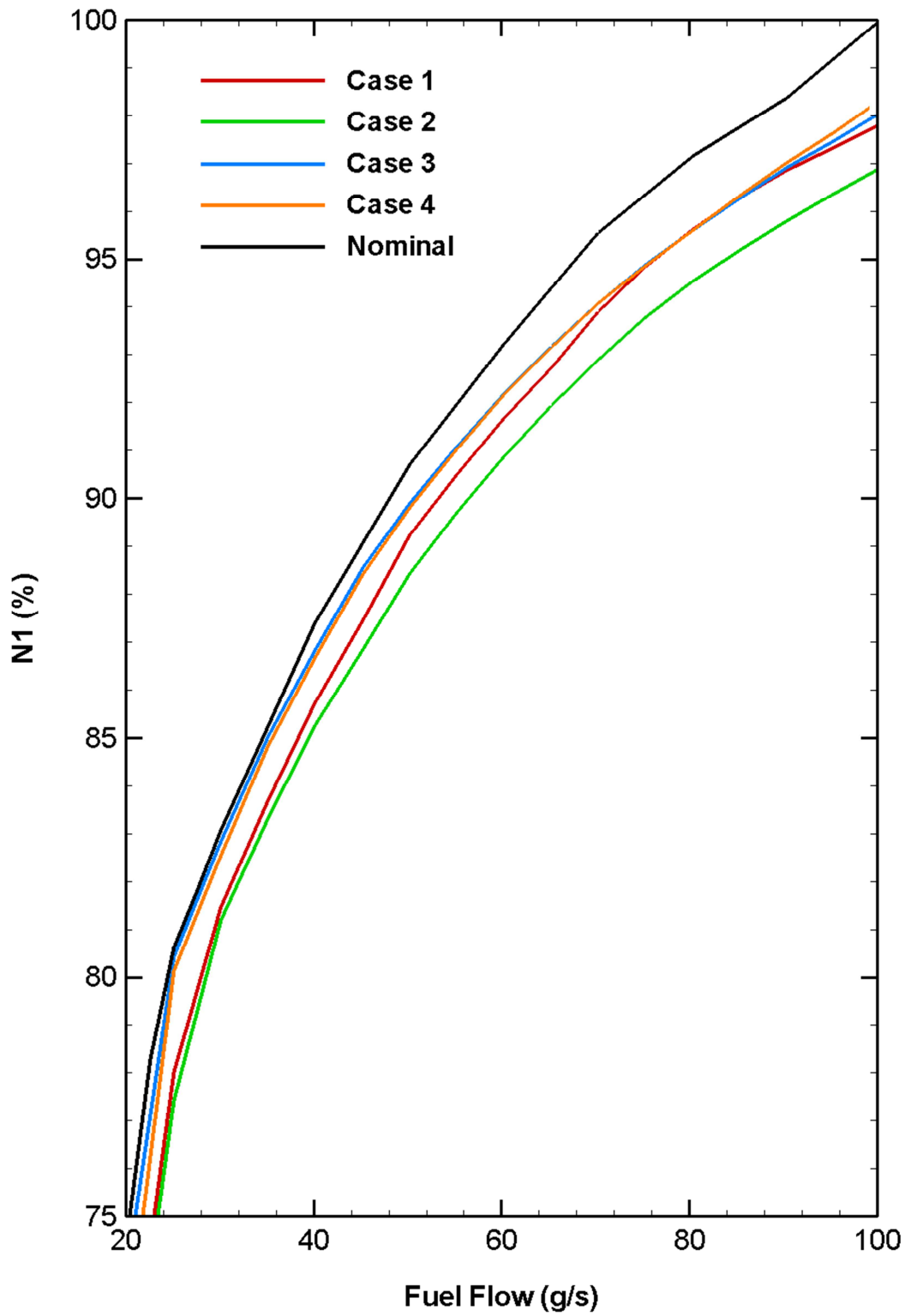


Figure 6.1: Variation of gas generator speed with fuel flow for different cases of engine deterioration

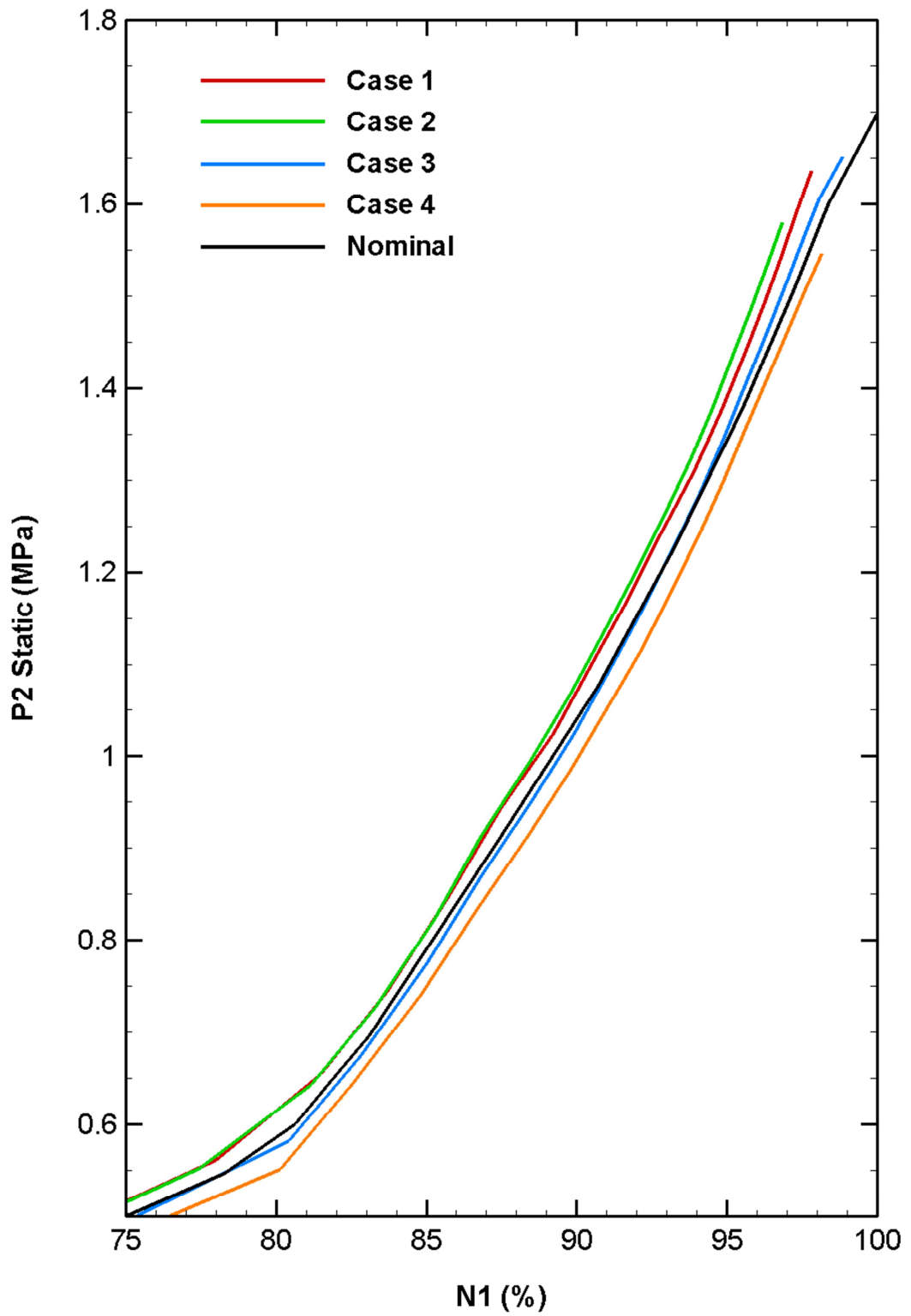


Figure 6.2: Variation of compressor outlet static pressure with gas generator speed for different cases of engine deterioration

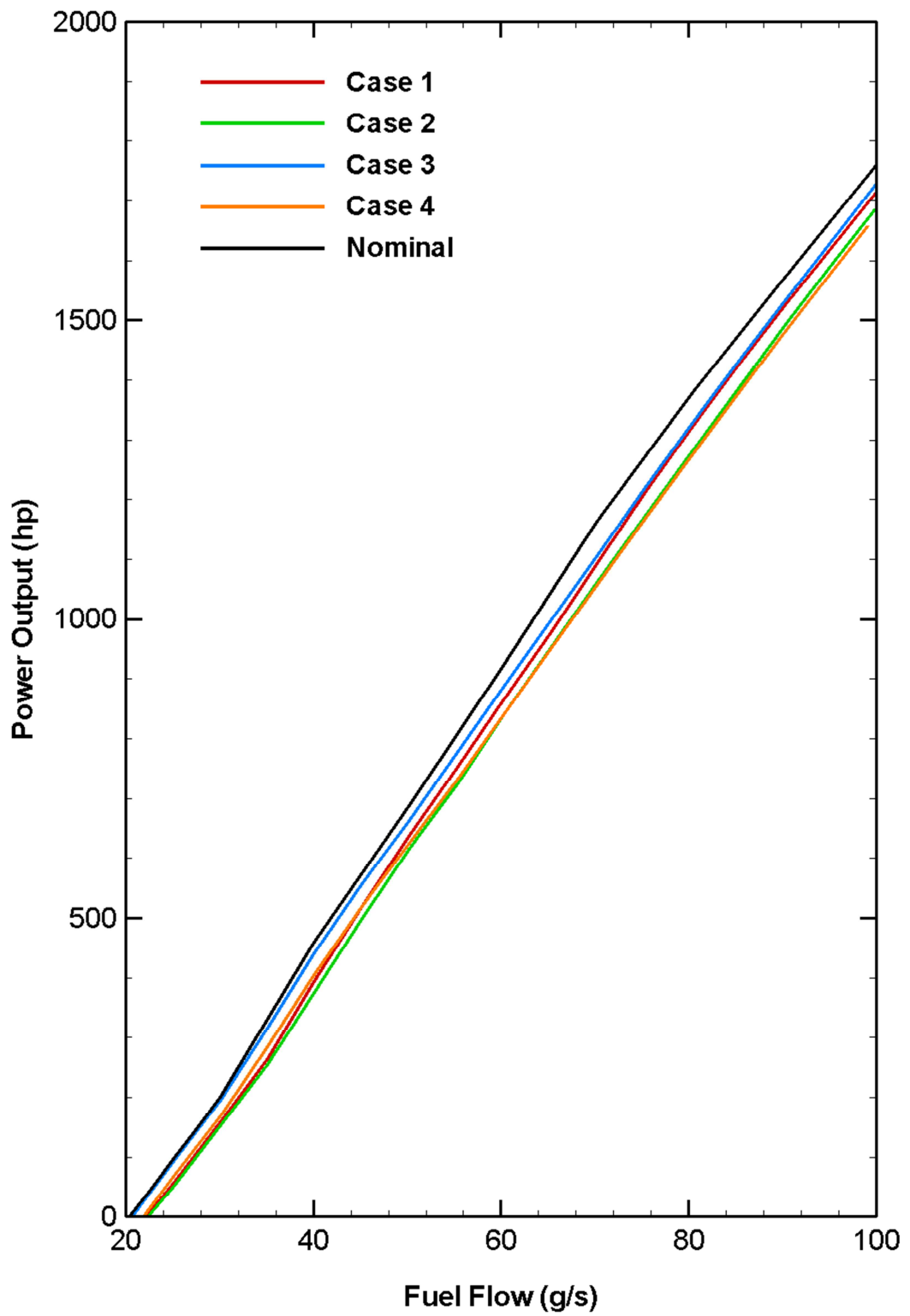


Figure 6.3: Variation of output power with fuel flow for different cases of engine deterioration

Figure 6.2 shows variation of compressor outlet static pressure as a function of engine speed. All the curves except for the nominal data were cropped for values at which gas generator turbine inlet temperatures exceeded the maximum value of 1575 Kelvin. As seen in the figure, for a given compressor outlet static pressure Case 2 results in the lowest engine speed. Case 1 is observed to produce an effect identical to that of Case 2 with only some slight deviations for engine speeds between 88% and 97%. In the operating range shown in Figure 6.2, Case 3 simulation results match fairly well with nominal performance data, while Case 4 produces the lowest pressure for a given engine speed.

Figure 6.3 gives the variation of power output as a function of fuel flow. For all simulated cases of engine deterioration, power output of the engine is seen to decrease. The most reduction is seen to occur for Cases 2 and 4 which for most of the operating range are almost coincident with each other. The substantial 4.1% decrease in power output (Table 6.1) in Case 2 is due to the decrease in power production of the gas generator turbine. As a result, the engine decelerates which leads to a reduction of ingested air mass flow and hence decrease in power output of the free turbine. The cumulative effect of engine deterioration as was simulated in Case 4 is to reduce power output by 4.8% and increase specific fuel consumption by 5%. Again, in Table 6.1 the power output for Case 1 is seen to decrease by 2.6% from the nominal. The least drop in power delivery of the engine is observed to occur in the case with eroded gas generator turbine: power decreases by about 1.8%, while specific fuel consumption increases by approximately the same amount.

Shown in Figure 6.4 is the plot of compressor operating lines. In all cases of engine deterioration compressor running lines are seen to shift towards the surge line, which is a common effect when engine operates under conditions that are far from the nominal. The largest decrease in stability margin is observed to occur for Case 2. Case 1 and Case 4 produce almost identical reductions in the surge margin, and the two fall very close to the running line produced by Case 2. Out of all simulated deterioration scenarios, Case 3 produces the least decrease in the surge margin of the compressor, and actually for low engine speeds it is even seen to produce a better surge margin than does the engine in its nominal operating state.

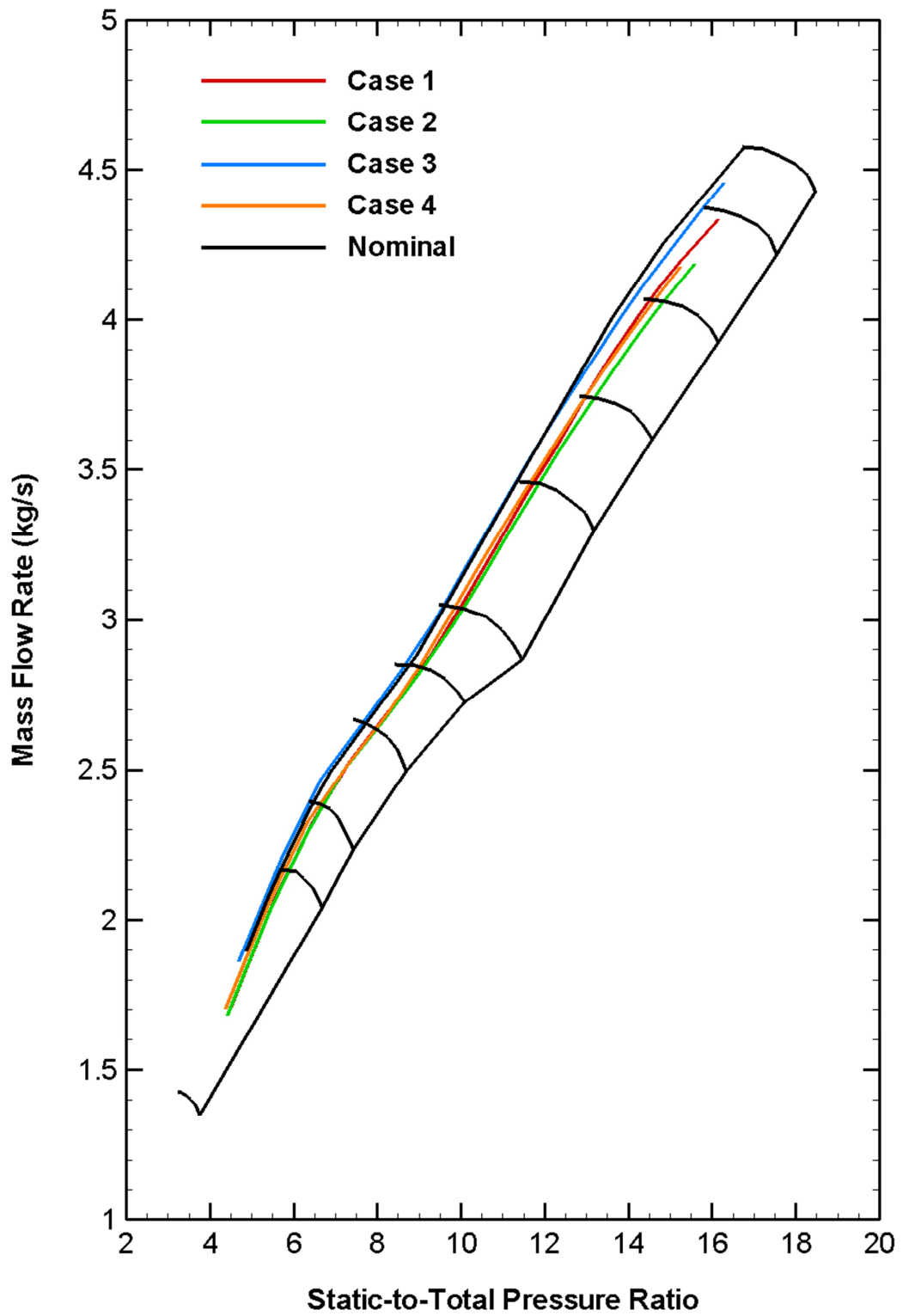


Figure 6.4: Compressor operating lines for different cases of engine deterioration

Presented in Table 6.2 are steady state parameters of the engine for the case in which gas generator turbine inlet temperature was set to 1575 degrees Kelvin. With increase in the value of turbine inlet temperature, the extent of degradation of engine performance due to component deterioration is rendered more apparent, thus allowing for a better comparison of each deterioration scenario relative to the others. When compared to nominal engine data at steady state, the cumulative effect of engine degradation simulated in Case 4 is to result in power reduction by a substantial amount of 10% and increase in specific fuel consumption by 11%. Similar performance degradation is observed to occur for the case with gas generator mechanical damage: 8.4% drop in power output and increase is specific fuel consumption by 9.1%. For the case with compressor mechanical damage output power decrease is a moderate 6.6% of the nominal with increase in the value of specific fuel consumption by 7%. As in steady state results presented in Figures 6.1 to 6.3, Case 3 is once again seen to produce very little loss in the performance of the engine: 0.6% power decrease with an increase in specific fuel consumption by 0.5%.

**Table 6.2: Engine steady state parameters for difference cases of engine deterioration  
(TIT = 1575 K)**

	$g_b$ (g/s)	$N_1$ (%)	Power (hp)	SFC $\left(\frac{kg}{hp \cdot h}\right)$
Nominal	104.2	100.55	1840.52	0.204
Case 1	100.22 (-3.8%)	97.81 (-2.7%)	1718.18 (-6.6%)	0.2183 (+7.0%)
Case 2	99.94 (-4.1%)	96.85 (-3.7%)	1686.15 (-8.4%)	0.2225 (+9.1%)
Case 3	105.20 (+1.0%)	98.85 (-1.7%)	1829.02 (-0.6%)	0.2051 (+0.5%)
Case 4	99.07 (-4.9%)	98.16 (-2.4%)	1656.81 (-10%)	0.2264 (+11%)

To summarize the results of the study, Case 2 in which simulated was the gas generator turbine mechanical damage which led to a 5% decrease in turbine efficiency, produced significant degradation of engine performance. For nominal fuel flow regime, this deterioration scenario was characterized by substantial decrease in power output and engine speed, which was also seen to be the case for engine steady state operation at gas generator turbine inlet temperature of 1575 Kelvin. The most significant deterioration of

engine performance was observed to occur for Case 4 in which both the compressor and turbine were assumed to have degraded with time. The characteristics of simulated deterioration scenario were the substantially decreased power output and some moderate decrease in engine speed. Erosion of the gas generator turbine with increase in the throat area by 2% was found to produce only small degradation of engine performance: for nominal fuel flow regime power loss was no larger than 1.8%. An even smaller reduction of engine power was seen to occur for TIT of 1575 Kelvin: a minor 0.6% drop from the nominal value.

## CHAPTER 7

### REAL TIME IMPLEMENTATION OF AEROTHERMAL MODEL

For the reason that aerothermal models achieve high levels of accuracy in simulating performance and transient dynamics of aero-engines, these constitute a solid foundation for development of engine control systems. Once tested and validated on the model which substitutes a test bed, developed control systems can be readily used on the real engines. By doing so, it becomes possible to prevent the possibility of incurring any damage to the real engine with a faulty control system. However, because increasing the level of physical accuracy of an aerothermal model by decreasing simulation time step and increasing the amount of calculations per each engine cycle for the purpose of designing more accurate control systems, developed engine models may lack real time capability, which is a must for developing such systems. Moreover, in order to obtain an accurate simulation model, it must display numerical stability at all times, which is a condition dictated directly by the choice of simulation time step. In Chapter 3 it was discussed that numerical stability of developed aerothermal model could be attained only for simulation time steps equal to, and smaller than  $10^{-4}$  seconds. It was shown that for time steps larger than  $10^{-4}$  seconds numerical instabilities caused cyclic oscillations in the outlet pressure of the second plenum which then propagated into the upstream and downstream of the engine via gas generator speed and pressure ratio, respectively. At the largest allowable simulation time step of  $10^{-4}$  seconds, however, it was not possible to realize real time capability of the model. This problem was overcome by scaling plenum volumes with simulation time step. By considering Equation 2.54 which defines Euler integration, change of simulation time step was reflected on the pressure integration, i.e.  $\frac{dP}{dt} \cdot \Delta t$  with  $\frac{dP}{dt}$  term per Equation 2.48 being directly proportional to the plenum volume parameter, in a way that preserves the product

of simulation time step with plenum volume parameter. Mathematically, time scaling of plenum volumes is defined by Equation 7.1:

$$(K_V \cdot \Delta t)_{\Delta t_1} = (K_V \cdot \Delta t)_{\Delta t_2} \quad [7.1]$$

Using the definition of volume parameter, Equation 7.1 can be written as follows:

$$\left(\frac{\Delta t}{V}\right)_{\Delta t_1} = \left(\frac{\Delta t}{V}\right)_{\Delta t_2} \quad [7.2]$$

Thus, if the simulation time step is varied by some factor, so must be the volume of the plenum. In other words, increasing simulation time step by, for example, a factor of five will require an increase in plenum volume by the same factor to, per Equation 7.2, keep the ratio of the two parameters constant. The idea behind this approach originates from the simple fact that a smaller volume will respond to perturbations much faster than would a larger volume. To accurately capture fast volume dynamics, use of a simulation time step smaller than the one used in the case of a larger volume is required, thus hindering the ability of the model to perform calculations in real time. Then, for the purpose of achieving real time capability, it is adequate to increase plenum volume for which a larger simulation time step can be employed.

A detailed description and successful application of time scaling of plenum volumes for real time realization of an aerothermal model is given in Reference 36. In their 9-state-vector aerothermal model for a military turbofan engine, Sanghi and Lakshmanan encountered stability issues for simulation time steps greater than  $10^{-4}$  seconds at which real-time implementation of the model was unattainable. By reducing the model to a 6-state-vector one in which engine operating point was uniquely defined by six parameters, it was possible to increase simulation time step by a factor of three. Real time capability was achieved by a further increase in simulation time step with application of time scaling of plenum volumes by a factor of four. It was shown by the authors that resulting model with simulation time step of 1.2 milliseconds produced negligible deviations from simulation results obtained with a time step of  $3 \cdot 10^{-4}$  seconds. Not only was the accuracy of the original 6-state model preserved, but numerical stability also achieved despite the increase in time step. It was, therefore, shown the possibility of real time implementation of an

aerothermal model by time scaling of plenum volumes at almost no cost of simulation accuracy and numerical stability.

In the current model, in attempt to decrease CPU time required per each second of simulation time, time scaling of plenum volumes was applied in accordance with Equation 7.2. To understand whether time scaling was to be applied to all plenum volumes at once or the smallest volume alone, each of these cases was run at a simulation time step of  $5 \cdot 10^{-4}$  seconds for step increase in fuel mass flow from 400 to 775 lbm/h. Simulation results are shown in Figures 7.1 and 7.2 where they are compared against baseline solution (i.e. model results obtained with time step of  $10^{-4}$  seconds without application of time scaling of plenum volumes) in terms of pressures at the outlets of the first and second plena (results were normalized with respect to design point parameters).

Baseline solution is indicated with solid red line. Indicated with solid blue line are simulation results obtained with the model in which only the volume of the smallest plenum (i.e. plenum between the turbines) was scaled with time (Case 1). As clearly shown in Figure 7.1, pressure dynamics predicted by the two models match very well. Only some minor discrepancies in the power turbine inlet pressure are observed in the second plot of the figure which shows the first 0.1 seconds after the application of step input in fuel mass flow. Solid green line shows simulation results obtained by scaling of both plenum volumes with simulation time step (Case 2). As can be seen in Figure 7.1, simulation results for Case 2 deviate to considerable extent from the baseline and yield a relative maximum error of 8.4%.

Shown in Figure 7.2 is the variation of compressor outlet static pressure. Again, considerable differences in pressure dynamics are observed between Case 2 and baseline solution results. The match between baseline model and Case 1 is once again perfect. All these findings are consistent with Sanghi and Lakshmanan [Ref. 37] who also arrived at the conclusion that time scaling of all plenum volumes results in wrongful engine dynamics: because the new simulation time step which was obtained by increasing the baseline time step (i.e.  $10^{-4}$  seconds for the current study) by some factor is still sufficient to accurately resolve pressure variations at plena having larger volumes, application of time scaling to these plena will result in the damping of pressure dynamics. It thus follows that time scaling of plenum volumes should be applied only to the plena having the smallest volumes.

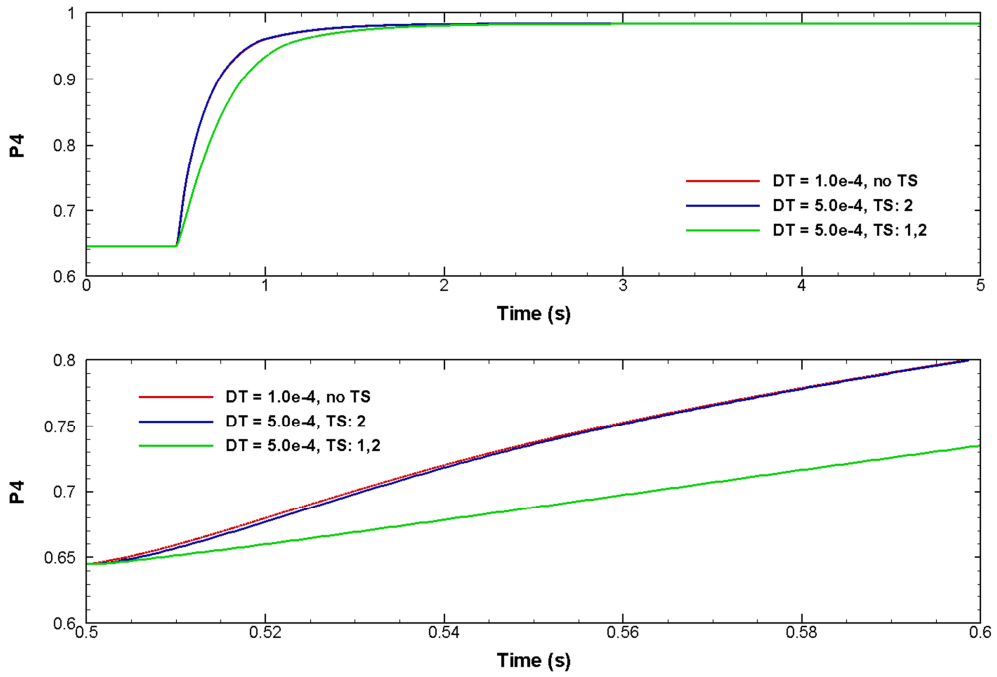


**Figure 7.1: Response of power turbine inlet pressure to step increase in fuel flow from 400 to 775 lbm/h (50.4 to 97.65 g/s) for the two cases of volume time scaling**

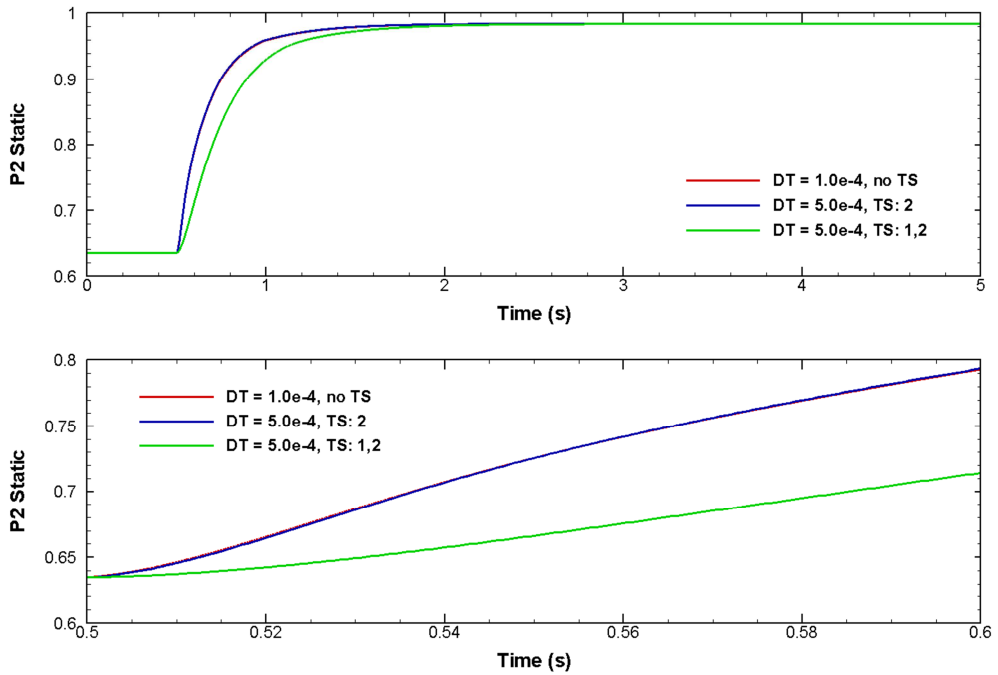


**Figure 7.2: Response of compressor outlet static pressure to step increase in fuel flow from 400 to 775 lbm/h (50.4 to 97.65 g/s) for the two cases of volume time scaling**

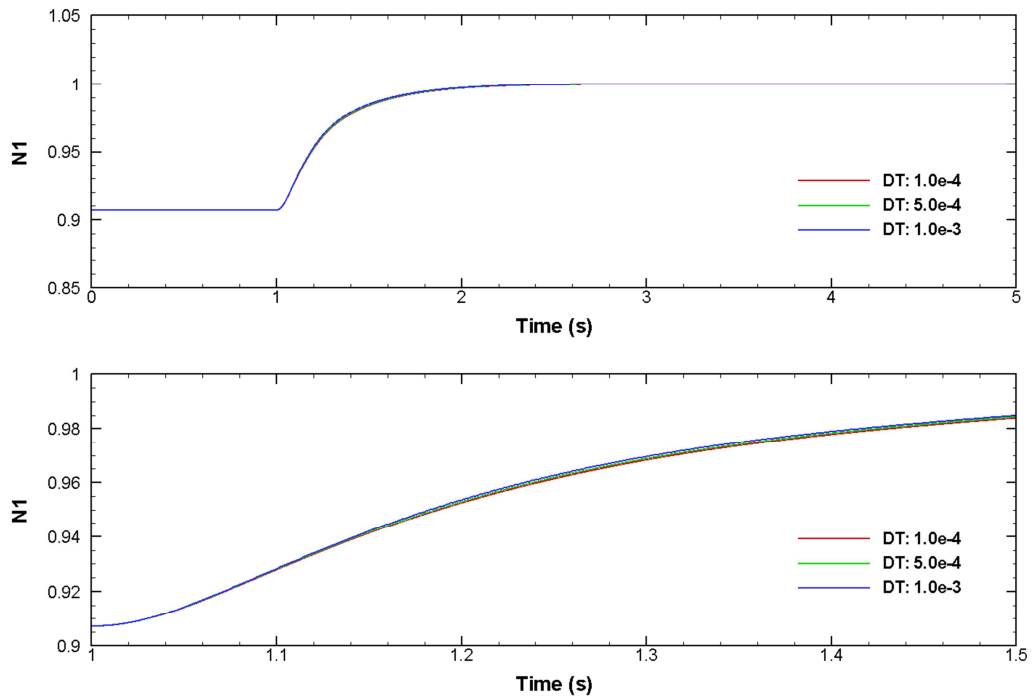


**Figure 7.3: Gas generator speed dynamics as a function of simulation time step for step increase in fuel flow from 50% to 100% of design value**

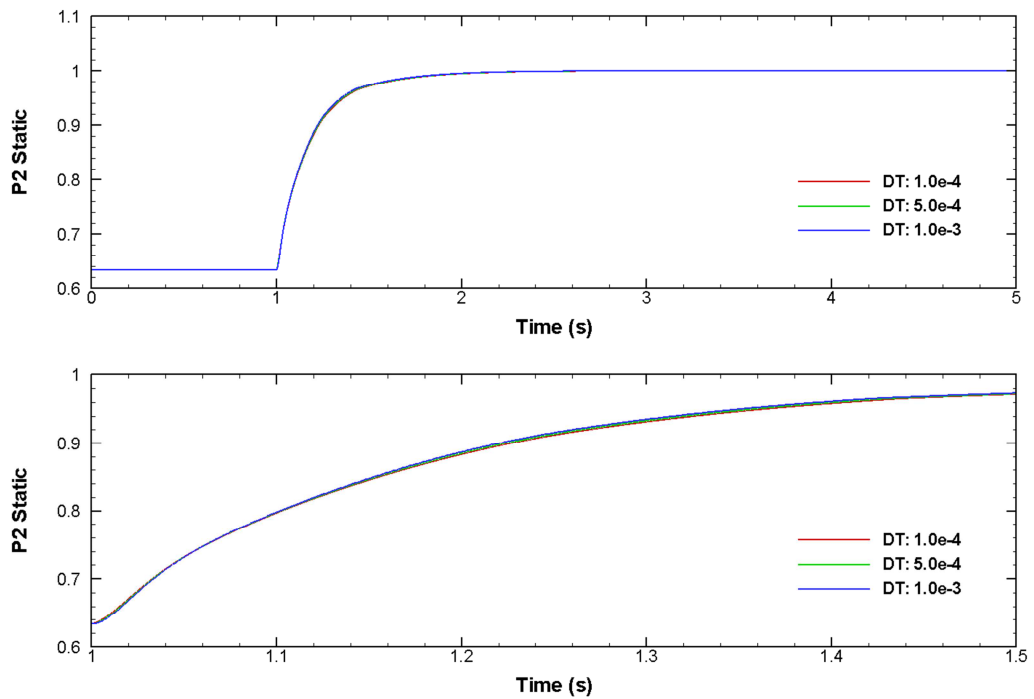


**Figure 7.4: Compressor outlet static pressure dynamics as a function of simulation time step for step increase in fuel flow from 50% to 100% of design value**

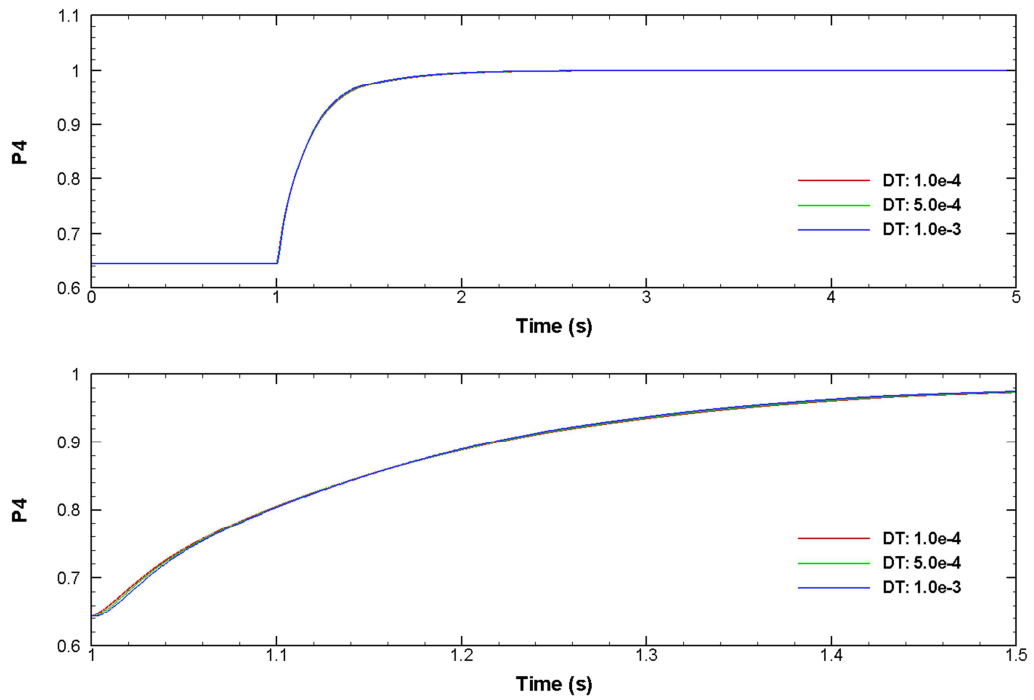


**Figure 7.5: Gas generator outlet pressure dynamics as a function of simulation time step for step increase in fuel flow from 50% to 100% of design value**

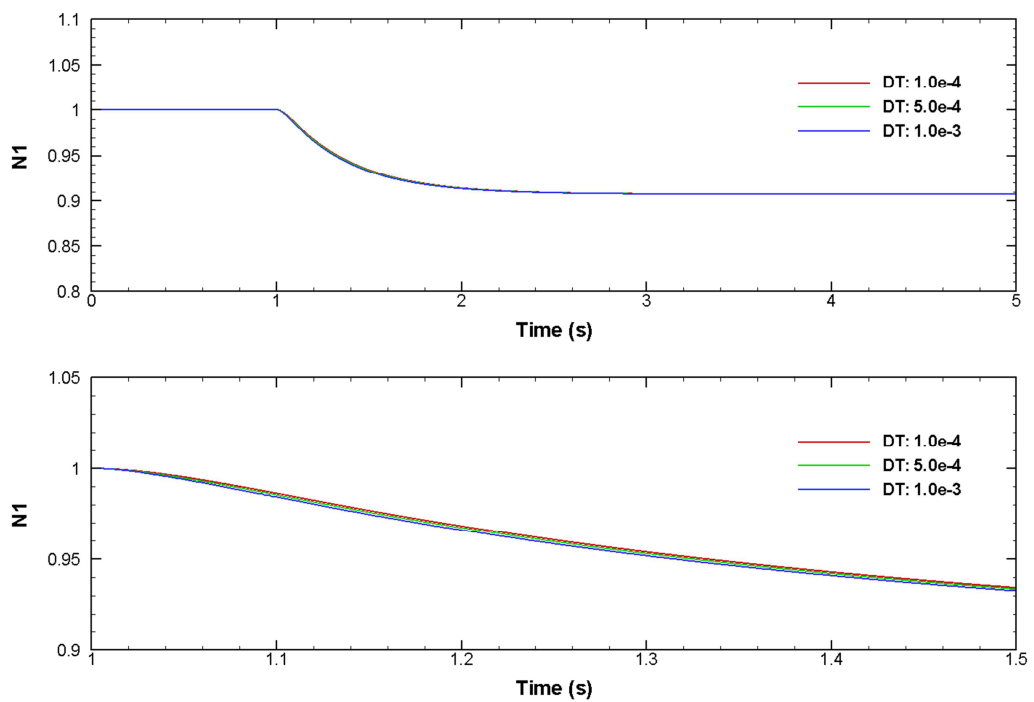


**Figure 7.6: Gas generator speed dynamics as a function of simulation time step for step decrease in fuel flow from 100% to 50% of design value**

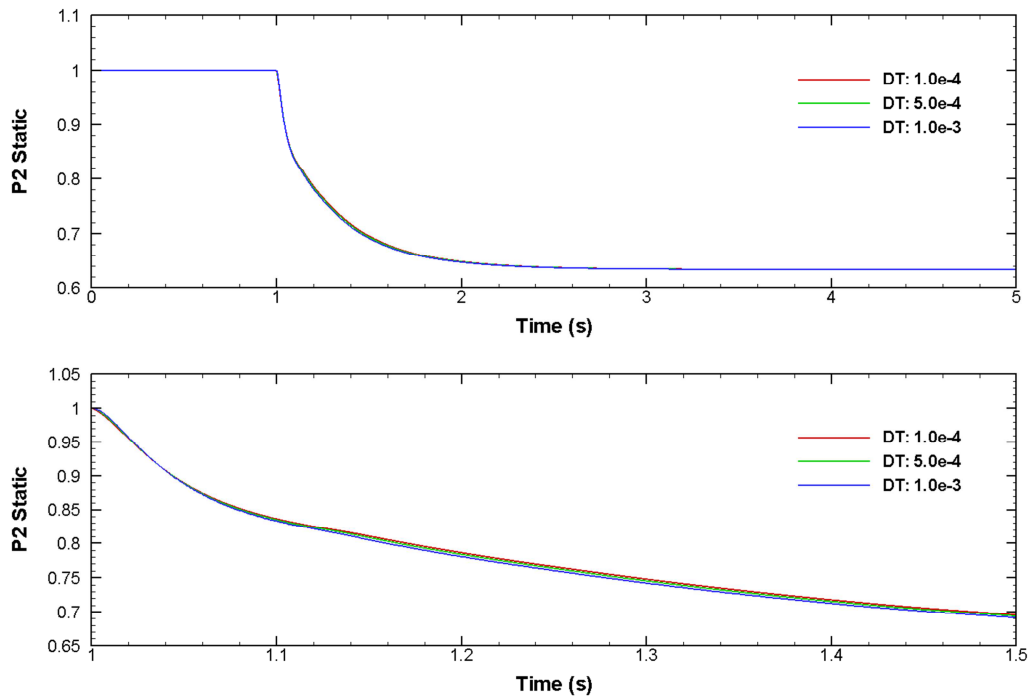


**Figure 7.7: Compressor outlet static pressure dynamics as a function of simulation time step for step decrease in fuel flow from 100% to 50% of design value**

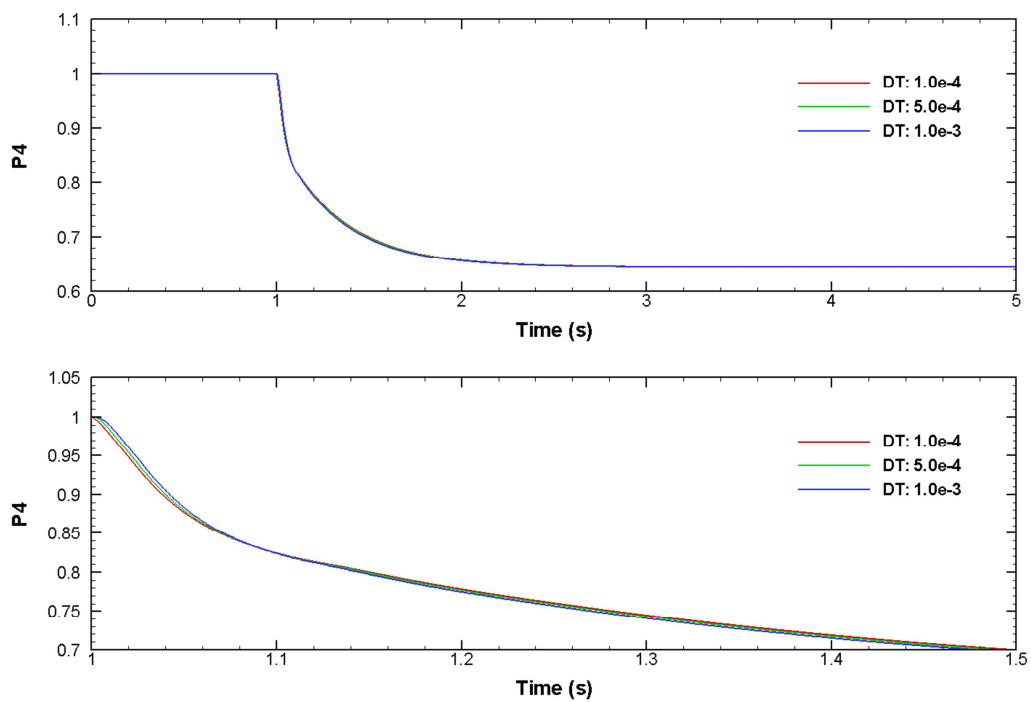


**Figure 7.8: Gas generator outlet pressure dynamics as a function of simulation time step for step decrease in fuel flow from 100% to 50% of design value**

In the current model, time scaling was applied to the second plenum as it had the smallest volume, and simulations were performed for time steps of  $5 \cdot 10^{-4}$  and  $10^{-3}$  seconds. Simulation results are given in normalized form for the gas generator speed and plenum outlet pressures, and are shown in Figures 7.3 to 7.5 for the case of step increase, and in Figures 7.6 to 7.8 for the case of step decrease in fuel flow.

Numerical stability was achieved for all time steps by scaling the volume of the second plenum in accordance with Equation 7.2. Engine dynamics obtained from simulations with increased time steps are seen to exhibit negligible deviations from the baseline. The largest deviations are observed to occur in the outlet pressure of the second plenum for a short duration starting from the moment of application of step input in fuel mass flow (Figure 7.8, second plot).

Table 7.1 presents maximum errors calculated with respect to the baseline solution for 4 different engine parameters. The smallest errors are generated for simulation time step of  $5 \cdot 10^{-4}$  seconds. As shown in the table, doubling of the time step results in increase of the relative error by an approximate factor of two. The errors peak at a value of 1.37% for the power turbine inlet pressure, and 1.33% for the gas generator turbine inlet temperature. Keeping in mind that these values correspond to the cases of step increase in fuel flow from 50% to 100% and step decrease from 100% to 50% of design value, relative errors which would be generated in a typical simulation with a realistic fuel variation will be much smaller. Therefore, magnitudes of relative errors presented in Table 7.1 fall within the tolerance band for a high-fidelity simulation model.

**Table 7.1: Percent errors introduced with time scaling of plenum volumes**

	Step Increase		Step Decrease	
	$\Delta t = 5 \cdot 10^{-4}$	$\Delta t = 10^{-3}$	$\Delta t = 5 \cdot 10^{-4}$	$\Delta t = 10^{-3}$
$N_1$	0.06	0.14	0.1	0.23
$P_2$	0.185	0.44	0.34	0.77
$T_3$	0.6	1.33	0.34	0.76
$P_4$	0.51	1.14	0.61	1.37

Table 7.2 shows the amount of CPU time it took to complete one second in simulation environment. Taking more than 5 seconds per each simulation second, baseline model exhibits the worst performance. Increase in simulation time step by a factor of 5 times decreases CPU time by approximately the same amount down to a value slightly larger than unity. At this point, developed SIMULINK® model can either be converted to a much faster C++ code to offer real time capability, or CPU time can be decreased by further increase in simulation time step and application of appropriate time scaling of plenum volume bearing in mind the rule of increasing errors (Table 7.1). Then, the simulation time step can be increased further to  $10^{-3}$  seconds and model can be run in real time directly in SIMULINK®. By taking approximately half a second of CPU time per each second of the simulation, this time step not only enables real time implementation, but also allows for further improvement of the model by inclusion of various engine-related phenomena such as calculation of engine emissions, modeling of engine surges etc. Thus, at very small cost of numerical accuracy, simulation time step of 1 millisecond offers considerable savings in computational time which can be effectively used for further development of the model.

**Table 7.2: CPU time per one second of simulation measured for different time steps**

<b>Simulation Time Step (seconds)</b>	<b>CPU Time (seconds)</b>
$10^{-4}$	5.67
$5 \cdot 10^{-4}$	1.117
$10^{-3}$	0.56

## CHAPTER 8

### DEVELOPMENT OF A GENERIC AEROTHERMAL MODEL

Developed aerothermal model for the T700 turboshaft engine included empirical relations which were used to evaluate specific heat capacities at different stations of the engine and enthalpy drop parameters for the turbines. Therefore, application of the model to simulate steady state and transient performance of another engine was impossible. To make the model generic, characteristics of the T700 engine were scaled with respect to design point parameters of the engine, and enthalpy-temperature relations were replaced with curve-fits for evaluation of specific heat capacities.

#### 8.1 Evaluation of Specific Heats

Curve fits for evaluation of specific heat values as a function of temperature and gas composition were previously published in the literature [Ref. 26]. These relations were implemented in the current model in the form of a function block which accepted two inputs: temperature of the flow and fuel-to-air ratio. The output was the value for specific heat capacity which, depending on the inputs, was evaluated by using one of the following relations.

Specific heat for air in 200 – 800 Kelvin temperature range:

$$C_{p_a} = 1.0189 \cdot 10^3 - 0.13784 \cdot T + 1.9843 \cdot 10^{-4} \cdot T^2 + 4.2399 \cdot 10^{-7} \cdot T^3 - 3.7632 \cdot 10^{-10} \cdot T^4 \quad [8.1]$$

Specific heat for air in 800 – 2200 Kelvin temperature range:

$$C_{p_a} = 7.9865 \cdot 10^2 + 0.5339 \cdot T - 2.2882 \cdot 10^{-4} \cdot T^2 + 3.7421 \cdot 10^{-8} \cdot T^3 \quad [8.2]$$

Specific heat for the gas is evaluated as a function of fuel-to-air ratio:

$$C_{p_g} = C_{p_a} + B_t \cdot \frac{FAR}{FAR + 1} \quad [8.3]$$

Where  $B_t$  in the 200 – 800 Kelvin temperature range is given as:

$$B_t = -3.59494 \cdot 10^2 + 4.5164 \cdot T + 2.8116 \cdot 10^{-3} \cdot T^2 - 2.1709 \cdot 10^{-5} \cdot T^3 \\ + 2.8689 \cdot 10^{-8} \cdot T^4 - 1.2263 \cdot 10^{-11} \cdot T^5 \quad [8.4]$$

$B_t$  for 800 – 2200 Kelvin range:

$$B_t = 1.0888 \cdot 10^3 - 0.1416 \cdot T + 1.916 \cdot 10^{-3} \cdot T^2 - 1.2401 \cdot 10^{-6} \cdot T^3 \\ + 3.0669 \cdot 10^{-10} \cdot T^4 - 2.6117 \cdot 10^{-14} \cdot T^5 \quad [8.5]$$

Enthalpy at turbine outlets was evaluated by using scaled T700 characteristic maps for enthalpy drop parameter for the gas generator and power turbines. Then, turbine outlet temperatures were calculated by using an iterative process in which an initial guess for the unknown value of the true temperature was required. The value of specific heat capacity was evaluated as a function of guessed temperature and fuel-to-air ratio, and the new guess for the unknown temperature was obtained through Equation 8.6 by using the known value of enthalpy. This iteration process was continued until calculated enthalpy matched its known value.

$$h = C_p(T, FAR) \cdot T \quad [8.6]$$

Thus, an iterative calculation technique was used to evaluate flow properties at turbine outlets. This iterative method, however, was found to occasionally enter an infinite loop in which temperature was iterated for between two repeating values. To eliminate this problem, evaluation of the temperature using Equation 8.6 was bounded with a loop of 20 iterations. Then, bisection method was applied to calculate the exact value of the unknown temperature which yielded an enthalpy value residing in the  $10^{-8}$  tolerance band from the known value of enthalpy.

## 8.2 Scaling of Component Maps

The following scaling factors were taken from Reference 38 and used to scale turbine maps of the GE T700 with respect to design operating point parameters of the engine:

$$SF_g = \frac{g}{g_{des}} \quad [8.7]$$

$$SF_\pi = \frac{\pi - 1}{\pi_{des} - 1} \quad [8.8]$$

$$SF_\tau = \frac{\tau^\alpha - 1}{\tau_{des}^\alpha - 1} \quad [8.9]$$

$$\alpha = \frac{\gamma}{\gamma - 1} \quad [8.10]$$

Per Equation 8.7, mass flows were scaled linearly. This definition was employed to scale mass flow parameter on the T700 power turbine map. For a turbine, Equation 8.8 scales down the pressure ratio of the component which, contrary to the definition employed until so far, is defined as the ratio of inlet pressure to the outlet pressure to yield a value greater than unity. Equation 8.9 was used to scale the temperature ratio map of the compressor. This way, efficiency variation defined for the T700 engine in terms change of temperature ratio across the compressor as a function of static-to-total pressure ratio was transferred to the generic model.

Turbine maps given for T700 engine were defined in terms of critical velocity parameter as given by Equations 2.33 and 2.43. By using the same definitions of critical velocities in the generic model, T700 turbine maps were used in the simulation of a characteristically similar engine by scaling them with the enthalpy drop parameter:

$$SF_{\Delta h} = \frac{\Delta h / \theta_{cr}}{(\Delta h / \theta_{cr})_{DP}} \quad [8.11]$$

### 8.3 Steady State Simulation of Lycoming T53-L11 Turboshaft Engine

Generic model was used to simulate steady state performance of Lycoming T53-L11 turboshaft engine. Similar in aerothermodynamic configuration to the GE T700, T53 has a 5 stage axial compressor followed by a radial compressor. Gas generator turbine consists of a single stage that drives the compressor. Power shaft is driven by the single-stage free turbine. Both turbines are uncooled. Data for design point parameters of the engine found in Reference 39 is presented in Table 8.1.

**Table 8.1: Lycoming T53-L11 design specifications [Ref. 39]**

Engine Parameter	Value
Gas Generator Speed	97.8% (100% = 25150 RPM)
Compressor Pressure Ratio	6.2:1
Mass flow rate	4.85 kg/s
Power Output	1070 HP

Initialization of the model was done by using engine thermodynamics to calculate design point engine parameters and flow properties at all stations of the engine. Since engine design speed was specified as 97.8%, all thermodynamic calculations were based on the data given for this particular speed (i.e. data shown in Table 8.1).

Compressor map of T53-L11 engine was adopted from Reference 39. However, due to limited amount of speed lines, linear interpolation for design speed of 97.8% between 100.4% and 93.4% speed lines did not yield the design mass flow and pressure ratio values as they are given in Table 8.1. Therefore, 97.8% speed line was added to the compressor map by applying linear interpolation between 100.4% and 93.4% speed lines using the known design values for compressor mass flow and pressure ratio.

As in the case with T700 engine, gas generator turbine of Lycoming T53 was assumed to operate under choked flow condition at all times. This assumption allowed evaluation of turbine mass flow rate using Equation 2.29.

Because no information about component efficiencies of the T53 engine was mentioned in the literature, compressor and gas generator efficiencies had to be assumed. As for the power turbine, component efficiency was calculated using the known amount of power it generated at design conditions. By using steady state simulation results and T53 data presented in Reference 39, it was possible to estimate the design value of fuel flow which served as a reference in estimating a value for the gas generator turbine inlet temperature. Then, design point parameters of Lycoming T53 engine were estimated by performing a thermodynamic analysis of the engine to produce the closest match to steady state performance results reported in Reference 39. These parameters are presented in Table 8.2.

**Table 8.2: Estimated performance parameters for Lycoming T53-L11**

<b>Parameter</b>	<b>Value</b>
Gas generator inlet temperature	1090 <i>Kelvin</i>
Fuel mass flow	93.763 <i>g/s</i>
Compressor isentropic efficiency	0.82
Gas generator turbine isentropic efficiency	0.86
Mechanical efficiency of the shaft	1.0
Combustor efficiency	0.95
Combustor pressure loss coefficient	0.96

Steady state simulation results are presented in Figures 8.1 to 8.3. A total of 4 different models were used to simulate the T53 turboshaft engine. Model 1 was based on constant efficiencies for the compressor, gas generator and power turbines. Mass flow of the power turbine was defined in terms of scaled T700 map. In Model 2, compressor and turbines were modeled using scaled T700 component maps. In Model 3, T700 component maps were used to model the compressor and power turbine, while gas generator turbine was modeled using variation of component efficiency as a function of component pressure ratio and rotational speed. Efficiency variation of a single stage of a two-stage turbine was taken from Reference 40, scaled with respect to design parameters of the turbine, and applied in the simulation of T53 engine. In Model 4, compressor and gas generator turbine were

modeled using constant efficiencies, while mass flow and enthalpy drop characteristics for the power turbine were defined by using scaled T700 component maps. Results of the four models were compared against T53 specification data which was reported in Reference 39 (to be referred to as “reference data” in the remaining of this chapter). In order to simplify the evaluation of engine parameters using component efficiencies, specific heat capacity ratios were assumed to remain constant at 1.4 at for air, and at 1.33 for gas. Moreover, the difference between specific heat capacity values at the inlet and outlet of the compressor and turbines was assumed to be negligible to allow for their cancelling.

Shown in Figure 8.1 is the change of fuel flow as a function of gas generator speed. A good match between T53 data and Model 1 is obtained for engine speeds between 97.8% and 85%. For lower engine speeds, T53 data deviates from an almost linear variation of Model 1 to higher fuel flow demand for a given engine speed. Results for Model 2 and Model 3 show considerable deviation from the reference data and Model 1 results.

Figure 8.2 is the plot of variation of compressor mass flow as a function of gas generator speed. All three models predicted a similar variation of compressor mass flow which is in good agreement with the reference. The only difference is in the trend of variation of mass flow: smooth, almost linear variation predicted by the three simulation models versus piece-wise-smooth variation of the reference data.

Model 4 results are not shown in Figures 8.1 and 8.2 since they coincide with those of Model 1: use of constant efficiencies for the compressor and gas generator turbine, and scaled T700 map for power turbine mass flow in both models results in evaluation of identical engine parameters and flow properties up to the inlet of the power turbine. The two models, however, differ in the evaluation of power output: constant efficiency in Model 1 versus scaled T700 map for power turbine enthalpy drop parameter in Model 4.

Shown in Figure 8.3 is the variation of power output with engine speed. A very good agreement is observed between results of Model 4 and reference data for engine speed higher than 85%. Below this speed value, Model 4 prediction deviates from the reference and underpredicts power output of the engine. Models 1 and 3 are observed to yield a less successful prediction for variation of output power of the engine, while Model 2 shows considerable deviations from the reference and results of Models 1 and 3.

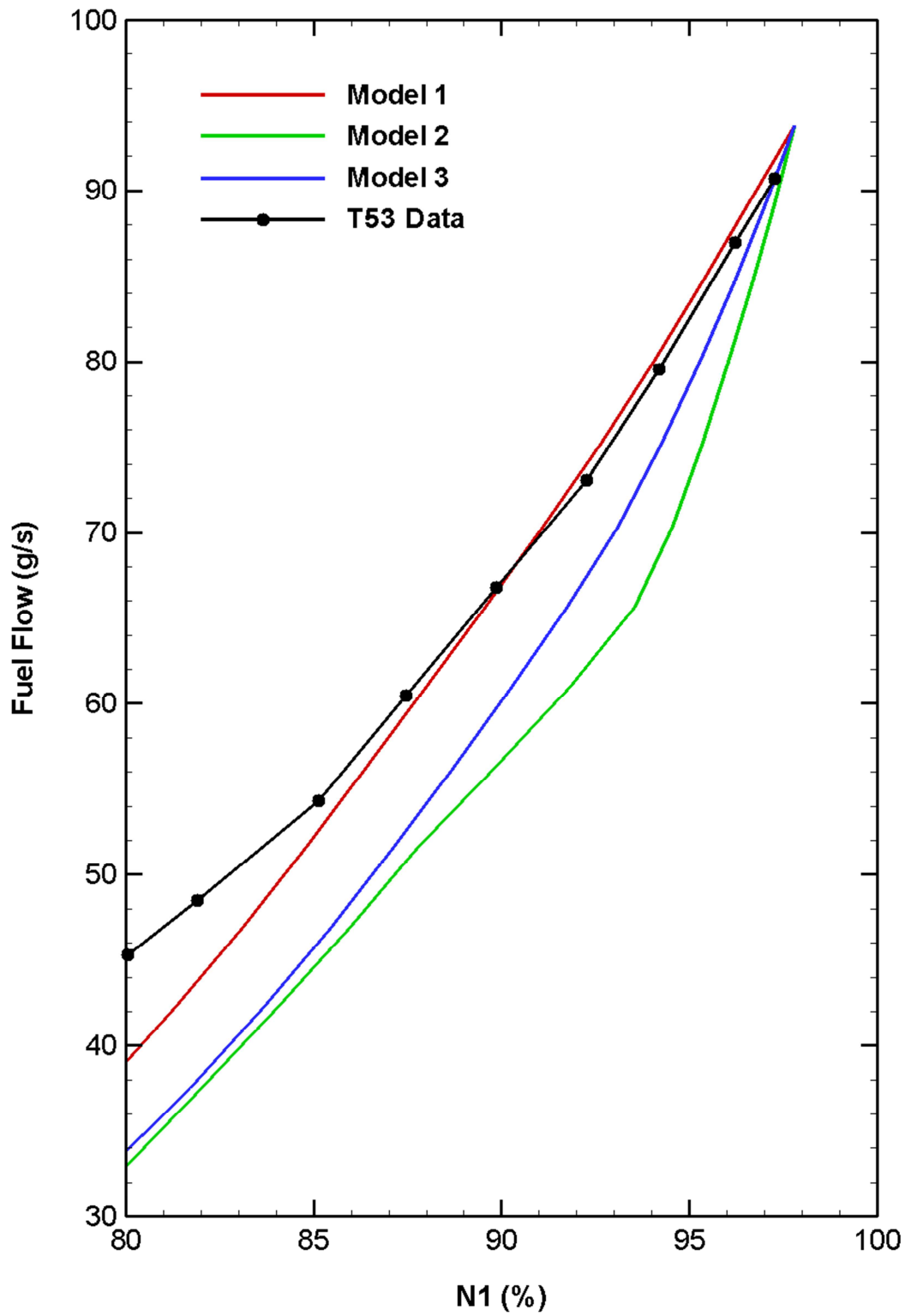


Figure 8.1: Variation of fuel flow as a function of gas generator speed

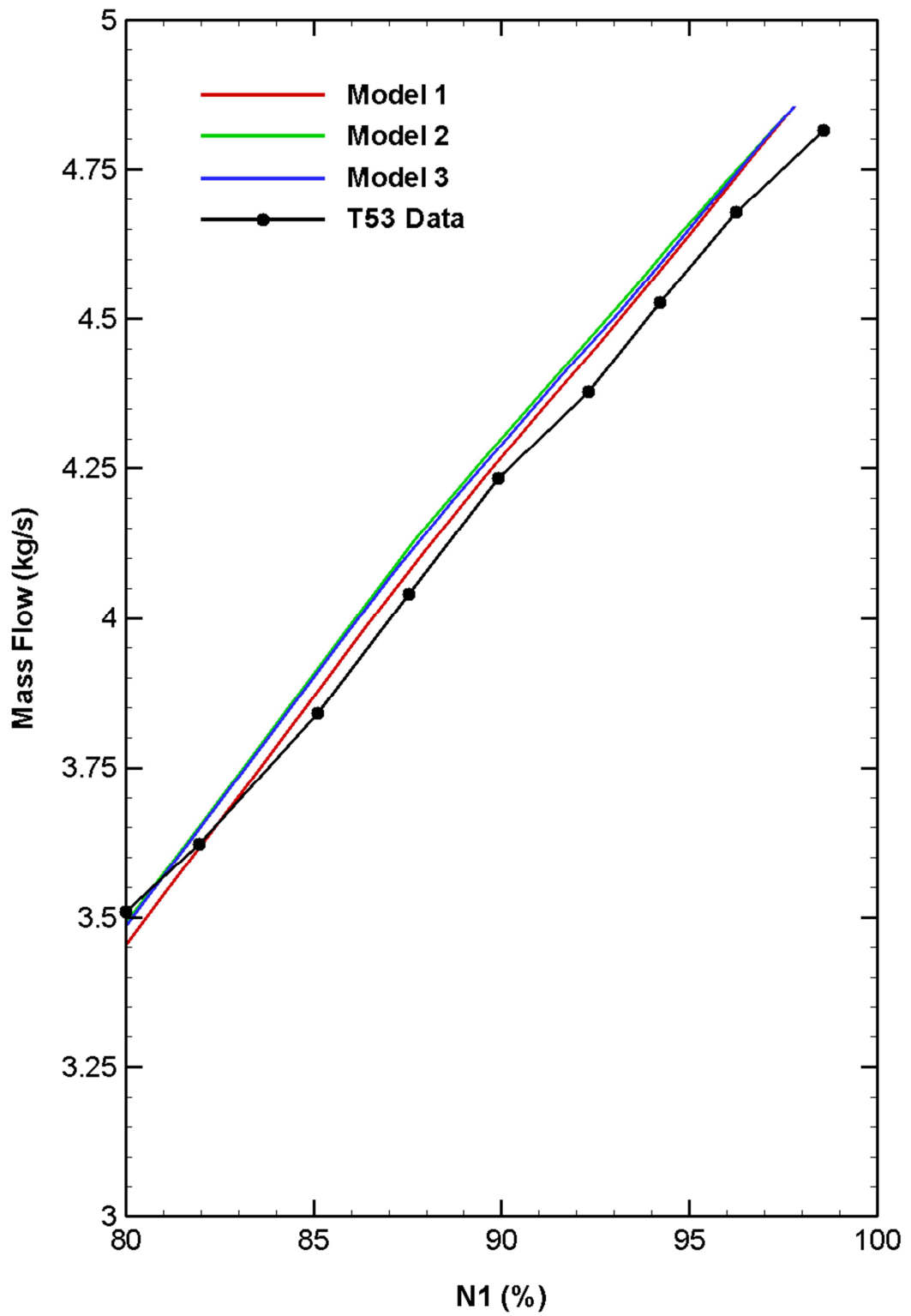


Figure 8.2: Variation of compressor mass flow as a function of gas generator speed

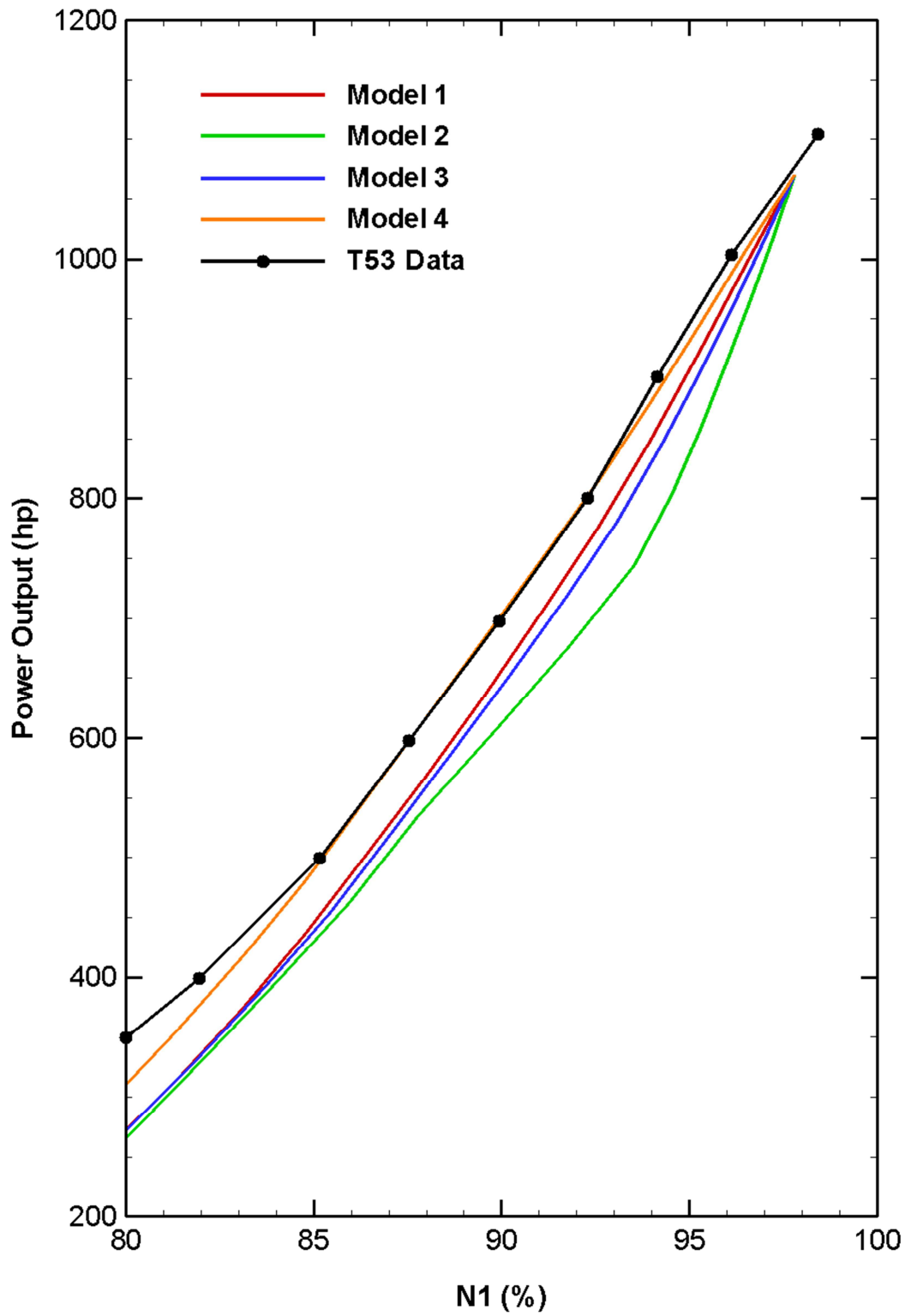


Figure 8.3: Variation of output power as a function of gas generator speed

From the three figures it is evident that although implementation of scaled T700 maps produced the least successful prediction for steady state performance of the T53-L11 engine, Model 4 which used constant efficiencies for the compressor and gas generator turbine, and scaled T700 maps for the mass flow and enthalpy drop across the power turbine produced a good match with reference data. The largest deviations between the two occur in the fuel flow and power output for engine speeds lower than 85%. Moreover, due to lack of engine data for lower engine speeds, no speculation can be made as to whether developed model accurately predicts steady state performance of the engine at speeds lower than 80%.

Deviation of simulation results from reference T53 data is attributed to the limited information which was available for initialization of the simulation: component efficiencies, burner efficiency, combustor pressure drop coefficient and gas generator inlet temperature were estimated by trial-and-error until good match with reference results was obtained at design operating point of the engine. As for the simulation part, it was speculated that scaling of T700 turbine maps could be the reason for the considerable deviations from the reference results. To eliminate the ambiguity, the plot of variation of efficiency for a single stage of a two-stage turbine as a function of engine speed and pressure ratio was adopted from Reference 40. Scaled with respect to turbine's design parameters which were given in the same reference, variation of turbine efficiency with engine speed and component pressure ratio was applied to model the gas generator turbine of the Lycoming T53 engine. Although some improvement is observed to take place in the variation of engine power output with the new map for the gas generator turbine, fuel flow is still underestimated by considerable extent, thus suggesting that discrepancies are not caused by the modeling of the gas generator turbine. Since compressor mass flow rates predicted by the 4 models are consistent with reference data, scaled map for the power turbine mass flow rate can also be eliminated as a possible cause for observed deviations from the reference. Then, the only possible explanation for discrepancies at engine speeds lower than 85% may be due to the compressor map which defined operating range of the engine from 100.4% to 69.6% RPM with only 5 speed lines. Previously it was mentioned that by using linear interpolation between 100.4% and 93.4% speed lines engine design parameters defined in Table 8.1 were not attainable, hence it was required to construct the 97.8% speed line by linearly interpolating between the two speed lines. This suggests that using linear interpolation

between 87.5% and 79.5% speed lines, i.e. the interval in which largest deviations of Model 1 results from reference data occur, will result in incorrect evaluation of compressor mass flow.

From the experience with T700 engine it can be stated that an accurate simulation model can be obtained if true component maps are available. Not only will the model faithfully predict correct steady state and transient performance of the engine, but design point of the engine can be calculated using iterative techniques with a high level of accuracy, thus contributing to the overall accuracy of the model. Although T53 simulation results leave some question marks about accuracy of the model which was caused by the lack of a reliable compressor map, additional engine parameters and simulation results which could be used to adjust engine parameters to match steady state results of the reference data, and, most importantly, lack of turbine maps, developed generic model can be rendered a high level of reliability by using true component maps as well as reference data of the engine for the purpose of adjusting some of the most critical performance parameters of the engine.

## CHAPTER 9

### CONCLUSIONS AND FUTURE WORK

#### 9.1 Conclusions

Out of a number different transient simulation model types widely used in the industry and academic research, aerothermodynamic gas turbine models provide one of the highest levels of accuracy in simulating steady state and transient performance of an aero-engine. This is due to the fact that these models rely on performance maps of major engine components and are based on the laws of thermodynamics which govern change of flow properties inside individual engine components. Due to their inherent structure which allows for the use of forward substitution solution methodology, these models can be run without employing time and power intensive iterative solution schemes. Offering significant savings in time and computational power, aerothermal models provide high numerical accuracy at very little cost of simulation time, which makes them the primary candidate for the use in simulating engine performance under different operating conditions. Because they combine high accuracy with superior execution time, aerothermal models are widely used for design and development of sophisticated engine control systems.

Developed in the current study was an aerothermal engine model for GE T700 turboshaft engine. Using genuine component maps of the engine as well as empirical relations governing change of flow properties inside the engine, an accurate simulation model was developed and successfully validated against previously published simulation data. The model was used to simulate different cases of inlet distortion as well as four common cases of engine deterioration.

In steady state HGI simulations, the model was run for elevated ambient temperatures. The effect of ingestion of hot air on engine performance was studied by keeping the rotational

speed of the power turbine at its design value by varying the fuel flow, and maintaining gas generator turbine inlet temperature at a certain value thus to provide the maximum power output of the engine. Using the two-parallel-compressor model in which one of the compressors was subjected to inlet distortion and the other was kept operating at clean inlet conditions with overall compressor performance determined via the angle of distortion to which the original compressor was subjected, it was possible to simulate the effect of increasing distortion angle on the overall performance of the engine with increasing ambient temperature. It was shown that for a given ambient condition and distortion angle losses due to hot gas ingestion could be reduced if higher turbine inlet temperatures could be sustained. Moreover, it was shown and discussed that increasing inlet distortion angle resulted in increased engine response to the distortion: since for a small distortion angle the overall effect of the distortion is small, distorted compressor is prone to surge more rapidly than in the case with a large distortion angle in which contribution of the clean compressor diminishes to yield a more pronounced response to the distortion. Thus, with increase in inlet distortion angle it becomes possible to keep the operating line of the compressor further from the surge limit. This conclusion, however, was reached by assuming that no mixing of hot and cold air streams took place inside of the compressor, which led to the possibility of treating hot and cold air streams separately by passing each of them through a separate compressor and accounting for the overall effect via the fraction inlet area to which each of the two compressors was subjected in the original compressor.

In another simulation investigated was the effect of hot gas ingestion with a realistic inlet distortion profile which was given in the literature for the case of rocket launch. Hot combustion gases being emitted from the nozzle rise and get ingested by the engine to cause a significant disturbance to the operating state of the engine. One of the effects recorded during a real flight was the high-amplitude engine torque variation which had the potential of causing significant damage to the power shaft and results in its failure. Simulated with developed aerothermal model was the case of hot gas ingestion with a similar inlet profile as in the case of the real flight. It was found that for the full inlet distortion torque spikes could reach up to 20% of design value, and pose a serious threat to the mechanical integrity of the drive train.

Inlet total pressure distortion was simulated by generating a signal applied to the ambient total pressure of ingested air. Simulations predicted a drastic variation in output torque as well as significant reduction in compressor surge margin. It was shown that to initiate a compressor surge at very short pulse duration times, it was sufficient to apply a 10% distortion at the inlet. As the time duration of the pulse was increased, allowable distortion extent first increased, and following a small decrease approached a limiting value which remained constant for very large pulse durations.

Different cases of engine deterioration were simulated by applying appropriate scaling factors to different components of the engine. Simulated were four cases of engine degradation: separately the mechanical damage of the compressor and gas generator turbine both leading to a 5% decrease in component efficiency, increase in the throat area of the gas generator turbine by 2%, and a combination of compressor and gas generator turbine efficiency drop by 3% and 1%, respectively, 2% increase in the throat area of the gas generator turbine and 5% decrease in the mass flow rate of the compressor as a result of fouling. Since decrease in gas generator turbine efficiency directly resulted in reduction of power required to drive the compressor under a given operating state, reduction in engine speed was associated with substantial reduction in the output power. Gas generator turbine erosion was found to produce very little performance degradation in terms of both the engine speed and power output. Compressor mechanical damage was found to produce moderate degradation of engine performance. The largest performance loss was produced for the combined effect of degradation of engine components: associated with some decrease in engine speed, overall engine deterioration was found to result in substantial loss in power and significant increase in specific fuel consumption.

Real time capability of the model was tested using sinusoidal variation in fuel flow to ensure that model consumed the largest amount of time require to complete one cycle. Since the model was numerical unstable at large simulation time steps, it was limited to a maximum time step of  $10^{-4}$  seconds at which real time capability of the model was not achievable. In order to render the model with the capability of real time execution and preserve numerical stability of the model, time scaling of control volumes was applied to allow for the use of simulation time steps as large as 1 millisecond. With this simulation time step, it was possible to reduce the true simulation time to 0.56 seconds per one second of the simulation. This substantial amount of time can be used to increase physical

faithfulness of the model by including a more detailed description of engine components. Thus, some of the shortcomings of the model can be alleviated and more detailed simulation of engine dynamics be done under different operating conditions of the engine.

Based on the experience with T700 engine model, a generic version of the model was developed in which T700 scaled maps were used to simulate T53 turboshaft engine. Modeled using 4 different approaches, it was possible to obtain a close simulation model of the T53 engine by using constant efficiencies for the compressor and gas generator turbine, and scaled T700 performance maps for the power turbine. Discrepancies in simulation results from reference data were attributed to the lack of engine data and the partial compressor map which for a wide operating range was defined with only 5 speed lines.

## **9.2 Future work**

Accuracy of developed aerothermal model was shown to be highly satisfactory for a wide range of applications. General understanding about engine dynamics can be gained, and sophisticated control algorithms can be successfully designed and validated using developed model. There are, however, a number of improvements which can be added to the model to increase its physical faithfulness.

### **9.2.1 Remodeling of the Compressor**

In present study, compressor model was based on a component map which was used to read compressor corrected mass flow rate as a function of corrected engine speed and component pressure ratio. Because component map is just an approximation of the real component performance, it may not yield accurate prediction of engine performance under certain circumstances. Therefore, a more complete compressor model which would include internal flow dynamics is required. To do so, one needs to consider blade angles and velocity triangles for every stage of the compressor, and calculate stage performance by considering the turning angles of the flow. This modeling approach can be easily extended to turbines as well. By considering internal flow dynamics of the compressor, it becomes possible to better understand the dynamics of the component, and simulations can be done for different cases of engine deterioration by applying degradation effects to any blade

row. Thus, with suggested modeling approach the simulation model becomes much more flexible when compared to the model which employs a static compressor map.

An additional inconvenience introduced by the use of a static compressor map is the instantaneous change of compressor parameters as a result of change in ambient condition: any variation in ambient temperature or pressure is directly reflected on the corrected engine speed and mass flow of the compressor without accounting for the lag time between ingestion of air by the compressor and its discharge into the diffuser. This problem can be overcome by supplying compressor dynamics in form of a transfer function, or by remodeling of the compressor to account for internal flow dynamics as was described in the previous paragraph.

### **9.2.2 Surge Modeling**

Described as a violent reduction in pressure delivery and flow direction reversal, engine surge is a dangerous phenomenon for gas turbine engines. Modeling of the surge was left out of the scope of present study. However, modeling of surge is important to understand dynamics of an engine which experiences a compressor stall.

### **9.2.3 Dynamics of Loss Coefficients**

In developed model, four loss coefficients were employed: burner efficiency to account for unburned fuel, combustor pressure loss to account for pressure drop across the burner, enthalpy and pressure losses due to cooling of the gas generator turbine. All these losses were modeled as fixed percentages which remained constant for all operating conditions of the engine. While assumption of constant coefficients may yield satisfactory results, because it does not include dynamic change of these parameters as a function of operating state of the engine, some loss in accuracy inevitably occurs.

### **9.2.4 Drive Train Model**

For the purpose of providing a more realistic dynamics of the engine, a drive train model is required so that more accurate variation of speed and torque of the power turbine can be obtained.

## BIBLIOGRAPHY

1. P. P. Walsh and P. Fletcher, *Gas Turbine Performance*, Blackwell Science Ltd, Oxford, 1998.
2. N. U. Rahman and J. F. Whidborne, "Real-Time Transient Three Spool Turbofan Engine Simulation: A Hybrid Approach", *Journal of Engineering for Gas Turbines and Power*, Vol. 131, No. 5, 2009.
3. S. M. Camporeale, B. Fortunato, M. Mastrovito, "A Modular Code for Real Time Dynamic Simulation of Gas Turbines in Simulink", *Transactions of the ASME*, Vol. 128, pp. 506 – 514, 2006.
4. R. Chacartegui, D. Sanchez, A. Munoz, T. Sanchez, "Real Time Simulation of Medium Size Gas Turbines", *Energy Conversion and Management*, Vol. 52, No. 1, pp. 713-724, 2011.
5. V. Panov, "GasTurboLib: Simulink Library for Gas Turbine Engine Modelling", *ASME Turbo Expo*, GT2009-59389, 2009.
6. V. Sanghi, B. K. Lakshmanan, V. Sundararajan, "Digital Simulator for Steady-State Performance Prediction of Military Turbofan Engine", *Journal of Propulsion and Power*, Vol. 14, No.1, pp. 74-81, 1998.
7. S. Martin, I. Wallace and D. G. Bates, "Development and Validation of a Civil Aircraft Engine Simulation Model for Advanced Controller Design", *ASME Journal of Engineering for Gas Turbines and Power*, Vol. 130, Issue 5, 2008.
8. R. Sekhon, H. Bassily, J. Wagner, J. Gaddis, "Stationary Gas Turbines - A Real Time Dynamic Model with Experimental Validation", *American Control Conference*, June 2006.
9. P. Tagade, S. K. Sane, K. Sudhakar, "Start-up to Shutdown Simulation of Single Spool Turbojet/Turboshaft Engine", *19th National Convention of Aerospace Engineers, Institution of Engineers, Jaipur*, November 2005.
10. J. Larjola, "Simulation of Surge Margin Changes Due to Heat Transfer Effects in Gas Turbine Transients", *International Journal of Turbo and Jet Engines*, Vol. 2, Issue 1, pp. 81–91, March 1985.

11. N. U. Rahman and J. F. Whidborne, "A Numerical Investigation into the Effect of Engine Bleed on Performance of a Single-Spool Turbojet Engine", *Journal of Aerospace Engineering*, Vol. 222, No. 7, pp. 939-949, 2008.
12. N. K. Vallabhaneni, "Continuously Variable Rotorcraft Propulsion System: Modelling and Simulation", M.Sc. Thesis, University of Tennessee, 2011.
13. S. Yarlagadda, "Performance Analysis of J85 Turbojet Engine Matching Thrust with Reduced Inlet Pressure to the Compressor", M.Sc. Thesis, University of Toledo, May 2010.
14. M. Montazeri-Gh, M. Nasiri and S. Jafari, "Real-Time Multi-Rate HIL Simulation Platform for Evaluation of a Jet Engine Fuel Controller", *Simulation Modelling Practice and Theory*, Vol. 19, No. 3, pp. 996-1006, 2011.
15. S. Vivek, B. K. Lakshmanan and V. Sundararajan, "Survey of Advancements in Jet-Engine Thermodynamic Simulation", *Journal of Propulsion and Power*, Vol. 16, No. 5, pp. 797-807, October 2000.
16. G. Kocer, "Aerothermodynamic Modelling and Simulation of Gas Turbines for Transient Operating Conditions", M.Sc. Thesis, Middle East Technical University, Turkey, June 2008.
17. G. Kocer, O. Uzol, I. Yavrucuk, "Simulation of the Transient Response of a Helicopter Turboshaft Engine to Hot-Gas Ingestion", ASME Turbo Expo, GT2008-51164, 2008.
18. O. Uzol, "A New High-Fidelity Transient Aerothermal Model for Real-Time Simulations of the T700 Helicopter Turboshaft Engine," *Journal of Thermal Science and Technology*, *accepted for publication*, 2010.
19. M. G. Ballin, "A High Fidelity Real-Time Simulation of a Small Turboshaft Engine", NASA-TM-100991, July 1988.
20. W. I. Rowen, "Simplified Mathematical Representations of Heavy Duty Gas Turbines", *Transactions of the ASME, Journal of Engineering for Power*, Vol. 105, pp. 865-70, 1983.
21. J. Mantzarisand and C. Vournas, "Modelling and Stability of a Single-Shaft Combined Cycle Power Plant", *International Journal of Thermodynamics*, Vol. 10, No. 2, pp.71-78, June 2007.
22. D. N. Gaonkar and R. N. Patel, "Modelling and Simulation of Microturbine Based Distributed Generation System", *IEEE Power India Conference*, pp. 256-260, 2006.

23. L. N. Hannett and A. H. Khan, "Combustion Turbine Dynamic Model Validation from Tests", IEEE Transactions on Power Systems, pp. 152-158, 1993.
24. L. M. Hajagos and G. R. Berube, "Utility Experience with Gas Turbine Testing and Modelling", IEEE Power Engineering Society Winter Meeting Conference Proceedings, pp. 671-677, 2001.
25. F. Tokarski, M. Desai, M. Books, R. Zagranski, "Hot Gas Ingestion Effects on Fuel Control Surge Recovery and AH- 1 Rotor Drive Train Torque Spikes", Army Research Laboratory, Contractor Report ARL- CR-13, 1994.
26. Q. Z. Al-Hamdan and M. S. Y. Ebaid, "Modelling and Simulation of a Gas Turbine Engine for Power Generation," Journal of Engineering for Gas Turbines and Power, Vol. 128, pp. 302–311, April 2006.
27. J. M. Spack, "Linear parameter varying controller for a small turboshaft engine", Electrical and Computer Engineering Master's Theses, Northeastern University, USA, 2011.
28. M. M. Maslennikov, Y. G. Behli, Y. I. Shalman, *Gas Turbine Engines for Helicopters* (in Russian), Moscow, 1969.
29. L. S. Rysin, "Investigation of Gas Turbine Engine Exhaust Emissions under the Main Rotor and its Effect on Air Surrounding the Helicopter" (in Russian), Moscow, 1966.
30. J. Berdy, P. G. Brown, J. G. Andrichak, S. B. Wilkinson, *High-Speed Reclosing System and Machine Considerations*, General Electric Company.
31. L. M. Wenzel and R. J. Blaha, "Analysis of dynamic inlet distortion applied to a parallel compressor model", NASA-TM-X 3522, 1977.
32. I. S. Diakunchak, "Performance Degradation in Industrial Gas Turbines", ASME Journal of Engineering for Gas Turbines and Power, Vol. 114, pp. 161-168, April 1992.
33. T. J. Carter, "Common Failures in Gas Turbine Blades", Engineering Failure Analysis, Vol. 12, pp. 237-247, April 2005.
34. P. Zhu, H. I. H. Saravanamuttoo, "Simulation of an Advanced Twin-Spool Industrial Gas Turbine", Journal of Engineering for Gas Turbines and Power, Vol. 114, pp. 180-185, April 1992.
35. R. Kurz and K. Brun, "Degradation in Gas Turbine Systems", Journal of Engineering for Gas Turbines and Power, Vol. 123, pp. 70-77, 2001.

36. V. Sanghi, B. K. Lakshmanan and R. Rajasekaran, "Aerothermal Model for Real-Time Digital Simulation of a Mixed-Flow Turbofan Engine", *Journal of Propulsion and Power*, Vol. 17, pp. 629-635, 2001.
37. V. Sanghi and B. K. Lakshmanan, "Timescaling Control Volumes During Real Time Digital Simulation of a Military Turbofan", *Journal of Propulsion*, Vol. 18, No. 4, pp. 964-966, 2002.
38. H. I. H. Saravanamuttoo and B. D. MacIssac, "Thermodynamic Models for Pipeline Gas Turbine Diagnostics", *Journal of Engineering for Power*, Vol. 105, pp. 875-884, October 1983.
39. J. Faragher, "The Development of a T53-L11 Engine Computer Model", *Propulsion Technical Memorandum 453*, April 1989.
40. R. G. Stabe, W. J. Whitney and T. P. Moffitt, "Performance of a High-Work Low Aspect Ratio Turbine Tested with a Realistic Inlet Radial Temperature Profile", *NASA-TM-83655*, 1984.

## APPENDIX A

### COMPRESSOR MAP READING

Compressor map given by Ballin in Reference 19 is digitized and stored in a “.mat” MATLAB file. Each RPM line is defined by 6 equally spaced points. A MATLAB subroutine is used to calculate compressor corrected mass flow rate as a function of inputted pressure ratio and corrected rotational speed of the component. The first step of calculating the mass flow is to find the operating range of the compressor by bounding the running RPM ( $N$ ) with a lower ( $N_0$ ) and a higher ( $N_1$ ) RPM line as it is given in the original compressor map by comparing stored values of compressor speed with the running speed (see Figure A.1).

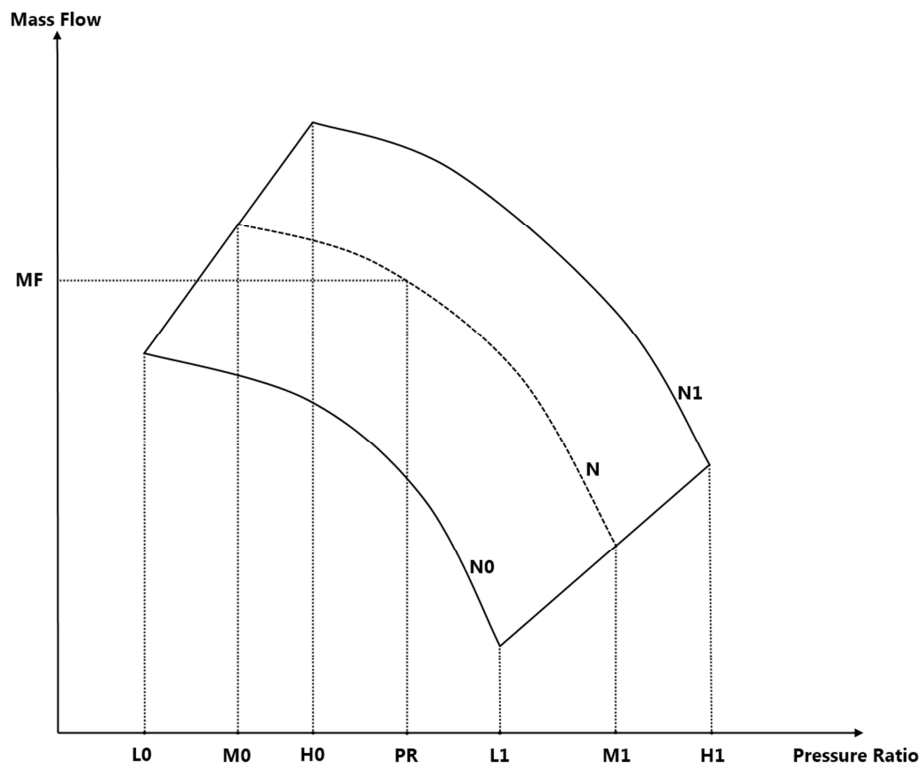


Figure A.1: Reading of the compressor map

Compressor speed is assumed to vary linearly between two bounding RPM lines. Then, the value of the running speed can be defined in percent form as follows:

$$dN = \frac{N - N_0}{N_1 - N_0} \quad [\text{A.1}]$$

Each bounding RPM line, i.e.  $N_0$  and  $N_1$ , spans over a certain range of compressor pressure ratio which is defined for every bounding RPM line as follows:

$$L_0 = \min\left(PR_{map}(N_0)\right) \quad [\text{A.2}]$$

$$L_1 = \max\left(PR_{map}(N_0)\right) \quad [\text{A.3}]$$

$$H_0 = \min\left(PR_{map}(N_1)\right) \quad [\text{A.4}]$$

$$H_1 = \max\left(PR_{map}(N_1)\right) \quad [\text{A.5}]$$

Similarly, the span of pressure ratio of the running RPM is limited by  $M_0$  and  $M_1$ :

$$M_0 = L_0 + (H_0 - L_0) \cdot dN \quad [\text{A.6}]$$

$$M_1 = L_1 + (H_1 - L_1) \cdot dN \quad [\text{A.7}]$$

Then, the ratio of operating pressure ratio with respect to the span is defined as:

$$dPR = \frac{PR - M_0}{M_1 - M_0} \quad [\text{A.8}]$$

Equation A.8 defines the percent shift of the operating point from the line defined by  $L_0$  and  $H_0$ . Using this shift to calculate mass flows of the two bounding RPM lines will yield the line on which operating point of the compressor is located. So,

$$MF_0 = \text{interp1}\left(PR_{map}(N_0), MF_{map}(N_0), L_0 + (L_1 - L_0) \cdot dPR\right) \quad [\text{A.9}]$$

$$MF_1 = \text{interp1}\left(PR_{map}(N_1), MF_{map}(N_1), H_0 + (H_1 - H_0) \cdot dPR\right) \quad [\text{A.10}]$$

Finally, operating mass flow rate is calculated using Equation A.11:

$$MF = MF_0 + (MF_1 - MF_0) \cdot dN \quad [\text{A.11}]$$

Method of the extrapolation used in Equation A.9 and A.10 is “linear”. This way, as long as the operating point lies inside the boundaries of the compressor map, linear extrapolation reduces to linear interpolation. If the point lies outside this boundary, mass flow rate is linearly extrapolated for by using built-in MATLAB subroutine called “interp1”.

## APPENDIX B

### T700 ENGINE CONSTANTS

Table B.1: T700 Engine Parameters

Parameter	Value	Unit
$N_{1des.}$	44700.0	<i>RPM</i>
$N_{2des.}$	20900.0	<i>RPM</i>
$LHV$	42.5658	<i>MJ/kg</i>
$K_{V1}$	26539.79	$1/m \cdot s^2 \cdot K$
$K_{V2}$	372925.0905	$1/m \cdot s^2 \cdot K$
$k_{h1}$	1000.6452	$J/kg \cdot K$
$k_{h21}$	1045.0253	$J/kg \cdot K$
$k_{h22}$	-19538.4	$J/kg$
$k_{h31}$	1260.2268	$J/kg \cdot K$
$k_{h32}$	-202141.0295	$J/kg$
$k_{T41}$	$8.404987 \cdot 10^{-4}$	$kg \cdot K/J$
$k_{T42}$	99.5	<i>K</i>
$k_{GG1}$	0.00329868	$1/K$
$k_{GG2}$	0.0856	<i>non – dimensional</i>
$k_{PT1}$	0.00329868	$1/K$
$k_{PT2}$	0.0856	<i>non – dimensional</i>

## APPENDIX C

### IMPLEMENTATION OF THE T700 ENGINE MODEL IN SIMULINK®

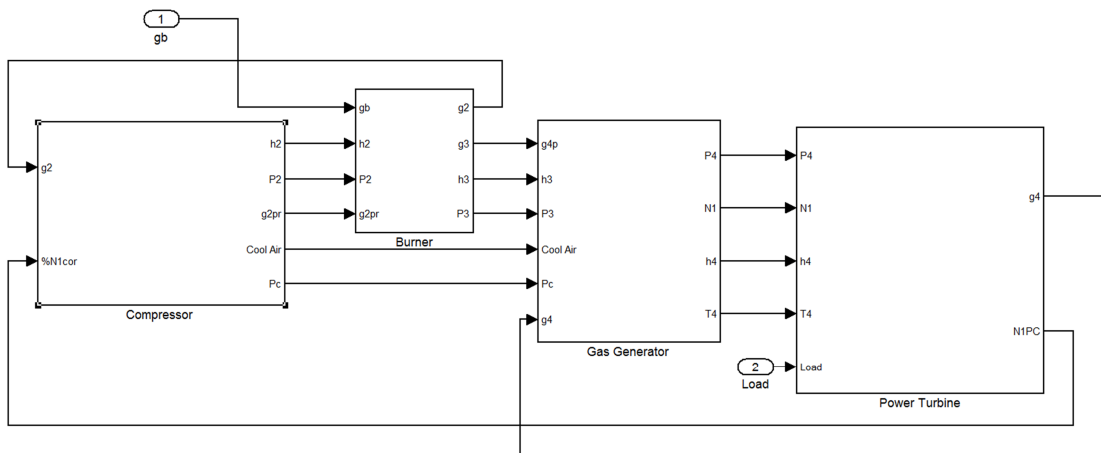


Figure C.1: Individual engine blocks of the SIMULINK® model

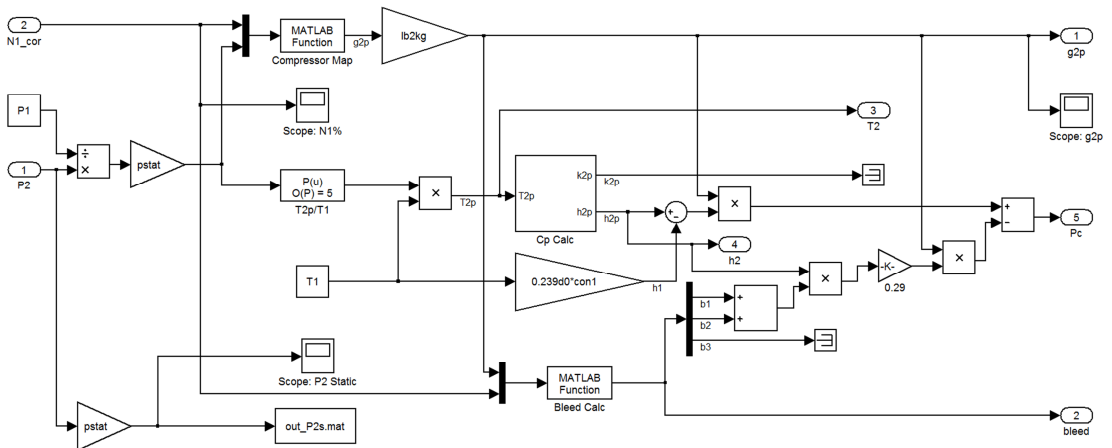


Figure C.2: Compressor model block

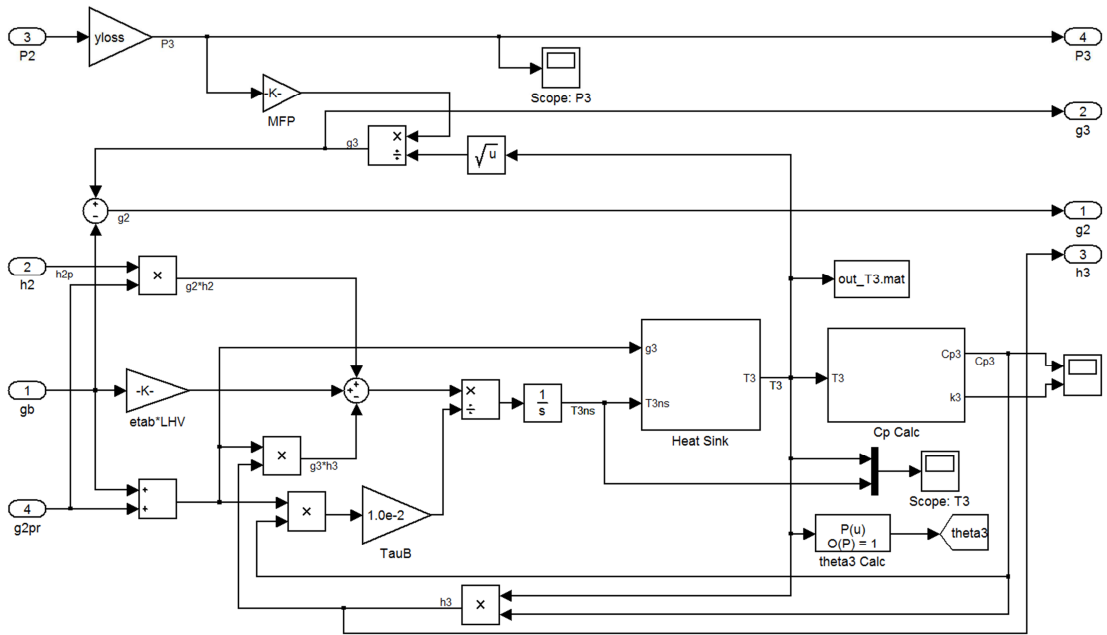


Figure C.3: Combustor model block

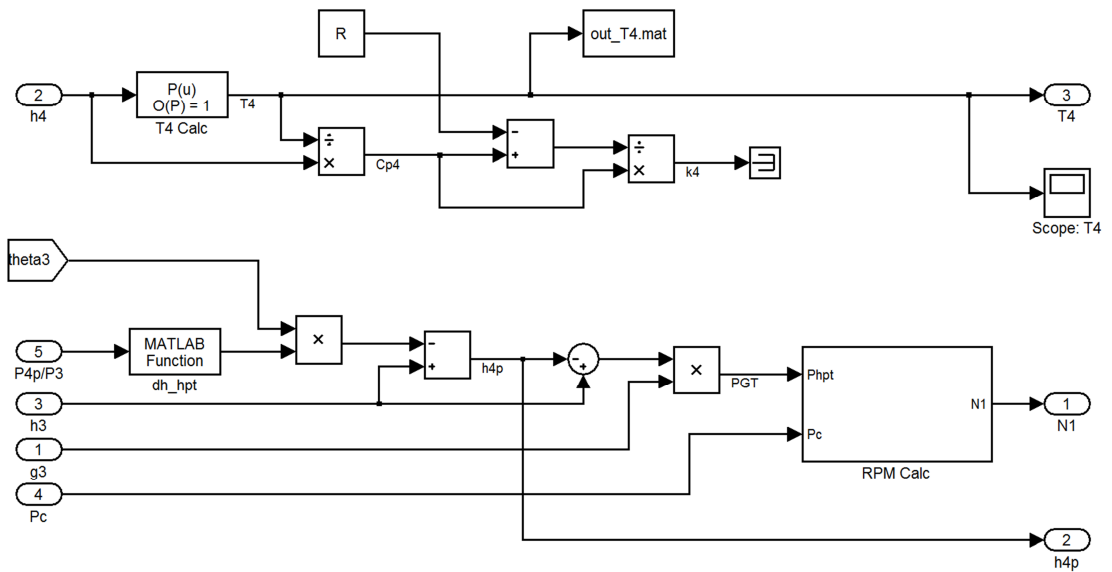
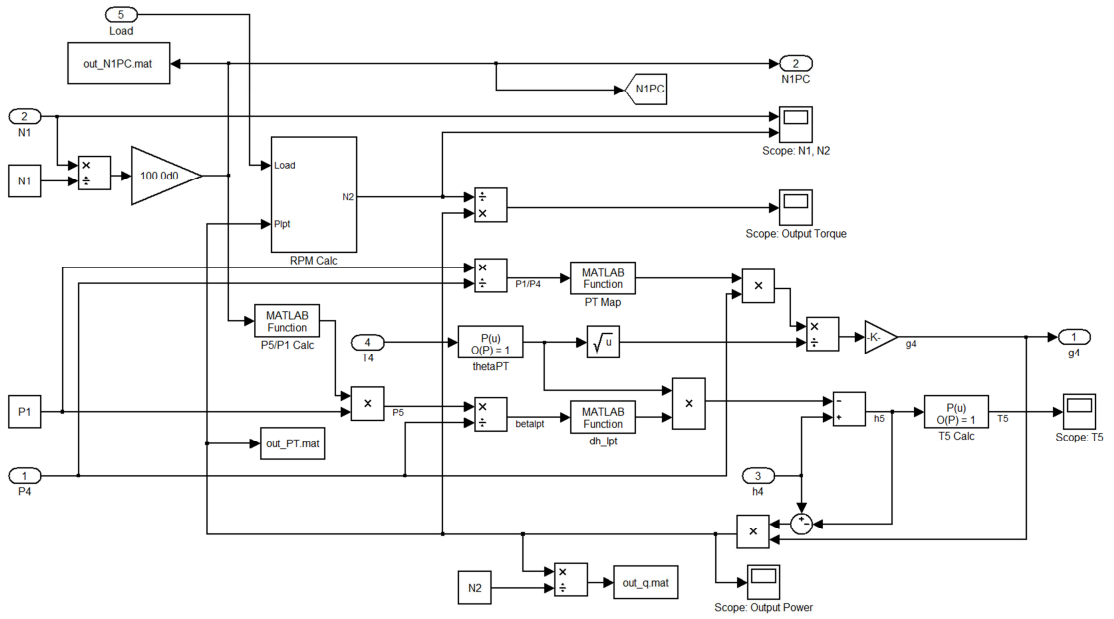


Figure C.4: Gas generator turbine model block



**Figure C.5: Power turbine model block**

# APPENDIX D

## GE T700 COMPRESSOR MAP

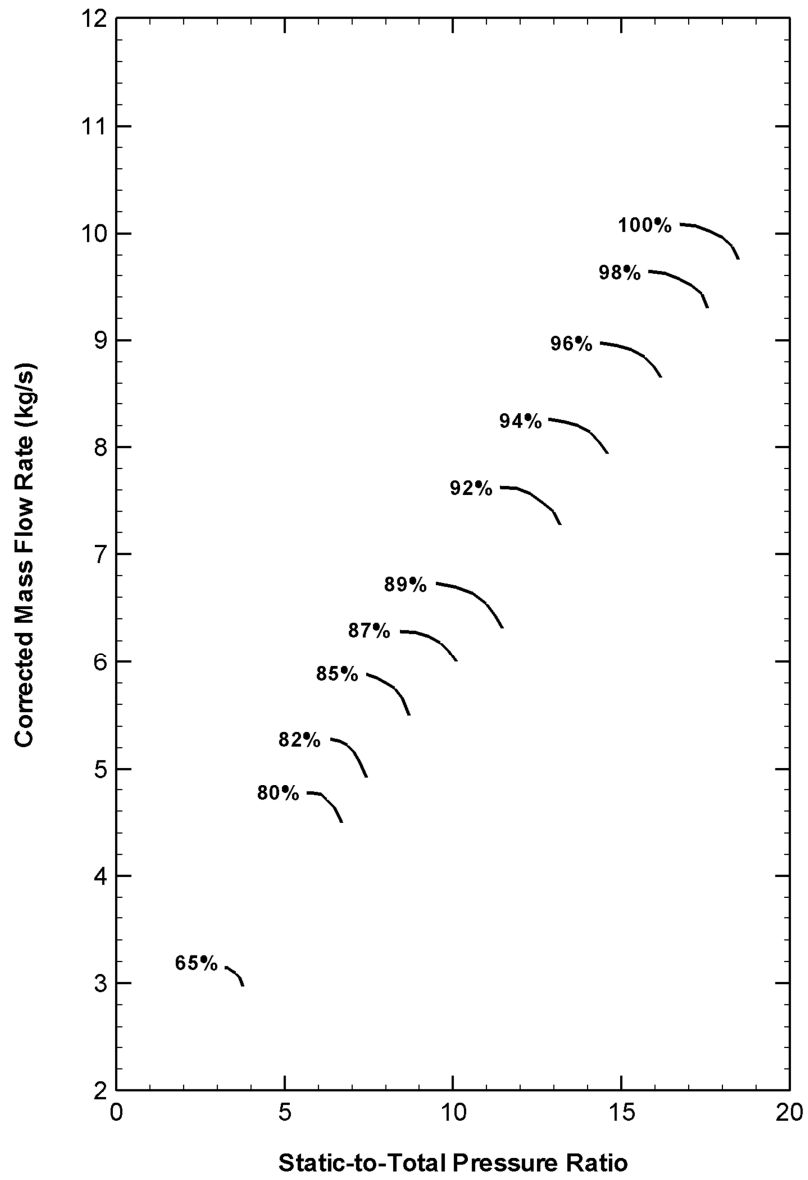


Figure D.1: GE T700 compressor map